EFFECTS OF LORENTZ FORCES ON FLAME HOLDING

by

ROGER ANGELO LUCHETA

S. B., Massachusetts Institute of Technology
(1961)

S. M., Massachusetts Institute of Technology
(1962)

M. E., Massachusetts Institute of Technology
(1964)

SUBMITTED IN PARTIAL FULFILLMENT

OF THE REQUIREMENTS FOR THE

DEGREE OF DOCTOR OF SCIENCE

at the

MASSACHUSETTS INSTITUTE OF TECHNOLOGY

September, 1965

Signature of Author_____
Department of Mechanical Engineering, July 1, 1965

Certified by_____
Thesis Supervisor

Accepted by_____
Chairman, Departmental Committee on Graduate Students

EFFECTS OF LORENTZ FORCES ON FLAME HOLDING

by

Roger Angelo Lucheta

Submitted to the Department of Mechanical Engineering on July 1, 1965 in partial fulfillment of the requirements for the degree of Doctor of Science

Abstract

A study of the alteration of the lean blowoff limits of a propane-air flame burning at 86 mm. Hg absolute pressure is described.

The fuel/air ratio at the lean blowoff limit for the flame, when subjected to Lorentz forces parallel to its direction of flow, is given. The Lorentz forces arose from magnetic fields applied to a five milliampere current flowing through the gas, and could either stabilize or reduce the stability of the flame. Stabilization was observed when the Lorentz forces decelerated the flow, and destabilization when the Lorentz forces accelerated the flow.

Visualization of the flow field demonstrated that the burning velocity of the gas flow was unaffected by the Lorentz forces, while the flow field of the gas downstream of the flame was severely changed

The effects of Lorentz forces on flame structure and burning velocity were evaluated, both by order-of-magnitude considerations and by solution of the flame structure equations, and were found to be negligable. Analysis and some limited experimental observations and measurements verified that the current flow between the electrodes remained downstream of the flame, and did not concentrate in the reaction zone of the flame.

It is concluded that Lorentz forces stabilize a flame by altering its flow field, but not its burning velocity.

Thesis Supervisor: Tau-Yi Toong
Title: Professor of Mechanical Engineering

ACKNOWLEDGEMENT

In the execution of this work, the writer has recieved a very great deal of indispensable aid and advice from very many people. It would be impossible to acknowledge all, but to each person who aided, a sincere "thank you" is offered.

Mr. Fred Ketterer's explanation of the character and mechanisms of gaseous discharges was the most important piece of information given the author; with this information, it was possible to plan experiments in which the flow of electric current could be manipulated in a controlled manner.

Messrs. Jon Kelly, Elazar Barak, and Edelbert Plett all assisted greatly in the planning and construction of experiments; in the execution of these, the writer relied heavily on the assistance of Messrs. Lawrance Johnson, William Day, Robert Silverstein, Isom Herron, and of the Sloan Laboratory Machine Shop.

The members of the author's Doctoral Committee - Professors Ascher H. Shapiro, Herbert H. Woodson, and William C. Moffat - provided very much extremely useful advice and aid; Professor Tau-Yi Toong filled the position of thesis supervisor and, in this capacity, definitely influenced the progress and direction of the work. It was Professor Toong's work, published and unpublished, which provided the initial impetus for undertaking this work.

The writer's support for the year 1962-1963 came from a fellowship granted by the National Science Foundation; an M.I.T. Research Assistantship, made possible by contracts DA-ARO-D-31-124-G190 and DA-ARO-D-31-124-G593, awarded by the United States Army Research Office (Durham), and by grant G-20880 of the National Science Foundation, provided for his support for 1963-1965. The former research contract also provided for experimental apparatus

The numerical solutions of the flame structure equations and of the current pattern equations were performed on the calculating machines of the M.I.T. Computation Center; many thanks to the Computation Center programming and operating staff for their assistance.

And to Karen, this thesis is dedicated as only a small token of recognition of her loyalty, steadfastness, help, and hope for the future which has added such meaning to this work.

TABLE OF CONTENTS

NOTATION

A list of the most frequently-used symbols in this thesis follows. Others which are less used are defined at the time of occurance

---

A - Burner area

a - One-half of electrode separation — location of poles in bipolar coordinates on X axis

B - Magnetic field intensity

C - Reactant molal concentration

C_A - Reactant mass fraction

C_v - Specific heat at constant volume

C_p - Specific heat at constant pressure

d - Burner diameter

D_c - Concentration gradient

D_T - Temperature gradient

$\mathcal{D}$ - Diffusivity of reactants into products

E_1 - Activation energy - burning velocity law

E_A - Activation energy - Arrhenius rate law

$\vec{E}$ - Electric field

$\vec{e}$ - Unit vector

f - Lorentz force applied to column of gas

F - Momentum flux (total) of column of gas

f_W - Particle size distribution function, by weight

f_N - Particle size distribution function, by number

g - Gravitational constant

h - Enthalpy

H - Hall parameter

i - Scaling factor in current distribution

$\vec{i}$ - Unit vector, X direction

I - Total current entering or leaving electrode, passing through gas

$\vec{J}$ - Current density vector

$\vec{j}$ - Unit vector, Y direction

K' - Scaling factor in electric field law

K - Reaction rate constant

K_A - Reaction rate - mass of reactants/unit time/unit volume

K_e - Boltzman's constant

L_M - Magnetic interaction length

L_T - Thermal interaction length

ℓ - Length of conducting region acted on by magnetic field - electrode separation

$\dot{m}$ - Mass flow rate (either total or per unit area)

m - Reaction order

m_e - Electron density

P - Gas pressure

q_c - Chemical heat release rate/unit volume

q_r - Chemical heat release/unit mass of reactant

q_J - Joulean heat release rate/unit volume

Q_{es} - Electron-neutral collision cross-section

q_e - Electronic charge

r_p - Particle radius

R - Perfect gas constant

r - Radial coordinate

S_u - Burning velocity

T - Temperature

T_i - Time

T_e - Electron temperature

t - Thickness of column of gas in Z direction

u, U, V - Gas velocity

X - Coordinate parallel to burner head - "horizontal" or "lateral"

X_o - Crossing point of particle track with flame surface

Y - Coordinate perpendicular to burner - "vertical" or "axial"; in Chapter 3, direction parallel to gas flow

Θ - Angular position, a polar coordinate; in Appendix 7, dimensionless temperature

β - Dimensionless magnetic field intensity

γ - Ratio of specific heats

$\bar{r}$ - Dimensionless reaction rate

δ - Dimensionless density; also Dirac delta function

ϵ_N - Parameter in expansion of Fourier series for current distribution

η - A bipolar coordinate

λ - Thermal conductivity

μ - Viscosity

μ_o - Permeability of free space

ξ - A bipolar coordinate

π - Dimensionless pressure

ρ - Gas density

σ - Gas electrical conductivity

τ - Dimensionless enthalpy

ϕ - Dimensionless burning velocity - flame Mach number

ψ - Potential function for current flow

β - Stream function for current flow

Ω - Dimensionless normalized reactant concentration

Subscripts

u - "Upstream" or "unburnt" conditions

b - "Downstream" or "burnt" conditions

x - Horizontal component of a vector- X direction

y - Vertical component of a vector - Y direction

ξ - ξ component of a vector

η - η component of a vector

TABLE OF FIGURES

CHAPTER I

INTRODUCTION

OUTLINE OF WORK REPORTED

The Purpose of this Thesis

This thesis is a study of the manner in which Lorentz forces may be employed to affect mechanisms of flame-holding. Emphasis is centered on the effect of Lorentz forces on two variables, which previous researches have shown to be significant in governing the equilibrium position of a flame over a burner. These are:

1) The burning velocity of the flame
2) The flow patterns and velocity of the flame gases.

The work in this thesis demonstrates that Lorentz forces may affect flame-holding by altering the second of these, but not the first.

Organization of this Thesis

The work presented in this thesis will be divided into four parts:

1) A quantitative determination of the alteration, by means of Lorentz forces, of a flame's resistance to extinction, in Chapter 2. It will be found that a flame's resistance to extinction may be either increased or decreased by the action of Lorentz forces, depending on the orientation

and intensity of the Lorentz forces.

2) An experimental determination, in Chapter 3, of the alterations of the flame gas flow patterns arising from the application of Lorentz forces to the flame gases. On the basis of these observations, it will be concluded that burning velocity is not altered by the Lorentz forces, but that the gas flow patterns are, in a manner similar to that in which a bluff body downstream of the flame alters the gas flow.

3) Calculations and order-of-magnitude evaluations of the possible effects of Lorentz forces and of Joulean heating on the transport processes in a flame, and on the burning velocity of the flame. These support the contention that the burning velocity would not be affected by the electric currents and magnetic fields applied to stabilize the flame.

4) A demonstration that the major features of the changes in flow pattern with the application of Lorentz forces occur in an analysis of a <u>two</u>-dimensional flow field and current pattern. This analysis ignores the effects of buoyancy, viscous drag, and the inherent three-dimensionality of the flow studied experimentally, and studies only the changes in flow patterns which would arise

from the Lorentz forces acting alone.

The Conclusion of this Thesis

The conclusion of this thesis is that the observed effects of Lorentz forces on flame-holding arise from alterations in the flow of the flame gases, and not from alterations in the flame's burning velocity.

Before embarking on the more detailed study of the character and causes of flame holding by Lorentz forces which comprises the subject of this thesis, we must first review some of the better known features of flame holding, and then examine the reasons why Lorentz forces might be expected to affect flame-holding.

BACKGROUND OF THE PRESENT WORK

Flame Stabilization - Governing Features

The behavior of flames and the study of flame stabilization can involve a combination of very many elementary phenomena, so that a complete study of the subject entails considerable complexity. Because of this, the study of some elementary, highly simplified phenomena, in isolation from the other processes usually present in industrial combustors, is essential to developing a conceptual understanding of the more complex phenomena at play in industrial combustors[31].

The first such separation which occurs in studies of flame-holding and blowoff is the separation between the "chemical-kinetic" and the "fluid-dynamic" features of the

flame and combustor. The independance of the two, in flames in fast, turbulent streams, was first brought out by Zukoski and Marble[70], and more aspects of the problem of flame holding in such streams were discussed by Weiss[64], Karlovitz[27], Wright[69], Wohl[67], Lewis and Von Elbe (Ref. 32, p. 436), Spalding (Ref. 52, p. 191), Wright's work being very noteworthy in its focus on the separation of chemical from fluid-dynamic effects. All of these studies appealed to the concept that, for purposes of evaluating the blowout behavior of fuels, it was possible to characterize the chemical kinetic features of combustible mixtures by some parameter, which did not vary as the combustor or the flow in the combustor was varied. (Which parameter to use, and how to use it to predict the blowout limits of a combustible were the questions which engendered so many different studies.)

The studies of Weiss[64], Spalding[52], and Putnam[47] showed that the normal burning velocity of the combustible mixture was a suitable measure of the combustible's chemical-kinetic character, significant in determining its resistance to blowout. Weiss' measurements showed - among other things - that, in situations where the flow patterns in a combustor were the same, mixtures of higher burning velocity would have higher blowout velocities as well. Spalding[52] and Putnam[47] were able to correlate a significant amount of data on the blowoff and blowout of different combustible mixtures in various combustors in terms of the

velocities of flow in the combustors, the geometry of the combustors, and the normal burning velocities of the combustible mixtures.

The role of the normal burning velocity in flame holding was brought out more directly in studies of the stability of laminar flames, in low-speed flows. In these studies, one necessary (though not sufficient) condition for flame stabilization was that, at some point in the flow field, the flow velocity should equal the burning velocity. This match could be produced, in slow moving fluids, under several conditions: upstream of a bluff body[36], in a boundary layer[57], in the diverging flow of gas from a flat flame burner[46], above a bunsen burner tube (Ref. 32, p. 220), or in the wake of a wire (Ref. 32, p. 238). In all the varied conditions of stabilization cited, the criterion that the local flow velocity had to equal the burning velocity was always met, either by affecting the flow velocities and patterns alone (as in Refs. 36 and 46) or by affecting the burning velocity simultaneously with the flow velocities (Ref. 57).

Despite differences of details of behavior, all flame holders decelerate some portion of the products of combustion, and lead to some sort of balance between the tendancy of the flame to propagate into the unburnt gas and the opposing motion of the unburnt gas. The action of the holder was summarized by Gammon's three concise criteria[16] for flame

holding:

a) That an element of charge from the main stream of combustible be in contact for a sufficient time with stagnated or recirculated burned or burning gas

b) That this stagnated or recirculated gas must be at a high temperature for ignition to occur in the time of contact available

c) The velocity gradient from the point of source of ignition out into the main stream must be low enough for the flame to spread into the stream.

In a similar attempt to extract a phenomonological model of the complex phenomenan of flame holding from the very complex detailed pictures which research had built up, Putnam[47] simply proposed that <u>any</u> sort of force which opposed the motion of the flow in a combustor would stabilize a flame, and (as pointed out earlier in this chapter) also adopted the view that mixtures of higher burning velocities were more resistant to blowout than mixtures of lower burning velocity. On the basis of this elementary viewpoint, Putnam argued that an experimental correlation of the ratio of blowoff velocity to burning velocity with the force applied to the flow would show no differance between different flame-holders, so long as the force applied to the gas flow was the same.

Putnam showed that published data on cylindrical rod flame holders and on opposed-jet flame holders did, indeed, display this similarity of behavior.

Electromagnetic Effects on the One-Dimensional Flame

Combustion in a one-dimensional flow of gas provides a simplified model for the theoretical analysis of flame structure and burning velocity. The conclusions of such an analysis may be applied to the behavior of bunsen or or of flat flames, so long as the flame is not so sharply curved that the thickness of the flame is comparable to the flame's radius of curvature.

The simplest possible study of the one-dimensional flame ignores the flame's structure, and treats the flame as a discontinuity in a one-dimensional flow, at which heat is released. In this approach, the conservation laws of fluid mechanics may be applied to derive the relations which hold, across the discontinuity, between the thermodynamic and gas flow properties (Ref. 50, p. 206). Such an analysis cannot predict the burning velocity of the mixture, which is governed by the detailed diffusion and chemical-kinetic processes within the flame structure.

Analyses which study the structure of a flame study solutions to a set of differential equations describing the interdiffusion and combustion of chemical species, and the conduction of heat from hot to cold

regions of the flame. The solution to these equations, with appropriate boundary conditions, involve the determination of the burning velocity concomitantly with the determination of the flame structure - the burning velocity is an "eigenvalue" of the equations (Ref. 65, p.102).

Electromagnetic effects are incorporated into these one-dimensional analyses by adding a Joulean heating term to the energy equation, and a Lorentz force term to the momentum equation. When the current flow, magnetic field, and flow velocity are assumed to be mutually perpendicular, the flame structure equations retain their one dimensional form, all changes taking place only in the direction of flow - the Y direction.

The previous studies of electromagnetic effects on combustion waves, which were the origional motivation for undertaking the present work, have been built on such one dimensional-analyses[3,8,9,12,20,22,23,45, 58]. With the exception of Beck's work[3], the analyses have treated the flame as a discontinuity, and concentrated on possible classes of discontinuity relations across the flame. (Beck's work - a study of electromagnetic effects on a flame of unity Lewis number - used an integral technique to determine the variation of burning velocity with applied magnetic fields.)

These previous analyses, while differing in many details of mathematical technique and physical models,

nontheless had the following two features in common:

1) The assumption that the flow velocity, electric current flow, and magnetic field were mutually perpendicular;

2) The assumption that the gas flow and magnetic field were coupled.

The first of these conditions is quite simple to obtain in the laboratory. The second (discussed in Chapter 4) demands that the gas be much more highly conducting than any combustion gas could be, or it demands that the length of the zone of interaction be so great as to be beyond the scale of any laboratory apparatus. Consequently, these earlier analyses are inapplicable to the situation studied in the present thesis, because they require gases with electrical conductivities much higher than were available for the present experiments, or because they require longer zones of interaction between the gas flow and the magnetic field than could be achieved in the laboratory.

A more subtle point is raised by inquiring after the mechanism in which these earlier analyses allowed electro-magnetic fields to alter burning velocities. As shown in Chapter 4, the mechanism - Joulean preheating of the flame gases - is conceivable in the experiments of this thesis, even though the coupling of the gas flow velocity and the magnetic field hypothesized in the

earlier analyses would not be present.

However, these previous analyses do not exhaust the possible effects of electromagnetic fields on the structure and propagation of flames, as they only include the Joulean heating and Lorentz forces acting on the flame gases as a whole, considering the flame gases to consist of a single molecular species. If, in contrast to this viewpoint, account is taken of the fact that the charged species actually acted on by the electric and magnetic fields comprise a very small portion of the gas, it is conceivable that electromagnetic fields could alter the structure of a flame by altering the diffusion of the charged species in the flame. Indeed, it is even conceivable that the mechanisms of the chemical reactions in the flame could be altered by magnetic fields. These possibilities will also be discussed in Chapter 4, and found to be unlikely.

The model of an ideally one-dimensional flame is, itself, impossible to achieve in practice. The flame studied in this thesis exhibited, to some extent, two or three dimensional behavior, which could not be ignored. Consequently, some of the known features of such laboratory flames will be reviewed, as well as relevant work on electromagnetic effects on such flames.

Electromagnetic Effects on Laboratory Flames

Experimentally, bunsen or flat flames provide very

simple premixed flames for the study of flame holding, flame structure, and flame aerodynamics[34]. In such flames, turbulence, excessive curvature of the flame surface, and flame stretch are either minimal or completely absent, so that the aerodynamics, stability characteristics, and burning velocity of these flames may be studied under conditions which are simpler than those encountered in industrial burners.

The propagation of the flame into the unburnt mixture proceeds by the same processes of preheating unburnt gas by conduction, followed by ignition and burning of the combustible mixture, which govern the propagation of the ideal, one-dimensional flame. The suitability of the bunsen flame for studies of burning velocity was investigated by Singer[51], Linnet[33], and Lafitte[34]. Singer's and Lafitte's conclusion was that the burning velocity of a combustible mixture could be accurately measured in such a flame as the velocity normal to the upstream edge of the flame.

In such measurements of burning velocity, the fact that the luminous zone of the flame does <u>not</u> coincide with the surface at which the initial heating of the flame gases occurs[31] gives a great difficulty in determining the upstream edge of the flame. However, Friedman's magnificant thermocouple measurements of the temperature structure of a flame[31] show that the <u>downstream</u> edge of the flame's luminous zone coincides with the surface at

at which the temperature gradients in the flame go to zero, so that the downstream edge of the flame is clearly marked by the downstream edge of the luminous zone. This fact will be of great significance in evaluating the data presented in Chapter 3, where it will be desired to interpret the velocity normal to downstream edge of the luminous zone of the flame as a measure of the burning velocity. The fact that the divergance of the lines of flow in passing through the flame surface is small (Refs. 21, 22, 40, 48) implies that the velocity normal to the upstream edge of the flame - U_u - may be inferred from the velocity normal to the downstream edge of the flame - U_b - if the ratio of the burnt to the unburnt gas' density - ρ_b/ρ_u - is known. The formula giving the desired relation for the burning velocity is

$$U_u = \frac{\rho_b}{\rho_u} U_b$$

The fact that the flow patterns of laboratory flames are not one-dimensional implies that aerodynamics plays a part in their behavior. The works of Ball[1], Gross[19], and Uberoi[60,61] are the most thouroughing and successful (in terms of being in accord with experimentation) studies of this subject. These analyses also assumed that the burning velocity of the flame was unaltered by the flow patterns of the surrounding gas or the flame surface. Thus, again the separation of the factors governing the flow patterns of the flame gases - the flow velocities and

pressures at the boundaries of the flame gas flow - are separated from the factors governing the burning velocity - the diffusion and chemical-kinetic features of the flame structure. Chapter 5 will take this viewpoint, in assuming that the flow leaving the downstream edge of the flame is a constant.

The experiments of Dimmock[10], in which Lorentz forces were applied to the products of combustion of a seeded nitric oxide-hydrogen flame, showed that, with currents of 175 ma. and magnetic fields of .1 Tesla, Lorentz forces could be applied to the flame gas flow which were large enough to deflect the flow of the jet of burnt gases. It is from this point that the theme of the present thesis can logically take its beginning.

Electromagnetic Effects on Flame Holding

The fact that Lorentz forces can alter the flow of products of combustion raises the possibility that these Lorentz forces can be used to oppose the flow of the products of combustion. If used this way, the Lorentz forces act in exactly the same way as the opposed-jet flameholders described by Cambel[6], in which a very tiny jet of fluid injected into the main stream of flow in a combustor, in a direction opposite the direction of the main stream, stabilized a flame. While a distribution of Lorentz forces is not the separate, opposed jet of fluid described by Cambel[6], nontheless it does apply a force

to the flame gases which is opposed to the main flow of gas. Consequently, Putnam's argument that a flame can be stabilized by any force which opposes the flow of gas could apply to the problem studied in the present thesis. While this is a reasonable concept, and should apply to the situation studied in this thesis, the stabilization of a flame by Lorentz forces must be demonstrated and studied experimentally before it can be taken to be a valid concept.

Heinshom's[21] and Putnam's[48] observations showed that electrostatic forces could affect the stability of a flame. What has never been established heretofore is whether or not Lorentz forces also may affect the stability of a flame, and, if they do, just what the Lorentz forces do to so affect the flame stability.

This, then, is the theme of the present thesis: To observe the stabilization of a flame by the action of Lorentz forces, to observe the manner in which the Lorentz forces and the current patterns giving rise to them affect the flame, and to determine, from these observations, if the burning velocity is altered, or if the effect of the Lorentz forces is solely to change the flow of the burnt gases, by this affecting the flame's stability.

Organization of the Thesis

The thesis will start from a demonstration of the fact that Lorentz forces can alter the stability of a flame, and proceed to an examination of the manner in

which the Lorentz forces affect the flow of the flame gases. These alterations of flow patterns will be used to determine whether or not the Lorentz forces alter the burning velocity of the flame, and how the Lorentz forces affect the flow of the product gases. The various means by which electromagnetic fields might affect the burning velocity of a flame will then be examined, and the distribution of Lorentz forces and electric current through the flame gases will be determined.

Chapter 2 will give a brief description of the combustor and flame employed for the work in this thesis, and present measurements of the alteration of the stability of the flame by the action of Lorentz forces.

Chapter 3 will present the measurements of gas flow velocities and patterns. On the basis of these measurements, it is concluded that the burning velocity is not changed, but that the flow patterns and velocities of the flame gases are changed. The observed changes in velocity will be found to be consistant with the viewpoint that these changes are caused by accelerations or decelarations of the flame gases by Lorentz forces.

Chapter 4 will consider the various means by which the diffusion of species and heat, and the kinetics of the chemical reaction in a flame may be altered by electromagnetic fields of the sort encountered in the present work. In addition to this, a one-dimensional analysis, based on the analysis of Toong[58], will also be

presented, and the conditions necessary to achieve a coupling between gas flow velocity and magnetic field intensity will be explored. These conditions will be found not to be met in the apparatus of this thesis.

Chapter 5 will analyze the flow of current between two cylindrical electrodes in a gas of constant conductivity and Hall parameter, in which the flow of current is assumed to be two dimensional. The electric field patterns calculated from this will be found to be close to the electric field patterns actually observed in the apparatus used for this thesis. The Lorentz forces arising from a magnetic field acting on these current patterns will then be calculated, so that the changes in velocity patterns due to these Lorentz acting alone can then be calculated. When this is done, the calculated flow patterns will be found to exhibit many of the features observed in the particle track pictures.

In Chapter 6, the conclusions of the thesis are summarized, and some of the questions raised in the course of the research for the present thesis are posed as subjects for further work.

CHAPTER II

EXPERIMENTAL OBSERVATIONS OF LORENTZ-FORCE EFFECTS ON FLAME HOLDING

INTRODUCTION

Purpose of this Chapter

This chapter presents the results of measurements of the effects which Lorentz forces have on the stability characteristics of a premixed laminar flame. The flame studied was a lean flame of propane and air, burning at a pressure of 85.5 mm. Hg absolute. The current through the gas, parallel to the flame surface and perpendicular to both the magnetic field and the gas flow direction, was 5 milliamperes.

The configuration of flame, burner, electrodes, and magnetic field considered throughout the remainder of this thesis is shown in Figure 1, and a complete description of the apparatus is in Appendix 1. As Figure 1 shows, gas flows vertically, and the flame takes the shape of a horizontal disc. A pair of coplanar wires, lying parallel to each other and to the flame surface, and perpendicular to the gas flow direction, serves as the electrodes. A magnetic field is applied perpendicular to the current flow and the gas flow directions.

Types of Observations

The quantitative measure of flame stability used in

these experiments was the fuel/air ratio at which, for a apecified air flow rate and electrode current, the flame blew off. It was found that, if care was taken to maintain the propane and air feed pressures constant to within .5% and the flame gas pressure constant to within .5 mm. Hg, then blowoff data was reproducable to within the limits of resolution of the flowmeters - approximately ±1.5% of the fuel/air ratio.

It should be noted that these measurements were obtained by varying the propane flow rate at a constant air flow rate, instead of by maintaining a constant total mass flow rate and varying the fuel/air ratio. However, since the variation in fuel flow rate was less than 2% of the total mass flow rate, the experiments presented in this chapter should not differ significantly from constant total mass flow rate experiments.

The effect of the Lorentz force on the flame stability was determined by measuring the flame stability with three different magnetic field intensities - .12, .24, and .46 Tesla - and with Lorentz forces both with the flow direction and against the flow direction.

A qualitative observation was also made of the effect of Lorentz forces on the stability of the flame when the fuel/air ratio was kept constant, and the mass flow rate increased, for a single value of magnetic field intensity.

Description of Results

The measurements presented in this chapter demonstrate that:

1) The lean blowoff limit of the flame described above is altered by the Lorentz forces, with the Lorentz forces capable of both stabilizing and destabilizing the flame.

2) Lorentz forces directed against the flow direction stabilize the flame; Lorentz forces with the flow direction reduce flame stability.

3) At a constant electrode current, these effects increase with increasing magnetic field intensity.

DESCRIPTION OF EXPERIMENTS

Apparatus

The layout of the experiment is shown in Figure 1, and was described above. The fuel and air, after being measured by rotameter flowmeters, were mixed and passed through the tubular matrix of the flat-flame burner, and burnt immediately above the burner. (The exact location and shape of the flame depended on the mixture flow rate, the fuel/air ratio, the electric current, and the magnetic field intensity.)

The electric current passed between the electrodes took the form of a normal glow discharge (Ref. 7, chapter 8). Since the diameter of the electrodes was very small

(.005 inch), and since the electrodes were very straight and parallel, current flowed to the electrodes along their entire length, as indicated by the luminosity of the electrodes. Consequently, the density of current normal to the electrodes at their surface was evenly and uniformly distributed along their entire length. (The exact character of the electric current pattern in the gas will be discussed in more detail in chapter 5)

Behavior of Flame near Blowout

As the fuel flow rate was decreased, with a five milliampere electrode current flowing and with no applied magnetic field, the flame would change from its initially flat shape to a more curved shape (see Figure 2). Simultaneously, the voltage between the electrodes would rise. As the blowoff condition was approached, the flame would begin to flicker, and finally blew off. When blowoff occurred, there was a sudden rise of voltage across the electrodes, and a change in the color of the electric discharge.

Behavior with Lorentz forces pointing with the direction of flow was similar, with the sole difference being that the blowoff took place at a higher fuel/air ratio, and that the scale of voltages was much higher, due to the Hall effect. If the Lorentz forces were against the flow direction, the voltage across the electrodes was much higher than the voltage was without a magnetic

field, due to the Hall effect.

The rise of voltage with reduced fuel/air ratio was probably due to the increased density of the products of combustion with the decreased temperature of the leaner flame, which reduced electron mobility. This reduced electron mobility would subsequently affect the other properties of the electric discharge - reducing the average electron energy and rate of generation of electrons in the same way as a rise in gas pressure at constant temperature would[30].

The disappearance of the flame was clearly marked by:

1) The disappearance of the blue reaction zone of the flame

2) The disappearance of the luminous region of the discharge passing through the products of combustion

3) A change in the color and intensity of the glow on the cathode.

4) A rise of several hundred volts in the voltage between the electrodes.

EXPERIMENTAL PROCEDURE

Establishment of Operating Conditions

In order to actually determine the blowoff limits, the operating conditions of flame gas pressure equal to 85.5 mm. Hg, with a five milliampere current passing through the flame, were employed. These particular

conditions were chosen when it was found that, at these conditions, the flame was quite free from any oscillations or drift of position with time. Further, at these conditions the electrodes had a reasonably long operating life so long as the electrode current was not raised above 7 ma. (Since the lifetime of the electrodes was the thing which imposed the greatest limitation on the extent and frequency of experiments, this latter was an important factor.)

In order to bring the flame to these conditions in the apparatus, without excessive wear of the electrodes, the following procedure was employed. The flame was ignited at approximately 180 mm. Hg pressure, in a rich mixture of combustible. The flow rate of air was then set to the desired flow rate for the experiment, with the propane flow rate in approximately stochiometric proportion. The pressure in the test section was then reduced to 90 mm. Hg, and an electric current flow of 1-2 milliamperes started through the gas. Then the pressure in the test section was reduced to 85.5 mm. Hg, the current between the electrodes was raised to 5 ma., and the search for the blowoff limit begun.

For a given air flow rate, the blowoff limit was first determined for the case of a five milliampere electrode current, and no magnetic field. Then, for each combination of magnetic field intensity and air flow rate, blowoff limits were observed in the following order:

1) I = 5 milliamperes, B = 0

2) I = 5 milliamperes, B ≠ 0, Lorentz force against flow direction

3) I = 5 milliamperes, B = 0

4) I = 5 milliamperes, B ≠ 0, Lorentz force with flow direction

Steps 1) and 3) served as a control, rather than to yield data. In this way, it was possible to verify that the observed blowoff data were, indeed, comparable.

In order to determine the blowoff limit for the case of a five milliampere electrode current and no applied magnetic field, the propane flow rate was reduced in steps until the flame blew off. At each step, the propane flow rate and electrode voltage were recorded. After blowoff, the flame was re-ignited and brought to operating conditions by the procedure previously described, and the propane flow rate was reduced to the previously-determined minimum which did not give blowoff. The propane flow rate was then reduced by steps much finer than those used before, until the flame blew off again. This procedure of determining the propane flow rates bracketing the blowoff limit, and then searching through this range for a new upper and lower limit was continued until a value was found which was reproducable to the limit of resolution of the rotameter scale - 1.5% of the rotameter reading.

In order to determine the blowoff limit with Lorentz

forces opposite to the flow direction, the procedure for determining a blowoff limit was, once that operating conditions were reached, the propane flow rate was reduced to a value slightly above the blowoff value for the I = 5 milliampere, B = 0 case, after which the magnet was switched on and the search for the blowoff limits begun.

In order to determine the blowoff limit with the Lorentz forces accelerating the flow, the operating conditions were established, and the propane flow rate reduced to a value somewhat above the flow rate at which the flame blew off with a 5 milliampere electrode current, but no magnetic field. The magnet was then switched on, and the search for the blowoff limit begun.

RESULTS

Description

The observed blowoff limits are plotted in Figure 3, giving the molal fuel/air ratio at blowoff as a function of the applied magnetic field, for two different air flow rates passing through the test section. An air flow rate of 15.2×10^{-6} kg./sec. corresponds to an air flow velocity, leaving the burner head at 70°F and a pressure of 86 mm. Hg absolute, of .75-.90 ft./sec., while an air flow rate of 22.7×10^{-6} kg./sec. corresponds to an air flow velocity, under the same conditions, of 1.14-1.36 ft./sec. (The uncertainty arises from the fact that the cross-sectional

area of the tube containing the burner matrix is partially obstructed by the tubes of the matrix. It seems likely, from the dimensions of the tubes comprising the matrix, that this obstruction does not exceed 20%.)

Figure 3 shows that the flame is stabilized by a Lorentz force which runs against the gas flow, and is made less stable by a magnetic field which accelerates the flow. (Just why the lower flow rate should be less stable than the higher flow rate flame will be discussed shortly.)

Alternate Observation

Blowoff and flame holding can be demonstrated either in a stream of constant reactant velocity and variable composition, when the burning velocity is reduced to too low a value, or in a stream of variable gas velocity and constant composition, when the gas velocity is raised to too high a value.

The choice to employ the former in the experiments described in the present chapter was made on the basis of experimental limitations. The latter involved flow rates which were found to be too large to be handled at the low pressures employed in the experiments of this thesis. (Very lean mixtures would have required lower total flow rates, but it was found almost impossible to keep these from being inadvertantly extinguished when the mass flow rate was changed.)

Nontheless, it was possible to demonstrate stabili-

zation in the second manner, as well. If the volumetric fuel/air ratio was fixed at .0309, a five milliampere current passed through the gas between the electrodes, and the mixture flow rate increased, the flame would rise higher and higher off of the burner, until a mass flow rate of 43.2×10^{-6} kg./sec. was reached, at which point the flame was blown off. Immediately before blowoff, the flame was about three inches above the burner, and oscillating with an amplitude of approximately one-quarter inch at about 2 cps.

Application of a magnetic field of .12 Tesla, oriented so that the Lorentz forces were against the direction of flow, to the flame when it was on the verge of blowing off caused the flame to immediately assume a very stable position between the electrodes; increasing the mixture flow rate (still retaining the fuel/air ratio of .0309) to a total mass flow rate of 60×10^{-6} kg./sec. did not lead to blowoff. However, if the magnetic field was switched off at this point, the flame would blow off immediately. Conversely, Figure 3 shows that, if the direction of the Lorentz force were <u>with</u> the direction of flow, a magnetic field of approximately .19 Tesla applied to the flame with a fuel/air ratio of .0309 and total air flow rate of 22.7×10^{-6} would cause blowoff, as would the application of a field of approximately .04 Tesla to a flame with the same fuel/air ratio, and a total air flow rate of 15.2×10^{-6} kg./sec..

These observations on the stability of a flame at a fuel/air ratio of .0309, and the alteration of this stability by Lorentz forces, are very relevant to the work to be presented in later chapters of this thesis. As the studies described in later chapters of this thesis were performed on flames at this fuel/air ratio, without blowing the flame off, it is necessary to be sure that the effects of Lorentz forces observed in these later chapters are of the same sort as can alter the flame's stability.

Discussion of Results

In order to determine how the Lorentz forces affect the stability of the flame, it is necessary to inquire into the manner in which the Lorentz forces act on the flame; posed as a direct question, this inquiry becomes: Do the Lorentz forces alter the gas flow patterns, the burning velocity, or both?

That the Lorentz forces can alter the gas flow patterns can be shown by comparing the total Lorentz forces applied to the gas to the total momentum flux of the gas. The total momentum flux of a column of gas of uniform velocity, of density ρ, with a cross-sectional area A and a total mass flow rate $\dot{m}$ is

$$F = (\dot{m}^2)/(\rho A)$$

The order of magnitude of the momentum flux leaving the burner may be obtained by taking the momentum flux of the reactants entering the burner head. With $\rho = 1.34 \times 10^{-4}$

grams/cc. (corresponding to a gas temperature of 70°F and a pressure of 86 mm. Hg abs) and $A = 4.9$ cm.^{2}, the relationship between mass flow rate and momentum flux becomes

$$F = 1.52 \times 10^{4} \times \dot{m}^2 \text{ newtons}$$

For comparison with the Lorentz forces applied to the flame gases, the total momentum fluxes corresponding to the two cases

$$\dot{m} = 15.2 \times 10^{-6} \text{ kg./sec.}$$
$$\dot{m} = 22.7 \times 10^{-6} \text{ kg./sec.}$$

are, respectively,

$$F = 3.5 \times 10^{-6} \text{ newton}$$
$$F = 7.8 \times 10^{-6} \text{ newton}$$

In order to estimate the Lorentz force applied to the flow of flame gases - f - applied by a magnetic field of strength B to a length of conductor - ℓ - carrying a current - I - applied to the situation of this thesis, represented in figure 1, the relation between the magnetic field intensity (in Tesla) and the force applied to the current-carrying gas between the electrodes is given as

$$f = (\ell I)B = B \times 9.0 \times 10^{-5} \text{ newton}$$

when ℓ was taken as .018 meter and $I = 5$ milliamperes. For a magnetic field of .14 Tesla, this formula gives a Lorentz force of 13×10^{-6} newtons. The fact that the total Lorentz

force applied to the gas is comparable to the total momentum flux of the gas flow implies that the Lorentz forces are capable of altering the gas flow velocities and patterns.

It is more difficult to appraise the possible effects of Lorentz forces on the burning velocity, but the evidence presented in Chapter 3, along with the calculations and physical reasoning of Chapter 4, shows that any possible effects are very slight.

Additional Effects

It should be noted that emphasis has been placed on the difference in flame stability observed when different Lorentz forces are applied to the flame gases, and not on the absolute level of such stability. This was necessary because of the probable presence of a large number of effects influencing the gas flow and burning velocity in addition to the Lorentz forces.

The magnitude of such things as buoyancy, heat loss to the burner, viscosity, boundary layer stability, etc. can (and will) be estimated, and are indeed found to be significant in the experiments presented here. However, before undertaking such an evaluation, it should be remembered that the thing of interest in the present thesis is the change of flame stability with Lorentz forces. Concequently, the significance of the effects mentioned above does not lie in their absolute magnitude, but in the size of their changes when Lorentz forces are applied, and

in the effect of these changes on flame holding. These effects will be discussed in the following chapters when they are relevant to the particular aspect of the flame's behavior under study. In each case, it will be shown that, while these effects are potential sources of significant effects on the flame, they are not the primary causes of the changes in flame holding observed when Lorentz forces are applied.

The effects of heat loss to the burner are relevant to the material presented in this chapter, and will be discussed now. Calculations of the flame structure by the methods of Appendix 7 show that the temperature gradient 3 mm. upstream of the luminous zone is of the order of 7×10^5 °C/meter. The thermal conductivity of the flame gases leaving the burner is of the order of .027 (Joules)/(°C-meter-sec), so that the heat flux across an area of 4.9 $cm.^2$ would be of the order of 9.2 Watts, which is significant by comparison with the chemical heat release rate of the flame - 45 Watts. Changes in flame position with the application of Lorentz forces would change the heat loss to the burner, and would thereby change the burnt gas temperature in the manner described in Ref. 35. This change in burnt gas temperature by heating or cooling the unburnt gas would, in turn, lead to a change in burning velocity[4,59].

Reference 35 reports that, when the Lorentz forces were directed against the direction of flow, the flame was

pushed closer to the burner, and the burnt gas temperature was reduced. This being the case, the burning velocity would be expected to be reduced, so that, if the effect of heat loss to the burner had any effect on the flame stability when Lorentz forces were against the flow direction, it would be to decrease the stability of the flame. Similarly, the effect of Lorentz forces with the flow direction would be to increase the flame stability. Since the behavior actually observed was exactly opposite to this, it is apparent that the observed changes in flame stability can not be caused by changes in the heat loss to the burner, although the particular value of the observed blowoff limit might be affected by the level of heat loss.

Whether or not the changes in heat loss to the burner actually do reach such important levels when Lorentz forces are applied to the flame gases is best determined by experiment, and it is to such experiments that we will now turn our attention. The chief cause of changes of heat loss to the burner comes by changes in flame position. The changes in flame position, at a constant fuel/air ratio, arise from two completely different causes: either a change in the total mass flow rate of combustible, or the application of Lorentz forces to the flame gases.

The changes in heat loss to the burner due to changes in mass flow rate are evident in Figure 3. As this figure shows, the flames at lower mass flow rates are less stable

than flames at higher flow rates, despite the fact that the velocities of gas flow in the former case must be lower than those of the latter case. In all probability, this arises from the fact that, at lower flow rates, the equilibrium position of the flame is closer to the burner, so that the proportion of the flame heat lost to the burner is greater. This being the case, the burnt gas temperature would be lower, for a given fuel/air ratio, at a lower mass flow rate than at a higher one. Consequently, the burning velocity would be changed in the same way as the burnt gas temperature, and the flame would be less stable at the lower mass flow rates. Even if the flame did not change position, a fixed heat loss rate to the burner would mean that, as the mass flow rate and chemical heat release were decreased, the fraction of the flame's heat which was lost to the burner would be greater, so that the temperature of the flame and the burning velocity would still be decreased.

This hypothesis was verified by direct measurement of the burnt gas temperature at the two flow rates, at a fuel/air ratio equal to .0309. Temperature was measured approximately 1 cm. downstream from the flame with a thermocouple of .0005 inch diameter wires, for which the radiation correction, at the measured temperatures, was approximately 20°C. The measured temperature of the burnt gas was 1091°C at the lower air flow rate, and 1238°C at the higher flow rate, for the same fuel/air ratio. This

11% change in the temperature of the burnt gas could quite significantly alter the burning velocity.

Changes in heat loss to the burner due to Lorentz forces were the probable causes of the changes in burnt gas temperature reported by Lucheta[35], using currents of 150 ma. and a magnetic field of .12 Tesla, in an apparatus with the same configuration of burner and flame as used in the present thesis, but different electrodes. In the early phases of the present research this work was continued, using a .24 Tesla magnetic field and electrode currents of 30 ma., where the electrodes were needles, pointed toward each other and placed 25 mm. apart on opposite sides of the burner. With a 30 ma. electrode current, temperature changes with changes of Lorentz force of up to 110°C were recorded by a Chromel-Alumel thermocouple placed in the exhaust line. However, this effect decreased both with decreasing magnetic field intensity and with decreasing electrode current, so that with a .12 Tesla magnetic field and a 14 ma. electrode current the change observed was 35°C. 35°C is only 3% of the observed absolute temperature of 1091°C, and it is unlikely that, at .12 Tesla and 5 milliamperes electrode current, the temperature change in the flame gases would be this large.

The changes in temperature cited in the previous paragraph were made in an apparatus of different electrode configuration, and at lower gas pressures than were used in the measurements of flame stabilization. An attempt to

measure changes in burnt gas temperature with the application of Lorentz forces with the .0005" diameter Pt-Rh thermocouple, in the apparatus used in the experiments which measured flame stabilization, was only partly successful. The data on the changes in temperature of the burnt products was scattered between measured rises of 0°-25° for five measurements, when Lorentz forces were with the direction, and measured drops of 5-18°C for six measurements, when Lorentz forces were against the direction of flow. While the very bad scatter precludes assigning a specific value to the change in temperature with the application of Lorentz forces, it is unlikely that the temperature change is above 35°C for either case of Lorentz forces with or against the flow, so that the expected change of less than 3% in temperature due to the application of Lorentz forces seems likely, and will be the value used throughout the rest of this thesis.

The effect of heat loss of the products to the surroundings is much more difficult to evaluate. However, it is questionable that this would appear in measurements taken within 1 cm. of the flame, and that such a heat loss in the burnt gas would affect the structure or burning velocity of the flame.

Interpretation of Results

The considerations in Chapter 1 on flame stabilization and blowoff bring out that the observed variations in flame

stability with applied magnetic field and electric current could arise either from changes in the flame's flow field, or could be due to changes in burning velocity. The objective of the remainder of this thesis is to demonstrate that Lorentz forces stabilize the flame by obstructing the flow of gas downstream from the flame, but not by altering the burning velocity. The details of the interaction will also be determined.

Attention will be focused on determining the effects of Lorentz forces on a premixed propane-air flame, with a fuel/air ratio of 0.0309, at a pressure of 86 mm. Hg, in an air flow of 15.2×10^{-6} kg./sec., and a total mass flow rate of 15.83×10^{-6} kg./sec.. The measured gas temperature of 1091°C or 2560°R will be the value of temperature assumed. Under these assumed conditions, the properties of the products may be summarized as:

gas pressure — 85.5 ± 1.0 mm. Hg
burnt gas temperature — 2560°R
mass flow rate — 15.83×10^{-6} kg./sec.
fuel/air ratio (molal or volumetric) — .0309
viscosity of burnt products — 5.0×10^{-4} poise
density of burnt products — 2.86×10^{-5} gm./cc.

The electrode current used will be 5 milliamperes, and the magnetic field used will be either .12 or .14 Webers/meter^2 (Tesla). Since the reactants - propane and oxygen - are typical of hydrocarbon oxidations, and since hydrocarbon

oxidations have similar reaction mechanisms[40], burning velocities, heat release, and structure[14], it is likely that the effect of Lorentz forces on the structure and propagation of all hydrocarbon oxidation flames should be similar to the behavior reported in this thesis.

In Chapter 3, direct observations of the flow field will be presented which yield information both on the burning velocity of the gas and on the flow field of the burnt gas. These data demonstrate that the burning velocity is not changed when the magnetic field is applied, but that the flow downstream of the flame is very much affected when the magnetic field is applied.

In order to demonstrate that the observed behavior is consistant with analytical models of flame structure, Chapter 4 discusses the effects of a magnetic field and of Lorentz forces on flame structure and propagation rate. Chapter 5 shows that the observed behavior is explicable in terms of the mechanical effects of the Lorentz forces on the flow of flame gases.

CHAPTER III

OBSERVATIONS OF THE FLOW FIELD

INTRODUCTION

Purpose of this Chapter

This chapter presents data obtained from measurements of the flame gas flow velocities and directions, showing the effects of Lorentz forces on the flame gas flow and burning velocity. The effects of buoyancy, viscous boundary layers, and turbulence are discussed, and these are shown to modify, but not to dominate, the changes of flame gas flow with Lorentz forces.

Methods of this Chapter

In a laminar, premixed flame, the burning velocity is a function only of the chemical-kinetic and transport properties of the flame gases, and the final temperature of the burnt gases. Consequently, if these transport or kinetic properties were altered by the magnetic field or the Lorentz forces, the effects would probably become apparent in a change in burning velocity. This change in burning velocity could be the cause of the flame stabilizations and destabilizations reported in Chapter 2.

Alternatively, the flame stabilization or destabilization might arise from a deceleration or acceleration of the flame gases. In this case, it is of interest to understand

where and how the Lorentz forces act on the flame gases.

In any event, the gas flow velocity is a parameter of prime interest, measurements of which yield the information on just what does go on when Lorentz forces are applied to a flame. In the flows studied in this thesis, where dynamic pressures of the order of 10^{-6} of the static pressure are typical, in a flow of hot, corrosive gas, the particle track technique[15,28] is the most suitable technique for measuring gas flow velocities. Such measurements are presented in this chapter. Their subsequent interpretation shows that burning velocity is not altered whan a magnetic field is applied to a flame through which an electric current is passing, and other measurements, made in the burnt gas, reveal features of the flow field which show that these are being decelerated or accelerated by the action of Lorentz forces.

Conclusions of this Chapter

The measurements presented in this chapter demonstrate that:

1) The burning velocity is not significantly altered in the presence of Lorentz forces in the flame gases.

2) The flame gas flow patterns are severely altered by the Lorentz forces decelerating the flow of burnt gas, much in the same way as more familiar flame holders do.

3) When the Lorentz forces accelerate the flow, certain regions of the flow field contain accelerations which are perpendicular to the total Lorentz force applied to the flow.

4) There is an asymmetry of accelerations in the flow when Lorentz forces are with the flow, with fluid particles on the cathode side of the center line of the flow field being accelerated differently from those on the anode side. There is evidence of an asymmetry of the decelerations caused by Lorentz forces against the flow, as well, but it is not as conclusive.

MEASURING TECHNIQUE

The Particle-Track Technique

In the particle-track technique, flow velocities and directions are determined by observing, at successive times of known interval, the positions of a dust particle being carried along in the flow.

The implementation of the method is shown, schematically, in Figure 4. As can be seen, the gas flow contains suspended particles. The region of interest is illuminated at fixed time intervals by a stroboscope; the particles scatter the light, so that they appear as brilliant spots. If a camera is focused on the region of interest, a particle will be imaged as a brilliant dot on the film,

and the successive positions of the particle will appear as a train of dots on the film. Then, knowledge of the scale factor between the image size on the film and the size of the object being imaged, along with knowledge of the flashing frequency, allows the velocities of the flow to be measured from the pictures. (Appendix 4 contains an analysis of the error inherent to this technique.)

Extent of these Measurements

The region of flow actually observed is represented in Figure 5, being a 2 to 3 mm. thick strip in the central plane of the gas flow, lying between the electrodes and extending from the burner head to a point approximately 12 mm. downstream from the flame. The thin strip in a plane of symmetry was chosen in order to have a region whose flow would be as nearly planar (though not two-dimensional) as possible.

That this was achieved is suggested by the fact that several very long particle tracks were observed, which completely traversed the 20 mm. length of the illuminated region without passing out of the 2 to 3 mm. deep illuminated region. This indicates that the velocities perpendicular to the plane of flow possibly were less than 10% of the velocities in the plane of flow, and certainly less than 15% of the velocity in the plane of flow.

Reduction of the Data

In these experiments, the flashing frequency used was

3000/second, with variations in shutter type and speed being such that single particles appeared from 5 to 40 times in a picture. Pictures taken were approximately 2-1/2 times life size, with the exact scale being obtained by photographing a piece of millimetric graph paper in the test section (see Figure 6) with all the optical components clamped in the same position that they would hold in the subsequent data-gathering session. (The rectangular - rather than square - appearance of the grid in the picture in Figure 6 was caused by the fact that the sheet of graph paper was tilted back 45° at the top. Consequently, the vertical lines of the grid appear shortened in the photo. However, the horizontals, which were used for scaling, projected their true length.) A picture was also taken of the test section without a flame, so that the position of the electrode images could be fixed relative to the edges of the picture, and a horizontal established parallel to the burner head image. In this manner, a coordinate system which was consistent from picture to picture and from day to day could be established, with the anode image location in the photograph serving as the center of the coordinates. With such a consistent coordinate system, it was possible to construct consolidated plots of the data from the particle-track pictures, plotting either velocity profiles or the history of an individual particle. Quantitative measurements of the velocities of flow were made by measuring the horizontal and vertical distance

between particle images on the origional pictures with a micrometer-driven traveling microscope; these measurements could then be reduced to velocity data, using the time interval between flashes and the scaling between the photographic image and the object. The analysis in Appendix 4 concludes that an error of ± .2 foot/second is the error expected of the technique.

The data so obtained can then be employed for comparisons between the three cases of:

1) I = 5 milliamperes, B= 0, no Lorentz force
2) I = 5 milliamperes, B ≠ 0, Lorentz force with flow direction
3) I = 5 milliamperes, B ≠ 0, Lorentz force against flow direction

It should be noted that the application of a magnetic field when no current was flowing between the electrodes never caused any change in any observed or measured property of the flame.

In order to assure that the flame was not disturbed by the particles, a picture of the flame in each of the three cases of interest was taken, without the addition of particles, at the start of each data-gathering session, to be used as a control. Particle-track pictures, in each of the three cases of interest, were compared with the corresponding control to assure that the flame had not been disturbed; pictures in which the flame was disturbed were not used. This was found to be an essential precau-

tion, as it was only too easy to disturb the flame by adding an excess of particles.

A total of 31 pictures of usable quality were obtained, in two series, referred to hereafter as series A and series B. Series A pictures were taken in the same apparatus in which all the other data presented in this thesis was obtained, and most of the data presented in this chapter will be from this series. Series B data was of a more preliminary sort, taken in a more primitive stage of the development of the apparatus. Despite this, the series B data shows all of the important features of the series A data, and shows certain features more clearly. The chief differences in the apparatus used for the different series were that, for series B data, the upper half of the test section lacked a large extension for mounting an electric field probe (see Appendix 1); for series B, the electrodes were 1.2 cm. apart, rather than 1.8 cm. apart as was the case for series A; and series A data was taken with a .12 Tesla magnetic field, while series B data was taken with a .14 Tesla magnetic field. Also, in taking the series B data, a lens with a between-the-lens shutter was used, rather than a focal-plane shutter, so that the observed particle tracks were not as long as for series A.

Presentation of Data

Three sample pictures from series B are presented in Figures 7a, 7b, and 7c, with corresponding idealized

representations in Figures 8a, 8b, and 8c, respectively. Sample series A pictures are shown in Figures 9a, 9b, and 9c. It is immediately obvious that differences exist between the three cases of interest; in brief, these are that:

1) The influence of applied Lorentz forces which are <u>with</u> the direction of flow is to raise both the axial and the lateral velocities of the flow from the values observed when I = 5 ma. and B = 0

2) The application of a Lorentz force against the flow direction causes the flow to be decelerated to a very low velocity which is very uniform and parallel.

<u>Results - Representation</u>

The basic data produced by the particle-track technique is the time history of a particle's position — a streak line, which, in a steady state, is also a streamline. This data can be used directly to plot components of velocity as a function of the position of a single particle. A particle is identified by its coordinate when it crosses the downstream edge of the flame's luminous zone. (For a steady flow, this initial position and one other coordinate suffice to completely specify the particle's position). In this thesis, this initial position is expressed as the fraction $\frac{X_o}{a}$, where X_o is the X distance <u>from</u> the point halfway between the electrodes <u>to</u> the particle's crossing-

point on the flame surface, while $2a$ is the distance between the electrodes. (It should be noted that $\frac{X_o}{a} = -1.$ at the anode, and $\frac{X_o}{a} = +1.$ at the cathode.) Alternatively, the more familiar plots of velocity profiles may be used. In order to bring out certain features of the flow field, both representations will be used here. However, when plotting the velocity history of individual particles, only particles which actually crossed the downstream edge of the flame's luminous zone will be plotted.

EFFECTS ON BURNING VELOCITY

As pointed out in Chapter 1, the downstream edge of the luminous zone of the flame corresponds to the "downstream" point of one-dimensional analyses of flame structure, so that, when the density of the burnt gas is known, the velocity normal to the downstream edge of the flame is a measure of the burning velocity (mass flow per unit area of flame) which is equivalent to the velocity normal to the upstream side of the flame. As pointed out in Chapter 2, a change of less than 3% is expected in the temperature of the burnt products on the application of Lorentz forces.

Thus, if

$$U_b = \frac{\rho_u}{\rho_b} U_u = \frac{T_b}{T_u} U_u$$

then the change in U_b with the changes in temperature ratio across the flame would be

$$\Delta U_b = \Delta\left(\frac{T_b}{T_u}\right) U_u + \frac{T_b}{T_u} \Delta U_u$$

The first term of this expression - $\Delta\left(\frac{T_b}{T_u}\right)U_u$ - is the change in the velocity at the downstream edge of the flame due to changes in density ratio with no change in burning velocity. With a 3% variation in burnt gas temperature, this would be less than .1 ft/sec, which could not be detected by the particle-track technique. The second term - $\frac{T_b}{T_u}\Delta U_u$ - is the change in velocity at the downstream edge of the flame with a constant density ratio, and a change in burning velocity ΔU_u . The size of this term would necessarily depend on the variation of the burning velocity $-\Delta U_u-$ with the change of heat loss to the burner. What is of most interest is the fact that the less than 3% change in the temperature ratio across the flame when Lorentz forces are applied would give no measurable error in measurements of the burning velocity with measurements of the velocity normal to the downstream edge of the flame.

As the downstream edge of the flame's luminous zone is clearly visible on the origional photographs, it is quite simple to measure the velocity of a particle when it crosses the flame surface. This is shown in Figures 8a, 8b, and 8c, for the series B data, where the velocities measured at the downstream edge of the flame were:

Condition	Velocity
Lorentz force against flow direction	$4.3\pm.2$ ft/sec
Lorentz force with flow direction, $\frac{X_o}{2}=-.3$	$4.0\pm.2$ ft/sec
" " " " " $\frac{X_o}{2}=0.$	$4.1\pm.2$ ft/sec

5 milliampere current, B = 0 $4.2 \pm .2$ ft/sec

Thus, the flow velocities at the downstream edge of the flame surface did not differ by an amount greater than the error of the particle-track technique, 4.2 ft./sec. lying within the range of all the measurements.

Series A data is more conclusive on this matter, as more points were obtained for each case. The flow velocities observed at the downstream edge of the flame surface were:

Lorentz Force Against Flow Direction

Position along flame surface - $\frac{X_o}{a}$	Velocity
-.37	$4.4 \pm .2$ ft./sec.
-.37	$4.7 \pm .2$ ft./sec.
-.10	$4.5 \pm .2$ ft./sec.
-.06	$4.5 \pm .2$ ft./sec.
0.	$4.5 \pm .2$ ft./sec.

with the range of 4.5-4.6 ft./sec. lying within the variation of all the measurements

Lorentz Force With Flow Direction

Position along flame surface - $\frac{X_o}{a}$	Velocity
0.	$4.5 \pm .2$ ft./sec.
0.	$4.8 \pm .2$ ft./sec.
+.02	$4.6 \pm .2$ ft./sec.
+.275	$4.5 \pm .2$ ft./sec.

with the range of 4.6-4.7 ft./sec. lying within the

variation of all the measurements

5 Milliampere Electrode Current, No Magnetic Field

Position along flame surface - $\frac{X_o}{a}$	Velocity
.13	4.7±.2 ft./sec.
.21	4.5±.2 ft./sec.
.22	4.4±.2 ft./sec.
.38	4.4±.2 ft./sec.

with the range of 4.5-4.6 ft./sec. lying within the variation of all the measurements.

It should be noted that the velocity of 4.6 ft./sec. lies within the possible range of all the measurements, so that the slightly higher range of measured values in the case of Lorentz forces with the flow is probably not significant. Even if it were, an increase in burning velocity could hardly explain the decrease in flame stability for the case of the Lorentz force with the flow.

The difference in burning velocity between the series A and series B data is difficult to account for; it is possible that the difference arises from a difference in heat loss to the burner due to a different mean position of the flame in the two cases, or the cause for the change might lie in a difference in Joulean heat input between series B, where the electrodes were 1.2 cm. apart, and series A, where the electrodes were 1.8 cm. apart. In either case, the difference is of little importance; what

is important is the fact that, in a given case, no significant change in burning velocity occurs when a magnetic field, of either orientation, is applied.

EFFECTS ON FLOW DOWNSTREAM FROM FLAME

Results - Presentation

Figures 10-18 give various types of velocity data, plotted in different ways to bring out different features of the flow field. Figures 10-16 are taken from series A data, and figures 17 and 18 are taken from series B data. In the notation used, $\frac{X}{a}$ increases from the X/a value of the anode to the X/a value of the cathode in going from -1. to +1., while Y is the distance downstream from the downstream edge of the luminous zone, in inches.

Two things are immediately obvious: In the case of Lorentz forces pointing <u>against</u> the flow direction, in which case Chapter 2 showed that the flame was most stable, the flow far downstream of the flame moves far more slowly than it does when <u>no</u> Lorentz force is applied to the gas, much as if some sort of obstacle had been placed in the flow. Conversely, in the case when the Lorentz forces are in the direction of the flow, which was shown to be the least stable case, the flow downstream of the flame is moving more rapidly than in the absence of Lorentz forces.

A more detailed discussion of the behavior exhibited in each of the three cases follows.

Results - Five Milliampere Electrode Current, No Lorentz Force

The data for this case is presented in Figures 7c, 8c, 9b, 11, and 13-16. Of special interest is the fact that the Y component of flow velocity rises to a peak at the downstream edge of the flame surface (see Figure 11), and that both the streamlines shown downstream of the flame in Figure 11 immediately begin to exhibit identical decelerations downstream of the flame. A deceleration of flow downstream of the flame is consistant with previous observations of free-standing flames[1,19,61], and is explained by the fact that, in surroundings of constant static pressure, momentum conservation demands that the volume expansion of the flame gases due to the heating of the flame gases by the flame be accomodated by a rise in the cross-sectional area of the column of flame gases far downstream, rather than by an acceleration of the flame gases, in the absence of buoyancy. Figures 8c and 9b clearly show a lateral velocity downstream of the flame surface, which, as figures 15 and 16 show, is very nearly symmetrical around the center line of the flow ($\frac{X}{a}=0.$)

Some Dimensional Considerations

At this point, the possible effects of Lorentz forces on the flow field downstream of the flame may be estimated.

In a flow of uniform density - ρ - and uniform velocity - V -, the momentum flux - ρV^2 - integrated over an area A

through which the mass flow rate is $\dot{m}$, is $\dot{m}V$; if the mass flow rate is kept constant, a force f applied to this flow will cause a change of velocity

$$\Delta V = f/\dot{m}$$

if this force is the only force acting on the flow.

While it is manifest from the data in Figures 13-16 that the flows downstream of the flame do not have flat velocity profiles, and it is also likely that buoyancy and viscosity are acting on the gas flows, it is, nontheless, of interest to calculate the change in velocity arising from Lorentz forces, and to compare the <u>observed</u> changes in velocity, on the application of Lorentz forces, with these.

Using the following parameters describing the experimental conditions, it is possible to make such estimates:

total mass flow rate — 15.83×10^{-6} kg./sec.

magnetic field intensity —

.14 Tesla (series B)

.12 Tesla (series A)

electrode separation —

.012 meter (series B)

.018 meter (series A)

total Lorentz force applied to gas by magnetic field acting on electrode current —

8.5×10^{-6} newton (series B)

10.5×10^{-6} newton (series A)

The expected changes in velocity downstream of the flame, given these parameters, are

$$\Delta V = 1.76 \text{ ft./sec.} \quad \text{(series B)}$$

$$\Delta V = 2.16 \text{ ft./sec.} \quad \text{(series A)}$$

and it will be found that the actually measured changes with Lorentz forces with the flow direction are very near to these - 1.8 and 2.2 ft/sec, at .5 and .38 inch downstream from the flame, respectively.

Results - Lorentz Force with Direction of Flow

Because the particles were moving fastest in this case, this case always yielded the longest particle tracks, which covored large portions of the flow field. As a consequence the behavior of this case is the best understood of the three cases. Further, the fact that the gas is accelerated demands that the diameter of the column of gas decrease from the case with no Lorentz forces, so that the edges of the column are drawn away from the walls of the test section. Consequently, in this case the effects of the test section walls are minimal, simplifying analysis.

The Y component of velocity .38 inch downstream of the flame was approximately 2.2 ft./sec. higher than the Y velocity component without the applied Lorentz force (Figure 14); in the less extensive series B data, the observed axial velocity of the flow .5 inch downstream was approximately 1.8 ft./sec. higher than the axial velocity without an applied Lorentz force. Lateral velocities also

became very large when Lorentz forces with the direction of flow were applied, as shown in Figures 15 and 16.

The very good agreement between the calculated and the observed changes are, perhaps, partially fortuitous, because, at the levels observed, not all of the gas particles have passed through all of the lines of electric current - some current flows downstream of the .38 inch level and the .5 inch level (as shown in Chapter 5), and the Lorentz forces acting on this current could further accelerate the flow.

Of very great interest is the fact that the observed accelerations are not uniform; particles near the centerline $-\frac{X}{a} = 0.$ - do not rise to as high a velocity as do particles near the cathode (Figures 10 and 17), and the X components of velocity are not symmetric about the center line of the flow, as particles near the cathode side (positive X/a) are accelerated much more rapidly than particles near the anode side (negative X/a), as can be seen in Figures 15 and 16. Finally, it appears that, on the anode side of the flow field, the rise in lateral velocity is delayed for some distance, after which there is a sharp jump in lateral velocity (Figure 18).

This asymmetry of velocity gradients caused by the Lorentz forces must arise from an asymmetry of the applied Lorentz forces. Just how these asymmetric Lorentz forces arise is the subject of Chapter 5.

Results - Lorentz Force against Flow Direction

In this case, the flow was decelerated to a very low velocity. In series A data, this velocity was approximately 1.0 ft./sec. lower than the velocity without Lorentz forces (Figures 12 and 14) .38 inches downstream of the flame. For series B data, the velocity .5 inches downstream of the flame surface was approximately 1.2 ft./sec. lower than the axial velocity in the absence of Lorentz forces. In either case, the deceleration is not as great as that which would be predicted if the reduction in flame gas momentum equalled the Lorentz force. The reason for this probably arises from the fact that, by continuity, the velocity of the flow in the 45 mm. tubes of which the test section is made cannot go below an average velocity of 1.1 ft./sec.; if a boundary layer grows on the walls of the test section, the velocity on the center line of the flow would have to be higher than this.

In actuality, the series A data were observations of the flow under the conditions depicted in Figure 19, in which the flame gases were not confined until a distance of approximately 3/4 inch downstream from the flame was reached. Also, the gases in this region were surrounded by static (and probably cooler) gas. While the flame gases were unconfined for some distance downstream from the flame and so were free to decelerate below 1.1 ft./sec., this would have required that they accelerate again once that they

entered the 45 mm. tube leading to the exhaust system. This deceleration followed by an acceleration was not observed, and it is likely that the portion of the Lorentz force which was not balanced by a deceleration of flame gases was balanced by a static pressure drop. (This could have been measured with a micromanometer, but such instruments take several minutes to reach their steady-state reading, and running times of such lengths were not available with the magnet used.)

From Figure 12, it appears that, in this case also, the flow is not decelerated uniformly, but that fluid nearer the anode - $\frac{X_o}{d} = -.38$ - is decelerated more rapidly than fluid equidistant from the electrodes - $\frac{X_o}{d} = 0$. Also, as Figures 15 and 16 show, the X component of velocity very quickly goes to zero.

Buoyancy, Heat Loss, and Viscosity

It should be noted that the dynamic head of the flame gases - $\frac{V^2}{2g}$ - is of the order of 1-12 cm. for the three cases considered, while the change in height of the flame gases under observation is 1.0-2.0 cm. The Froude numbers of 0.5 - 12.0 corresponding to these values indicate that gravity might affect the flow field. Nontheless, it is difficult to see how buoyancy could account for the changes in flame stability described in chapter 2, or for the changes in velocity observed in the series A data. Buoyancy is simply the result of an imbalance between the

weight of a column of hot gas and the static pressure change, over the height of the column, caused by an enviroment of cold gas. This can only change if the pressure gradient of the enviroment changes (for instance, if the cold gas is displaced by a warmer gas) or if the density of the hot gas changes. In the apparatus used for the series A data and the experiments of Chapter 2, the column of flame gases was surrounded by a sizable volume of cooler, static gas, which did not appear to be displaced by the hot flame gases when Lorentz forces were applied. Thus, it is probable that the static pressure gradient applied to the flame gases did not change when Lorentz forces were applied, so that the effects of buoyancy were the same in all three cases. Further, the estimated 3% change in burnt gas density with the changed heat loss to the burner would probably not severely alter the effects of the buoyant force. It is difficult to conceive of any effects which these changes of buoyant forces could trigger which would be so large as to dominate the behavior of the flame.

Experimentally, it is known (Ref. 32, p. 402) that, when the Reynolds number of the flow based on the burner diameter exceeds 2000, the flame becomes turbulent. Turbulent flames exhibit a higher "burning velocity" (based on a time-averaged surface area) and are much more stable than laminar flames. Thus, if the burner Reynolds number were

were in the vicinity of 2000, it is conceivable that the rise in velocity when Lorentz forces accelerated the gas flow would cause a laminar flame to go turbulent. Alternatively, if the flame were already turbulent and Lorentz forces decelerating the flow were applied, the flame might become laminar, either case affecting the stability of the flame. In order to avaluate this, the Reynolds number based on burner diameter - d

$$R_{E_d} = (4\dot{m})/(\pi \mu d)$$

may be calculated for the burner inlet conditions (temperature of 70°F, pressure of 86 mm. Hg absolute), and is found to be 44. Thus, it is rather unlikely that conditions of turbulence ever be approached in the experiments used in this thesis. An additional point is the fact that the observed particle tracks are very regular, showing none of the fluctuations of position which would be expected if the flow were turbulent, and if the turbulence were coarse enough and of low enough frequency to be followed by the particles.

It is more difficult to assess the effects of viscosity on the flow of the flame gases and the stability of the flame. It is first necessary to get some estimate of the growth of the viscous boundary layer between the moving column of flame gases and the surrounding static gas. Figure 19 sketches the region of flow observed in the series A data, and the probable effect of viscous entrain-

ment of the surrounding fluid. At the boundary between the flow issuing from the burner and the surrounding still air, the surrounding air must be entrained by viscosity, much as occurs in a laminar viscous jet. However, this flow differs from jets in an infinite sea of fluid in that there must be no net flow of entrained fluid, so that a reverse flow of fluid further away from the free boundary of the jet compensates for the entrained mass flow at the boundary. The flow field which results is, basically, a vortex. It should be possible to estimate the initial growth of the boundary layer between the jet and the vortex by use of the known solutions for the development of a boundary layer on a viscous jet in an infinite sea of fluid. This initial development is, in turn, given by the behavior of the boundary layer growing between two fluids of different velocity, as analyzed in Reference 42. If the edge of the boundary layer is taken to be the surface at which the boundary layer has reduced the gas velocity by 10%, the distance of the edge of the boundary layer from the outer edge of the jet is

$$\delta' = 2.5\sqrt{\frac{\mu Y}{\rho V_f}}$$ *

If the initial flow velocity of the jet, inside of the boundary layer, is taken to be 3 ft./sec. (a velocity intermediate between the highest and lowest velocities observed in the present chapter), and if the boundary layer is assumed to begin to grow at the flame, then, .19 inch

* Strictly valid only for thin boundary layers

downstream of the flame, δ' is .3 inch, and 0.38 inch downstream of the flame, δ' is 0.41 inch. As the diameter of the jet of fluid must lie in the range of 1.0 - 1.7 inches, it can be seen that viscous boundary layer effects might be significant in the flow field. Indeed, if the plots of Figures 13 and 14 are again inspected, it is seen that the Y component of velocity does fall off rather sharply near the outer edges of the jet, which could be due to viscosity.

Just what effect this vortex has in stabilizing the flame is difficult to appraise, although it is certain that the growth of the boundary layer into the fluid downstream of the flame in some way affects the flow field in the immediate vicinity of the flame. The vortex and boundary layer probably tend to stabilize the flame: experiments in which a flow of nitrogen surrounded the flow from a flat-flame burner, initially moving at the same speed as the flame gases, showed that the flame was less stable than it was without this shielding flow[34], although it is not completely clear just why this should be so. The fact that the boundary layer thickness <u>increases</u> with a decreasing flow velocity, while the total momentum loss to the boundary layer <u>decreases</u> with decreasing velocity makes a determination of how the stabilizing effect of the vortex would <u>vary</u> with the changes in burnt gas velocity more difficult.

In all events, it is likely that these viscous effects, whatever they be, would not change the burning velocity of the flame. Further, the likelihood that the boundary layers are very thin in the immediate vicinity of the flame means that the flame is not being stabilized in a viscously decelerated region of flow, but that, at most, the viscous boundary layer only indirectly affects the flow in the immediate vicinity of the flame (since it has not grown to any appreciable size at the location of the flame) while the Lorentz forces are being applied in the immediate vicinity of the flame. Also, the changes in viscous effects on the flow field do not occur spontaneously, but are a result of changes caused by the Lorentz forces, and it is unlikely that the fluid-dynamic effects of the changes in the viscous boundary layer be triggered into greater effects on the flow field outside of the boundary layer than are caused by the Lorentz forces.

SUMMARY

This chapter has presented data showing that:

1) Burning velocity is not altered when Lorentz forces are applied to flame gases under conditions which lead to alterations of flame stability.

2) The Y component of the flow velocity of the burnt gas is accelerated or decelerated, in accordance with the direction of the Lorentz force.

3) The increases in velocity are very close to those which would arise if these forces were used only to change the momentum flux of the gas; decreases in velocity are not as great, probably due to the limited cross-sectional area available to the gas flow.

4) In both cases, the variation of velocity with distance downstream from the flame is asymmetric about the center line of the flow. Further, in the case when the net Lorentz force is with the flow, components of velocity are produced perpendicular to the direction of the total Lorentz force.

The remainder of this thesis will be devoted to demonstrating that such behavior is reasonable. Chapter 4 will analyze flame structure and burning velocity as affected by magnetic fields, while Chapter 5 will analyze a situation similar to the experiments to demonstrate that the features of the flow patterns downstream of the flame can be accounted for on a purely dynamical basis.

CHAPTER IV

ELECTROMAGNETIC EFFECTS ON FLAME STRUCTURE AND PROPAGATION

INTRODUCTION

The Purpose of this Chapter

This chapter investigates the possible effects of Lorentz forces on a flame, where the only features of the flame considered are the one dimensional flow, kinetic, and transport processes which determine the structure and the burning velocity of the flame. As such an analysis includes the chemical-kinetic and transport processes which directly control the flame structure and burning velocity, and ignores the effects of flame curvature, two and three dimensional gas flow patterns, etc., which only indirectly affect the structure and burning velocity of a flame, it is suited to calculations of the flame's burning velocity.

The work of this chapter is split into two separate parts:

1) Order-of-magnitude evaluations and qualitative inspections of the effects of Joulean heating, Lorentz forces, and electric and magnetic field effects on several chemical-kinetic and transport phenomena in flames, under the conditions actually encountered in the present thesis.

2) An investigation of the effects predicted from

solutions to the one-dimensional, continuum equations for flame structure and burning velocity, with special emphasis on the physical configuration of electrode and magnetic field necessary to achieve the boundary conditions on the magnetic field equations employed in previous analyses.

Some effort is taken: to demonstrate that achievement of the boundary conditions employed in previous analyses of the problem require physical configurations which are not achievable in the experiments described in this thesis; to determine by what mechanism these previous analyses allow the magnetic field to modify the burning velocity; and to demonstrate that this mechanism, alone, would not be altered by the presence of a magnetic field.

Methods of this Chapter

As the structure and propagation of a flame is governed by a balance of diffusion and kinetic processes, alteration of the diffusion of charged species might affect the flame's structure. Various ways in which electric and magnetic fields could do this will be evaluated in this chapter, and be shown to be negligable compared to the processes normally occuring in a flame.

A completely different possibility is raised by previous analyses of magnetohydrodynamic effects in combustion, in which the assumption of a coupling between the gas flow and the magnetic field leads to predictions

of changes of burning velocity with the application of a magnetic field. This chapter will examine the physical conditions necessary to achieve this coupling, and show that these require electrode lengths or electrical conductivities which are far greater than can be achieved in the present experiments. Further, some attention is paid to the mechanism by which, in these analyses, the burning velocity of the flame is altered, to see if this mechanism of alteration of the burning velocity can be achieved without the assumption of a coupling between the magnetic field intensity and the gas flow velocity.

Conclusion of this Chapter

On the basis of this chapter's evaluation of the two possible classes of electromagnetic field effects on flame structure and propagation - i.e., the alteration of the diffusion of charged species through the flame, and the coupling of the gas flow velocity to the magnetic field intensity - it is concluded that there is no reason to expect that electromagnetic fields of the sort employed in the present research alter the structure or burning velocity of the flame.

EFFECTS ON THERMODYNAMIC OR TRANSPORT PROPERTIES

Physical Conditions - Variation in Thermodynamic Properties

The propagation of a flame is a process in which heat and energetic chemical species generated at high temperatures

diffuse forward into the unburnt gas, heating and igniting it. The governing factors in this process are the transport properties and the reaction kinetics of the particular combustion reaction involved: these, in turn, rely on the local thermodynamic state - pressure, temperature, and composition.

If the flame is considered as burning in a single component mixture, in a perfectly one-dimensional flow, electromagnetic effects directly enter the governing equations for flame structure twice - once in the energy equation, as a Joulean heating contribution, and once in the momentum equation, as a pressure drop term. Thus, within the physical model implied by these equations, electromagnetic effects on flame structure and propagation would arise either from heating the gas or from altering its static pressure.

A very simplified model of flame structure, which treats the entire chemical reaction as taking place at the temperature of the burnt gases predicts (Ref. 65, p. 99) that the burning velocity should vary as

$$S_u \sim P^{\frac{n}{2}-1} e^{-E_1/RT_b} \qquad (4\text{-}1)$$

where, for a hydrocarbon-air flame, the reaction order, n, is assumed equal to 1.8, and E_1 is assumed to be approximately 40 kcal/mole (Ref. 39, pp. 310-315). While E_1 is generally assumed to vary only with the combustible mixture, it cannot be assumed to be the same as E_A - the

activation energy in the Arrhenius reaction rate law. Equation 4-1 is a strong function of the final temperature of the gas (and a weak function of the pressure of the gas) which, in conjunction with the experiments of Botha and Spalding[4] showing that the burning velocity of a propane-air flame could be reduced by precooling the flame gases, raises the possibility that a Joulean preheating of the flame gases would raise the burning velocity.

A comparison of the maximum possible energy input from the Joulean heating with the chemical energy input due to combustion allows some appraisal of the magnitude of the effect of the Joulean heating on the properties of the flame. The total voltage drop across the electrodes multiplied by the total electrode current gives the electrical power being dissapated in the test section. (Not all of this is dissapated in the gas. There is a large voltage drop and energy dissapation in the region immediately surrounding the cathode, which heats the cathode to a temperature at which it glows brightly and probably radiates off a sizeable amount of power.)

At the operating conditions used for this thesis, the voltage across the electrodes was ~500 volts without an applied magnetic field, and ~900 volts with an applied magnetic field. This voltage was the same, at 5 milliamperes, for either direction of magnetic field, despite the fact that,

at current levels from 14-25 milliamperes, with electrodes in the shape of needle points pointing towards each other, placed on opposite sides of the burner, the voltage drop was higher when Lorentz forces were <u>against</u> the flow direction than when Lorentz forces were <u>with</u> the flow direction. The observed change in voltages across the electrodes corresponds to a power input change, at 5 ma., from 2.5 to 4.5 watts - a variation of 2 watts when the magnetic field is applied. The heat of combustion of propane is 526 cal./gm.-mole[71], which corresponds to a heat release rate of 45 watts for a rate of combustion of 8.0×10^{-4} gm./sec. of propane. The addition of 4% to the heat input rate due to Joulean heating would give a proportionate rise in T_b, and possibly a disproportionate rise in the burning velocity, as equation 4-1 is extraordinarily temperature-sensitive. However, if this were the case, it could not account for the changes in flame stability reported in Chapter 2, as this is independant of magnetic field orientation, while the effects reported in Chapter 2 very definitely <u>do</u> depend on magnetic field orientation.

It is quite possible that this electrical heat input change will not alter the burning velocity at all, as evidence presented in Chapter 5 suggests that the major part of the electric current through the flame gases passes <u>downstream</u> of the luminous zone of the flame, where the gas is <u>already</u> burned, so that Joulean heating occurs where the

reaction rate can no longer be affected by changes in temperature.

The possible effect of Lorentz forces on static pressure would be absolutely negligable insofar as concerns any physical or thermodynamic properties of the gas. The total Lorentz force applied to the gas, as stated in Chapter 3, is 10.5×10^{-6} newtons (series A) while the total force of an 86 mm. Hg absolute pressure acting on a circle 28 mm. in diameter (a value representative of the diameter of the column of gas) is 7.1 newtons, so that the Lorentz forces applied during the experiments of this thesis are absolutely negligable by comparison to the static pressure of the gas. This being the case, it is unlikely that any property of the gas depending on the total static pressure of the gas would be changed by the application of Lorentz forces.

Variations in Rate and Transport Processes

The effects of the electric and magnetic fields on the rate of diffusion of heat and charged species, and on the chemical-kinetic processes in the gas, are more difficult to appraise conclusively. However, it is possible to make some estimates of the degree of alteration of the diffusive processes in a flame by electric and magnetic fields, and some qualitative experimental observations which bear out the contention that flame structure is not altered by electric or magnetic fields.

A small but very important piece of information is given by the observation that there is no visible change in the flame whatever when it is subjected to magnetic fields of up to .79 Tesla (the maximum available from the magnet used for this thesis) with the electrodes open-circuited, so that no current passes through the flame from the electrodes. Thus, it seems that the magnetic field, alone, has no effects on the diffusive or kinetic processes taking place within the flame. This is quite reasonable with respect to the diffusive processes, as the ionic Hall parameter is of the order of 10^{-2}, showing that the motion of the molecular ions is not affected by the magnetic field. The fact that the Debye length (Ref. 53, p. 17) - of the order of 2×10^{-4} cm. for a gas with an electron concentration of 10^{12}/cc. and a temperature of 1090°C - is so much less than the flame thickness makes it probable that the electron distribution in the flame will not be different from the molecular ion distribution. A related item of information comes from Kelly's measurements of the structure of detonations under conditions similar to those studied in this thesis[29]. These showed that the distribution of radiation from the reaction zone of C_2H_2-O_2 detonations, which characterizes the distribution of the reaction processes in the detonation, was nearly unchanged with the application of a magnetic field. Further, by a similar technique, Nakamura[41] concluded that electric fields would not affect the reaction processes of a propane-air flame.

It is possible to imagine that a powerful electric field might alter the diffusion of charged species within the flame, possibly altering the flame structure. During the course of the electric field measurements described in Chapter 5, electric fields typically of the order of 5000 volts/meter were observed near the downstream edge of the reaction zone. It is possible to decide whether or not these electric fields would affect the distribution of charged radicals in the flame by comparing the two terms of the formula for the effective driving force (Ref. 7, p. 54) causing diffusion of a singly charged particle under the combined effects of an electric field and a gradient of concentation

$$E + E' = E - \frac{K_e T_e}{m_e q_e} \frac{d m_e}{d y}$$

Taking for E a typical experimental field strength of 5000 volts/meter, and, for $m_e(Y)$ a distribution rising to 10^{18} ions/meter^3 over a distance comparable to the thickness (of the order of 1 mm.) of the luminous zone[5], with $K_e T_e \approx 1/8$ electron volts (T_e equal to 1400°K), $q_e = 1.6 \times 10^{-19}$ couloumb[71], and $E' = \frac{K_e T_e}{m_e q_e} \frac{\Delta m_e}{\Delta Y}$, yields an E' of the order of 8×10^{20} volts/meter, so that, in the reaction zone, the diffusion of charged species would be governed completely by the driving force arising from concentration gradients $-E'-$ with the diffusion due to the electric field $-E-$ of relative insignificance.

The fractional ionization, given an electron density of approximately 10^{12} electrons/cc. and a gas density of

5.9×10^{17} molecules/cc. (corresponding to a temperature of 2560°R and a pressure of 86 mm. Hg absolute) is 1.7×10^{-4}%. Since the specific heat per mole of electrons in a gas would be of the same order as that of the gas molecules, and since the alterations of diffusion of the electrons in the reaction zone due to the changes in the electric and magnetic fields are negligable, it is apparent both that the gas may be assumed to be slightly ionized, and that the effect of electric and magnetic fields on the diffusion of heat through the reaction zone may be considered as negligable.

SOLUTION OF THE FLAME STRUCTURE EQUATIONS

Presentation of the Equations

The foregoing portions of this chapter have investigated the possible effects of the Lorentz forces and Joulean heating actually present in the present thesis on flame structure and propagation. This investigation did not purport to deal with the solutions of the formal equations of flame structure including electromagnetic effects, but only evaluated the order of magnitude of possible electromagnetic effects on the physical processes in the flame and on the properties of the flame gases.

In contrast, some early work in the study of electromagnetic effects in combustion was built around a study of electromagnetic effects on the structure and propagation of a flame[3,58], and did work with the formal

equations of flame structure.

The equations of flame structure used for such analyses are strictly one-dimensional, involving: the diffusion, convection, and consumption of reactants; Bernoulli's equation; the equation for the diffusion, convection, and chemical release of heat; the equation for conservation of mass; Ampere's circuital law (in differential form); and various algabraic relations between the thermodynamic, transport, and chemical kinetic properties of the gas.

Electromagnetic effects are assumed to arise from an electric field of specified intensity and a parallel flow of current, both perpendicular to the gas flow direction. A magnetic field is assumed perpendicular to both the electric current and the gas flow direction. If the flame gas is assumed to have no thermodynamic properties which depend on the electric or magnetic field intensity, the effects of the electromagnetic field are restricted to a Joulean heating of the flame gases and a Lorentz force term in the Bernoulli equation. We will now undertake such an investigation in order to find out if such analyses predict anything of relevance to the experiments described in this thesis.

The equations used in this thesis were derived starting from those given by Toong and Chen[59]. The concentration, or species continuity equation, is unchanged from the form given by Toong and Chen; it is (with a change

in notation)

$$D_c \equiv {}^{dC_A}/_{dY}$$

$$\rho U D_c - \frac{d}{dY}(\rho \mathcal{D} D_c) - K_A = 0$$

In the energy equation, the "heat loss" term of Toong and Chen is replaced with a Joulean heating term $-\sigma E_u(UB+E_u)$ as given by Pai (Ref. 43, p. 113) and becomes (again with a change in notation)

$$D_H \equiv {}^{dh}/_{dY} \qquad D_T \equiv {}^{dT}/_{dY}$$

$$\rho U D_H - \frac{d}{dY}(\lambda D_T) - q_c - \sigma E_u(UB+E_u) = 0$$

The mass conservation equation is unchanged from Referance 59; it is

$$\dot{m} = \rho_u U_u = \rho_b U_b = \rho U$$

A different form of the momentum equation must be used from that in Reference 59; it is derived from a one-dimensional formula given by Pai (Reference 43, p. 100) under the assumption that the gas is inviscid and has a negligable dynamic pressure compared to its static pressure; this, then, is

$$P + \frac{B^2}{2\mu_o} = P_u + \frac{B_u^2}{2\mu_o}$$

Ampere's law must be added to this set of equations; it is (Ref. 43, p. 100)

$$\frac{dB}{dY} = \sigma \mu_o (E_u - UB)$$

(References 24 and 25 develop the equations of flame

structure from fundamental principles, while Reference 43 - in Chapters 2, 3, and 14 - develops the equations of magnetohydrodynamics, allowing for chemical heat release and reaction of species, beginning from a kinetic-theory basis. The interested reader should refer to these references.)

The form of the electrical conductivity function - σ - must take into account the fact that, in experiments, the flow of current through the flame is affected by the location of the electrodes as well as by the state of the gas. Within the framework of the one-dimensional analysis, the effect of this may be expressed by making the conductivity a function of position - Y - as well as of the state of the gas, so that the electrical conductivity becomes zero at those values of Y where there are no electrodes. Consequently, the function for the conductivity - σ - becomes

$$\sigma = \sigma(T, P, C_A, Y)$$

The Arrhenius reaction rate law used in the present work was obtained starting from the form

$$\frac{dC}{dT_i} = K' C^{1.8} \sqrt{T}\, e^{-\frac{E}{RT}}$$

which gives the molal rate of consumption per unit volume per unit time - $\frac{dC}{dT_i}$ - where the reaction order -1.8- was taken from well-stirred reactor data[39] on hydrocarbon-air flames. K' is independant of temperature, and C is the molal density - (moles reactant)/(unit volume) - of

reactants. Defining the mass rate of production of reactant per unit volume as

$$K_A = (\text{molecular weight of reactant}) \cdot \frac{dC}{dT}$$

a temperature independant reaction rate constant as

$$K = K' / [(\text{molecular weight}) \cdot R]^{.8}$$

and the reactant mass fraction - C_A - as

$$C_A = (\text{molecular weight}) \cdot C/\rho$$

allows K_A to be written as

$$K_A = K \rho P^{.8} C_A^{1.8} T^{-.3} e^{-E_A/RT}$$

In order to permit solutions to the governing equations to be obtained, it is known that the reaction rate must be set equal to zero for some distance surrounding the upstream boundary (Ref. 65, p. 110) so that the reaction rate law finally becomes

$$K_A = K \rho P^{.8} C_A^{1.8} T^{-.3} e^{-E_A/RT} \quad ; \quad \frac{C_A}{C_{A_u}} \leq .9$$

$$K_A = 0 \quad ; \quad \frac{C_A}{C_{A_u}} > .9$$

Finally, it is necessary to use the perfect gas law, defining certain relations between gas properties

$$dh = C_p(T)\, dT$$

$$\rho = P/RT$$

$$C_p - C_v = R$$

as well as the heat release rate

$$q_c = q_T K_A$$

and functional expressions for the transport properties

$$\lambda = \lambda(P, T, C_A)$$

$$\sigma = \sigma(P, T, C_A)$$

Appendix 7 discusses these equations and their solution. It suffices here to state that a necessary and sufficient set of boundary conditions for a solution include, at an upstream boundary Y_u where $C_A = C_{Au}$, the conditions

$$D_c = 0$$
$$T = T_u$$
$$B = B_u$$
$$D_T = 0$$
$$P = P_u$$

the specification that

$$\dot{m} = \rho_u U_u$$

and the condition that, when K_A goes to zero at Y_b, D_c will also go to zero (when $m \geq 1$). For consistency, D_T must also be zero at Y_b, to prevent divergence of equation (A7-20).

The point at which the analyses in references 3, 20, and 58 become inapplicable to the present experiments is in the assumed behavior of solutions to Ampere's law

$$\frac{dB}{dY} = \sigma \mu_0 (E_u - U B) \qquad (4\text{-}2)$$

in that it is assumed that σ is never equal to zero (effectively, that current can always flow through the gas) and yet that $\frac{dB}{dY}$ goes to zero simultaneously with D_c and D_T. This necessarily demands that

$$E_u = U_u B_u = U_b B_b \qquad (4\text{-}3)$$

which is then adopted both as a specification of E_u and as a condition to be obeyed by the values of B at the boundaries. Such a condition, demanding that the change in magnetic field intensity over a length of channel L, caused by a flow of current arising from an electric field of order of magnitude UB acting on a material of conductivity σ, be of the same order of magnitude as the applied magnetic field is, very simply, a stipulation that the magnetic Reynolds number $\sigma\mu_0 UL$ be of order unity. Just why this should be unlikely in the present experiments may be seen after a discussion of some dimensional considerations.

Dimensional Considerations - Magnetic Interaction

We turn our attention to a situation in which the magnetic field intensity and its changes are assumed coupled to the flow of a conducting fluid moving with a velocity U, by virtue of currents generated in the fluid by the fluid's motion relative to the magnetic lines of flux and an electric field of the order of UB. In this case, if the changes in magnetic field are comparable to the applied field over a distance L_M, then the diffusion of the magnetic field upstream and the convection of magnetic field downstream are competing processes[68]. These competing diffusion and convection processes come to

a match over a distance such that the magnetic Reynolds number $-\sigma\mu_o U L_M$ is of order unity[68]. This, in turn, implies that L_M is approximately $\frac{1}{\sigma\mu_o U}$. Outside of the "magnetic shock" where the diffusion of magnetic field comes into balance with the convection of magnetic field, the gradient of magnetic field is zero. (Again, it should be noted that this is the case only when E is of the order of UB.)

In a similar manner (Ref. 65, p. 98), the structure of a flame may be considered to involve a balance between the convection and diffusion of heat, such that a balance is attained over a distance

$$L_T = \lambda / c_p \rho U$$

outside of which gradients of temperature go to zero. The ratio of the distance L_M over which magnetic diffusion matches magnetic convection, to the distance L_T over which thermal diffusion matches thermal convection, is

$$L_T / L_M = \frac{\lambda \mu_o \sigma}{c_p \rho} = Pr_M$$

which is called the magnetic Prandtl number, and is a function only of the properties of the gas.

For the values of c_p, ρ, and λ typical of the gases used in this thesis, and with σ = 1.0 mho/meter, this L_T/L_M parameter is of the order of 10^{-8}, implying that the distance over which the convection of magnetic field balances diffusion of magnetic field is 10^8 times as great as the distance over which convection of heat matches diffusion of heat - the flame thickness. Alternatively,

for these distances to be of the same order of magnitude, so that the gradient of magnetic field will approach zero simultaneously with the gradient of temperature, the magnetic Prandtl number must be of order unity. A magnetic Prandtl number of 1.0 implies that $\sigma \approx 10^8$ mhos/meter, which is an unrealistically high value of electrical conductivity to expect for a gas. (The conductivity of copper is 5.8×10^7 mhos/meter[71].)

It follows, then, that the assumption of a coupling between the gas flow and the magnetic field intensity implicit in equation 4-3 demands either that the gas conductivity be $\sim 10^8$ mhos/meter (if the coupling takes place over a distance comparable to the flame thickness), or that the length of the interaction zone between the flow and the magnetic field be of the order of 10^5 to 10^8 meters (σ = 1.0 to 0.001 mhos/meter). Obviously, such a coupling cannot be achieved in the laboratory.

Solutions and their Physical Mechanisms

Despite the unrealistic boundary condition, it is of interest to solve these equations using this boundary condition, using a Lewis number = .78, a chemical heat release = -24.9, magnetic Prandtl numbers = 10^{-7} to 10^{-10}, a ratio of specific heats = 1.4, a magnetic field intensity from 0 to .37 Tesla, a reactant concentration $C_{A_u} = .192$, a gas pressure = 86 mm. Hg absolute, and an activation energy equal to 48 kcal/gm-mole. All these values are

typical of a propane-air flame. When such solutions are obtained (by the methods of Appendix 7) it is found that a strong variation of burning velocity with magnetic field is predicted, along with a slight variation of final temperature with magnetic field intensity. The computed variation of burning velocity with magnetic field is plotted in Figure 20. The rise in temperature must come about from the Joulean heating in the energy equation, as the chemical heat release is assumed constant, and the energy equation contains no kinetic energy terms. Further, it may be demonstrated that, in this situation[38], all of the current must flow upstream of the reaction zone, so that the Joulean heating due to this current flow preheats the gas, before it burns, thereby raising the reaction rate when burning finally does take place. It is possible to get some idea of how this operates by correlating the data from the numerical solutions with equation 4-1.

The variation of burning velocity with final temperature predicted by equation 4-1 is

$$S_u/(S_u)_{B=0} = e^{+E_1/R(T_b)_{B=0}} \cdot \left(\frac{T_b - (T_b)_{B=0}}{T_b}\right)$$

or

$$\log\left[S_u/(S_u)_{B=0}\right] = \frac{E_1}{R(T_b)_{B=0}} \cdot \left(\frac{T_b - (T_b)_{B=0}}{T_b}\right) \quad (4-4)$$

and Figure 21 shows that this relation does describe the behavior of the solutions to the flame structure equations obtained using the boundary condition (4-3). What is very relevant is that the identical dependance of burning

velocity ratio - $\frac{S_u}{(S_u)_{q_T=0}}$ - on the ratio $\frac{T_b-(T_b)_{q_T=0}}{T_b}$ is obtained if no electromagnetic effects are assumed, and the final temperature is changed by varying the heat released chemically - q_T - from an initial value - q_{T_0} . The effective activation energy which may be calculated from the data in Figure 21, using equation 4-4 in the form

$$E_1 = R(T_b)_{\beta=0} \cdot \frac{T_b}{T_b-(T_b)_{\beta=0}} \log\left[S_u/(S_u)_{\beta=0}\right]$$

is 56 kcal./gm.-mole, while the activation energy used in the Arrhenius rate law - E_A - was 48 kcal./gm.-mole. However, despite the fact that the effective activation energy - E_1 - is not the same as the activation energy used in the Arrhenius rate law does not detract from the fact that the "electromagnetic effects" on flame propagation seem to be simply another heat source.

Thus, the predicted dependance of burning velocity on magnetic field intensity is simply a manifestation of the fact that " ... a flame could be made to propagate faster by adding heat." (reference 35, p. 11), and that the voltage drop and current flow giving this electrical heat addition is forced, by equation 4-3, to depend on the applied magnetic field intensity. Indeed, the assumption of (4-3) may be shown[35] to demand that the electrical power input to the flame - q_J - is given by

$$q_J = \frac{S_u(B_u)\,B_u^2}{\mu_0}\left(1-\frac{\rho_b}{\rho_u}(B_u)\right) \qquad (4\text{-}5)$$

which must go completely into Joulean heating when the kinetic energy of the fluid is negligable, and when there are no time-varying electromagnetic fields. It should be noted that, in formula 4-5, S_u and $\frac{\rho_b}{\rho_u}$ are functions of B_u, so that this formula is not a complete, explicit algebraic relation between the Joulean heating and the applied magnetic field. Nontheless, (4-5) does show that the Joulean heating, under the assumption of equation 4-3, is dependant only on the applied applied magnetic field intensity.

Despite the fact that the boundary condition (4-3) is inapplicable to the problem studied in this thesis, the basic mechanism of altering burning velocity by a Joulean preheating of the flame gases, where the electric field and electric current are not coupled to the magnetic field, is a possibility. This could be achieved, in the present experiments, by passing the current upstream of the reaction zone. However, the evidence from Chapter 5 seems to be that, at best, the greatest portion of the electric current passes through the gas downstream of the luminous zone of the flame, with only a small fraction of the electric current possibly passing through the reaction zone

SUMMARY

This chapter has discussed a variety of possible mechanisms for the alteration of flame structure and burning velocity by electromagnetic fields, and concluded

that any such alteration is unlikely.

The mechanisms discussed were:

1) Joulean heating of the flame gases, altering the reaction rate;

2) Alteration of the diffusion of charged species by electric or magnetic fields;

3) Alteration of the reaction kinetics and diffusion properties of the flame by a magnetic field alone;

4) Alteration of the heat transport by electrons.

Some attention has also been paid to the applicability of earlier analyses of magnetohydrodynamic effects on flames to the present work. It was found that the situation studied experimentally in this thesis was different from that analyzed in these works, so that their conclusions would be inapplicable to the present work.

CHAPTER V

ANALYSIS OF TWO-DIMENSIONAL EFFECTS

INTRODUCTION

Purpose of this Chapter

The purpose of this chapter is to obtain an idea of the distribution of current flow and Lorentz forces in the flame gases which gives rise to the flame stabilization and destabilization observed in Chapter 2, and accounts for the changes in flow patterns reported in Chapter 3. With this information, it becomes possible to visualize the details of the action of the Lorentz forces on the flow field.

Due to viscosity, buoyancy, and the fact that the flow from the burner is initially radially symmetric, while the current from the electrodes suffers fringing effects at the ends of the electrodes, a complete analysis would be a quite complex problem. As a first approximation to this complex problem, the present chapter will undertake a study of a much simpler problem, which idealizes the flow of gas and of current as being two-dimensional, and treats the effects of Lorentz forces as acting alone (no viscosity, buoyancy, or pressure gradients) on the flow of gas. While this analysis cannot predict every detail of the observed patterns, it does predict many of the features of the changes in flow field with Lorentz force observed in Chapter 3.

Only the effects of Lorentz forces, the Hall effect, and the hypothesized stratification of conductivity at the flame surface are retained, in order to see what arises from just these alone. The electric field calculated from this model is verified experimentally

Methods of this Chapter

The pattern and distribution of Lorentz forces in the flame gases can be determined either from knowledge of the magnetic field intensity and electric current patterns, or by a differentiation of observed fluid velocities. The latter, involving a numerical double differentiation of the experimental particle-track data, is very prone to error and probably would be of no value whatever. The former method, used in the present chapter, also has limitations; there is apparently no experimental method for directly measuring electric current densities in a gas. However, the distribution of luminosity of the gas in the discharge can be used for a rough estimate of the distribution of current density[62]. Further, Ohm's law, with the Hall effect included, gives a relation, between the direction of the local electric field and the direction of the local current, which is independent of the ion density in the gas or of the density of the local current. If the Hall parameter - H - is known, the direction of the local current flow is known to lie at an angle of $\tan^{-1}(H)$ to the observed direction of the local electric field, so that measurements of the electric field

direction (which are relatively easy to perform) immediately give the local current direction.

With this evidence, it is then possible to formulate an idea of the features of the current distribution in the gas - and to develop an analytical model of the current patterns.

The distribution of Lorentz forces in the gas can be immediately calculated from the known distribution of current in the gas. From the known distribution of current in the gas, the distribution of Lorentz forces can be calculated; from this, the equations of motion allow the determination of fluid particle trajectories

Conclusions of this Chapter

This chapter concludes that:

1) The current distributes itself behind the flame, in the burnt gases, and does not concentrate itself in the reaction zone (although some small fraction of the current might pass through the reaction zone).

2) The gas behind the flame, conducting electricity in the form of a glow discharge, behaves similarly to a uniform conductor with a constant Hall parameter

3) The Hall effect leads to distortions of the current patterns, making the field of electric current and of Lorentz forces asymmetric.

4) The field of velocity changes arising from

these Lorentz forces is also asymmetric, and demonstrates the features pointed out in Chapter 3.

ANALYSIS OF CURRENT PATTERN - OBSERVED BEHAVIOR

Gross Behavior of the Electric Discharge

Figure 22 gives the voltage vs. current curve across the electrodes in the apparatus used in this thesis, for the case of no applied magnetic field. As can be seen, with increasing current the voltage rises to a value of approximately 1200 volts, and then falls off to a value of 500 volts, where it remains with increasing current. (Application of a magnetic field gives identical behavior, but with the voltages at every current level being higher.) Direct observation of the discharge shows that the cathode and the surrounding gas glows brilliantly, but uniformly, over the length of the cathode, while the anode has a row of very tiny, very brilliant spots on its surface, on the line on its circumference parallel to the electrode surface, and nearest the cathode. Finally, the region of gas reaching from roughly midway between the electrodes to the surface of the cathode is luminous. Such behavior is typical of glow discharges, and known features of the glow[7,62] and of the electrical conductivity of flames[5] will be reviewed at this point. (Some of the early history of the study of electricity in flames - historically interesting but technically irrelevant to this thesis - is in Appendix 3.)

The Glow Discharge

The glow discharge is self-sustained; i.e., the electrons and molecular ions carrying the electric current are generated by violent collisions of electrons with neutral species, where the kinetic energy making such violent collisions possible comes from the same electric field which causes the current to flow[30]. A glow occurs when the rate of creation of new ions by this process exceeds the overall recombination rate of ions with electrons, a situation called an "avalanche". Once the avalanche has occured, the limitation on the level of total current flow lies in the rate of emission of electrons from the cathode.

In a glow, this limitation is overcome by the fact that the current through the last few mean free paths (the "cathode sheath") to the cathode is carried by positive ions, rather than by electrons leaving the cathode. At the anode, there is no limitation on the electron current density which can flow at the anode surface. What is observed to occur at the anode is that electrons flow into the anode at a very few points, each marked by a brilliant, glowing spot on the anode surface. Such points are at the metallurgical inhomogenieties located in regions of the anode surface where the highest local electrostatic fields prevail. In a glow, the cathode sheath carries a fixed current per unit area, whose density is much less than the current density in the concentrations at the anode. Thus, increases in the total

current will lead to an increase in the area covered by the sheath, the voltage drop between the electrodes remains constant, and the discharge is called a "normal" glow.

The Ionization of Flames

The equilibrium thermal ionization of a flame, as determined by Saha's equation, is very low[17], except if materials having low ionization potentials (K, Cs, Na) are added to the gas. However, in flames[5] and detonations[29] of hydrocarbon oxidations, there is an abnormally high level of conductivity and ionization in the luminous region of the flame. A matter which must be dealt with in the present thesis is the role which this ionization plays in determining the electric current patterns. Experiments with traveling detonation waves in tubes[29] have shown that this highly ionized zone can conduct a significant part of the total electric current of a discharge through the detonation gases; it is not unrealistic to consider the possibility that a similar behavior would occur in the experiments reported in this thesis.

Were this the case, the luminous zone of the flame would behave as an actuator disc when a magnetic field was applied, giving a fixed change in velocity simultaneously to all the fluid particles passing through it, uniformly and with no asymmetry. If it were not the case, the observed acceleration patterns will show inhomogeneous or even asymmetric accelerations resulting from asymmetric or inhomogeneous current distributions. The data presented in Chapter 3 showed that

the latter was the case in the experiments reported in this thesis.

The Electric Discharge in Flames

The rate of creation of new ions at a given point in a glow discharge is a function of the local electric field and gas density[62]. However, the fact that the diffusion of ions is a very significant part of the behavior of a glow discharge[30] makes it likely that local inhomogeneities in the creation of electrons are smoothed out by diffusion, so that nonuniformities in ion generation might be expected to be of little importance insofar as the uniformity of the ionization and conductivity distribution in the products of combustion are concerned.

However, the flame is a region of very high gas density gradients; the higher a gas' density, the lower is the mobility of ions in it (Ref. 7, Chapter 2) so that, in the colder gas upstream of the luminous zone, the acceleration of electrons to the high energies necessary to maintain a glow discharge would be inhibited, as well as the diffusion of ions from the highly ionized regions of the discharge. Thus, it is likely that, somewhere in the flame structure, a boundary exists upstream of which there is neither the creation nor the diffusion of ions, so that upstream of this boundary the flame is an insulator.

Visually-Observed Character and Behavior of Discharge

In the conducting regions of a glow discharge, there is

a balance between the generation, diffusion, and recombination of ions. The recombination leads to the emission of light, so that regions of high current density glow brightly. In the present experiments, the shape and position of the discharge varied with the magnetic field, so that it is probable that the current distribution varied as well.

Figures 23 and 24 show the flame and discharge, in the cases where the Lorentz force is, respectively, against the direction, and with the direction of the gas flow. As can be seen, in the case in which the Lorentz force is <u>against</u> the direction of gas flow, there is an intense concentration of luminosity at the flame surface, near the anode. Further, the current seems to flow downward from the anode, as if it were being forced to run along a surface in the luminous zone of the flame. Figure 23, (taken with a 10 ma. current to emphasize the appearance of the effect) shows the opposite behavior, occuring when the Lorentz force is <u>with</u> the direction of gas flow. Here, the electron flow to the anode seems to be from <u>downstream</u> of the anode. Consequently, it might be suspected that, near the anode, a larger fraction of the total current flows in the region <u>upstream</u> of the electrodes when Lorentz forces are <u>against</u> the flow direction than flows when Lorentz forces are <u>with</u> the flow direction. In the case of Lorentz forces <u>with</u> the flow, the total Lorentz force along a line of constant

X would be low until some point above the level of the anode were reached, where the intensity of the Lorentz forces would rise rapidly. This should be visible in the velocities of the fluid near the anode. Near the anode, such a distribution of current would demand that the acceleration of the fluid be delayed until some point downstream of the anode be reached.

The insulating character of the flame surface is most clearly seen in Figure 25 (taken with a 3 ma. current to emphasize the effect). The sharp boundary of the discharge lumonisity at the flame surface shows that the flow of current upstream of the luminous zone of the flame is inhibited.

It should be noted that, in all the photographs presented in this thesis, the very brilliant glow of the cathode and of the anode causes the photographic images of the cathode and anode to appear very much enlarged and distorted. In actuality, the physical cathode and anode are much smaller than they appear on the photographs.

The Hall Effect

The presence of the Hall effect is obvious from the observed behavior of the voltage across the electrodes when a magnetic field is applied. The voltage across the electrodes was typically 480-500 volts in the absence of a magnetic field, and rose to 860-940 volts with an applied magnetic field of .12-.14 Tesla.

Calcote gives data[5] on the effective collision cross-section of the products of combustion of a propane-air flame, pointing out that there is a significant variation in published and observed values of the electron-neutral collision cross-section - Q_{es} - with values ranging from 1.6 to 2.1×10^{-15} cm.^{2}. Adoption of a working value of 1.8×10^{-15} cm.^{2} gives a Hall parameter of .95 with the following gas conditions:

pressure = 86 mm. Hg
temperature = 1090°C
molecular density = 5.9×10^{17} molecules/c.c.
magnetic field intensity = .12 Tesla

ANALYSIS OF SIMPLIFIED MODEL

Analysis of Electric Current Patterns

A complete analysis of the electric current patterns between the electrodes would be a formidable problem, involving a three-dimensional problem dealing with all the interacting effects at play in a glow discharge. Rather than attempt such a complete analysis, this section will study a two-dimensional situation having, in common with the experimental situation, a pair of parallel and coplanar electrodes, and an insulating surface parallel to the electrodes.

The major features of the current flow patterns, however, should be governed by the boundary conditions placed on the

current flow. Consequently, in the following analysis a two-dimensional viewpoint will be taken, retaining the same boundary conditions at the electrodes and at the flame surface as must hold in the three-dimensional case, but ignoring any Z components of current. Further, the gas will be assumed to have a Hall parameter of + or - .95 in the presence of a magnetic field (the sign of the Hall parameter depending on the direction of the magnetic field), and a zero Hall parameter when no magnetic field is applied.

At the electrodes, there is at least one boundary condition which always must hold - that the integral of the current density over the entire surface of the electrode must equal the total current being passed through the gas. Further, the lines of current must lie at an angle of $\tan^{-1}(H)$ to the lines of electric field.

In the apparatus used for this thesis, the electrodes were .005" diameter wires, separated by a gap of 1/2 inch to 3/4 inch. Consequently, the patterns of current flow at the electrode surface would be of negligable significance as far as the current flow in the main body of the gas is concerned; all that would be of significance would be the relative positions of the electrodes and the flame surface, where the flame surface is assumed to be an insulating boundary. As pointed out above, a Hall effect of the order of .95 would be expected in this apparatus.

A situation with all of these features is depicted in

Figure 26b, in which the nomuniform, concentrated character of the current source at the anode is neglected. Thus, the effect of each electrode on the field of current and electric field in the body of the gas is one of a two-dimensional line source (or sink) of current and of electric field. It must be noted that it is not possible to treat the source and sink functions for the electric and current fields as having identical forms, as the Hall effect causes the current flow lines to lie at an angle to the electric field lines. If <u>each</u> separate electrode is considered to be a simple, two-dimensional line source of electric field, the electric field due to each electrode is given by

$$E_r = \pm K'/r$$

where r and θ are the familiar cylindrical polar coordinates.

The lines of <u>current</u> must always lie at an angle of $\tan^{-1}(H)$ to the lines of electric field; for the current flow due to a single electrode this can be obtained by treating the current flow as a source function

$$J_r = \frac{\sigma}{(1+H^2)} E_r$$

added to a free vortex

$$J_\theta = H J_r$$

so that the total current flow is

$$\vec{J} = \frac{\sigma}{(1+H^2)} (\vec{e_r} + H \vec{e_\theta}) E_r$$

Then, the total current pattern due to the cathode and anode, in the <u>absence</u> of the insulating boundary at the flame surface, is a superposition of four singularities - (anode source + anode vortex) + (cathode sink + cathode

vortex). The current flow due to these in the presence of the insulating flame surface may be obtained by the method of images, where the flame surface is the surface across which the cathode and anode are imaged. Thus, the final current field is a superposition of eight singularities - four vortices, two sources, and two sinks.

A somewhat more involved analysis was employed in this thesis, which <u>did</u> take the detailed behavior near the anode into account. The anode and the cathode were treated as follows: in order to simulate the localized flow of current at the anode on the point of the anode surface nearest the cathode, the anode current boundary condition was that the anode be an insulating cylinder, except for a line source of current (line sink of electrons) along the line on the cylinder's periphery nearest the cathode. Cathode behavior was assumed to be the behavior of the outer edge of the cathode sheath (the "virtual cathode"), characterized as an equipotential surface (justified by the fact that the voltage drop from the outer edge of the sheath to the electrode surface is a constant for a given gas and electrode[7]). Since lines of electric field are normal to equipotentials, the boundary condition on the electric <u>current</u> must be that the lines of current flow into the cathode lie at an angle of $\tan^{-1}(H)$ to the normal to the cathode surface.

The equivalence of the two analyses may be checked by

comparing the computed components of the normalized current density - $\vec{J}ta/I$ - as a function of $\frac{Y}{a}$ along the lines $\frac{X}{a} = \pm .93$ (where $2a$ is the electrode separation and t is the length of the electrodes, or the depth of the region through which current is flowing), as computed both by the singularity distribution outlined above and by the methods to be described later in this chapter. Figures 27 and 28 give such a comparison, where the crosses are the values calculated by the singularity distribution, and the continuous line shows the values as calculated by more detailed method. As can be seen, at the points compared the two analyses are very close to each other. This similarity is a quite strong indication that the effect of the localized current flow to the anode is of no significance in the determination of the current flow in the body of the gas.

Nature of the Electric Current Pattern

Appendix 5 contains a demonstration that a two-dimensional field of electric current in a gas of uniform conductivity and constant Hall parameter is rotation-free. Consequently, the steady current patterns obey Laplace's equation, which can be solved with the boundary conditions of Figure 26a. First the field of electric current due to the source and image cathode and anode can be solved separately, with the effect of the insulating flame surface then obtained by the method of images.

Solution

Representation of the parallel, cylindrical cathode and anode in the bipolar[54] coordinate system (Fig. 26c) allows the electrode surfaces to be represented as straight lines in the transformed plane. The rules for the transformations between bipolar - ξ, η - and cartesian - X, Y - coordinates are as follows, where the coordinate system is shown in Figure 26c.

conversion from (ξ, η) to (X, Y)

$$X = (a \sinh \xi)/(\cosh \xi - \cos \eta) \qquad Y = (a \sin \eta)/(\cosh \xi - \cos \eta)$$

angle between a curve of constant ξ and the X axis

$$\angle_\xi = a(1 - \cosh \xi \cos \eta)/(\cosh \xi - \cos \eta)$$

angle between a curve of constant η and the X axis

$$\angle_\eta = \angle_\xi - 90^\circ$$

the length of a line segment - dS - in terms of the change of ξ or η

$$dS = \frac{a}{\cosh \xi - \cos \eta} d\eta \quad ; \quad dS = \frac{a}{\cosh \xi - \cos \eta} d\xi$$

definition of h

$$h = \frac{a}{\cosh \xi - \cos \eta}$$

conversion from (X, Y) to (ξ, η)

$$\xi = \coth^{-1}\left([X^2 + Y^2 + 1]/2X \right), \quad \eta = \tan^{-1}\left(2Y/[X^2 + Y^2 - 1]\right)$$

Since the electric current is the gradient of a potential (see Appendix 5), it follows that

$$\vec{J} = \vec{\nabla} \psi = \frac{1}{h}\left(\frac{\partial \psi}{\partial \xi} \vec{e}_\xi + \frac{\partial \psi}{\partial \eta} \vec{e}_\eta \right)$$

where ψ satisfies Laplace's equation in bipolar coordinates:

$$\frac{\partial^2 \psi}{\partial \xi^2} + \frac{\partial^2 \psi}{\partial \eta^2} = 0$$

The form of Laplace's equation in bipolar coordinates is the same as the form of Laplace's equation in cartesian coordinates, so that ψ may be expressed as a Fourier series, or:

$$\psi = A\xi\eta + B\xi + C\eta + \sum_{N=1}^{\infty} \sin(N\eta)(A_N e^{N\xi} + B_N e^{-N\xi}) + \cos(N\eta)(C_N e^{N\xi} + D_N e^{-N\xi})$$

The Fourier coefficients must be obtained subject to the boundary conditions that: the lines of current must lie at an angle of $\tan^{-1}(H)$ to the surface $\xi = \xi''$, the "virtual cathode", assumed to be an equipotential surface, or

$$\left(J_\eta / J_\xi\right)_{\xi=\xi''} = H \longrightarrow \frac{\partial\psi}{\partial\eta} = H\frac{\partial\psi}{\partial\xi} ;$$

that the current distribution at the anode surface $\xi = \xi'$ is an impulse function, with all the current flowing into one point - $\eta = \pi$, or

$$(J_\xi)_{\xi=\xi'} = \left(\frac{1}{h}\frac{\partial\psi}{\partial\xi}\right)_{\xi=\xi'} = i \cdot \delta(\eta - \pi)$$

(where i is a coefficient given in terms of the total electrode current and the dimensions of the current-carrying region); and that the integrated current density normal to a cylinder of length t surrounding either the cathode or the anode must equal the experimentally measured current - I, or

$$I = \int_0^{2\pi} t \cdot J_\xi \, ds = t \int_0^{2\pi} \left(\frac{\partial\psi}{\partial\xi}\right) d\eta$$

The final solution may be written as

$$J_\eta = \frac{I}{ta} J_\eta^P \quad ; \quad J_\xi = \frac{I}{ta} J_\xi^P$$

where $\vec{J}$ is the physical current density and $\vec{J^P}$ is a normalized current density which may be determined by the methods given in Appendix 7. (It should be noted that $\vec{J^P}$ is the function plotted in Figures 27 and 28). It is then

a simple procedure to transform J_ξ and J_η, once obtained by the methods of Appendix 7, back to the X, Y components of current density by the formulae:

$$J_x = \cos(\angle_\xi) J_\xi + \cos(\angle_\eta) J_\eta$$
$$J_y = \sin(\angle_\xi) J_\xi + \sin(\angle_\eta) J_\eta$$

Solutions so obtained are not complete, as they are only the current patterns arising from the source anode and the source cathode. At the same value of (X, Y), the X component of current due to the image electrodes is the same as the X component of current of the source electrodes at $(X, 2Y_f - Y)$, where Y_f is the Y coordinate of the flame (or insulating boundary) location. Similarly, the Y component of current from the image electrodes is the negative of the Y component of current of the source electrodes at $(X, 2Y_f - Y)$. The detailed program for doing these calculations - given in Appendix 2 - involves: transformation from (X, Y) to (ξ, η); calculation of J_ξ and J_η; the conversion of (J_ξ, J_η) to (J_x, J_y); calculation of the image coordinate $(X, 2Y_f - Y)$; the calculation of the image current components; and the summation of the components of the source and the image current. In the solutions presented in this thesis, the flame was assumed to be at $\frac{Y_f}{2} = -.5$ for the cases of no Lorentz force or Lorentz force against the flow, and $\frac{Y_f}{2} = -.2$ for the case of Lorentz force with the flow.

Solutions so obtained are plotted in Figures 29, 30, and 31. As can be seen, with a nonzero Hall parameter the

solutions are quite asymmetric. What is even more interesting is the fact that, for the case when the Lorentz force is against the direction of flow, there is a large fraction of the total current which flows upstream of the electrodes, and downstream of the insulating boundary, near the anode, just as was suspected from Figure 24. (It should be noted that each line plotted in the figures is a line of constant current stream function, each pair of lines bounding 10% of the total current. The entire field of current, of course, cannot be plotted, as it extends to infinity.)

Experimental Check on Calculated Current Patterns

It is quite simple to calculate the angle of the electric field (with respect to the X-Y coordinates) from the angle of the lines of current. An especially interesting feature is the variation of the angle of the electric field at the flame surface, as the behavior of this angle with varying Hall parameter is very relevant to an understanding of the effectiveness of the flame surface as an insulating boundary. If the electric field and its changes with applied magnetic field indicate that the flow of current is always parallel to the downstream edge of the flame, then the flame is, indeed, an insulating boundary.

Experimentally measured electric fields are shown in Figures 29-31, and compared with theoretically calculated values at the same points. The data was obtained by placing

a probe of two parallel wires (see Appendix 1) into the flame gas - the wires being parallel to each other and to the electrodes - and rotating the probe until the voltage between the wires went to zero. The test section was then photographed, and a system of coordinates was established on the pictures from a given run by the same technique as was used in reducing particle-track pictures. The perpendicular besector of the line between the electrode tips was then used to define the local electric field direction.

In view of the uncertainty of H and the fact that data could be reduced with an accuracy of little better than $\pm 10°$, (as determined by having two independent workers measure some sample points) the agreement shown between theory and experiment in Figures 29-31 is rather good.

Field of Flow Due to Lorentz Forces

The column of gas leaving the burner flows into a region where no walls are immediately adjacent to the column; consequently, for some distance downstream of the burner, the flow is similar to that of a free jet. The field of Lorentz forces applied to this initially axisymmetric flow is not axisymmetric, so that the flow which finally results is three-dimensional.

In order to obtain a first approximation to the expected behavior, the analysis of the flow field, like the analysis of the current patterns, will be drastically

simplified from reality. The flow will be assumed to be two-dimensional, and subjected only to Lorentz forces. Obviously, then, this flow field does not describe the flow actually encountered experimentally, which certainly was subjected to pressure gradients and viscosity. It does allow a first approximation to be made of the effects of Lorentz forces on the flow field, by showing what effects the Lorentz forces, acting alone, have.

As pointed out in Chapter 3, the effects of viscosity are likely to be significant only near the outer edges of the flow field, decelerating the flow. The effect of buoyancy would be to add a fixed velocity head to the flow, though just how this would vary with the applied Lorentz forces is difficult to appraise without completely solving the problem.

The effects of the three-dimensionality of the flow would be to resist the changes in thickness of the column of gas, setting up pressure gradients from the outer edge of the column of gas inwards to the central core of the gas flow. However, it is likely that this would only reduce the effect of the Lorentz forces, and not eliminate it.

Under these assumptions, the equations of motion simply involve an acceleration of fluid particles - $\frac{D\bar{V}}{DT_i}$ - by a Lorentz force/unit mass of fluid - $(\vec{J}\times\vec{B})/\rho$ - or, treating the flow as two-dimensional

$$DV_x/DT_i = J_y B_z/\rho \qquad DV_y/DT_i = -J_x B_z/\rho$$

If the field of electric currents flowing through the gas is assumed to be the same as that calculated earlier in this chapter, the equations of motion become

$$D\left(\frac{V_x}{a}\right)/D T_i = (I B_z J_y^p)/(\rho a t \cdot a)$$

$$D\left(\frac{V_y}{a}\right)/D T_i = -(I B_z J_x^p)/(\rho a t \cdot a)$$

If the gas flows in at the downstream edge of the insulating boundary with an initially uniform velocity - $(V_y)_o = V_o$ - these can be integrated

$$V_y/a = V_o/a + \int_o^{T_i} -\frac{i}{\rho a t \cdot a} J_x^p B_z \, d T_i'$$

$$= V_o/a \left(1 + \int_o^{T_i} \frac{-i}{V_o \rho a t \cdot a} J_x^p B_z \, d T_i'\right) \qquad (5\text{-}1)$$

and, similarly

$$V_x/a = \frac{V_o}{a} \int_o^{T_i} \frac{i}{\rho a t V_o} J_y^p B_z \, d T_i' \qquad (5\text{-}2)$$

These must solved simultaneously with

$$X/a = \int_o^{T_i} \frac{V_x}{a} \, d T_i' \qquad (5\text{-}1a)$$

$$\frac{Y}{a} = \int_o^{T_i} \frac{V_y}{a} \, d T_i' \qquad (5\text{-}2a)$$

It is desired to use a coefficient $\frac{I}{\rho V_o a t}$ which gives some correspondence between these formulae and experiment. I is given by the total electrode current, which is easily measured; t, the depth of the region through which current

is flowing, is difficult to determine experimentally, due to the fringing of the lines of current flux at the ends of the electrodes and the three-dimensionality of the gas flow. If t is assumed to coincide with the depth of the column of flame gas (whatever this happens to be), the parameter $\rho V_o a t$ becomes the total mass flow rate passing through the discharge, which may be assumed to be the mass flow rate measured by the flow meters. (This is a rather sizeable assumption, as the design of the apparatus is such that gas can flow around the region not enclosed by the electrodes and, further, the shape of the gas column's cross-section is continually changing, as shown in Figure 32.) If V_o is taken as the velocity at the downstream edge of the flame, as measured by the particle-track pictures, then, from equations 5-1 to 5-2a, the rise of velocity above the inlet velocity $-V-V_o-$ may be calculated, as well as the lateral velocity engendered by the Lorentz forces.

The results of such calculations are plotted in Figures 33-36. As can be seen, certain features of the patterns of flow observed in Chapter 3 are evident here.

Considering first the case of Lorentz forces <u>with</u> the flow direction, Figure 33 shows that there is, indeed, an asymmetry of the axial velocity gradients, with the Y component of velocity rising more quickly near the cathode side of the flow field than at the centerline of the flow field, in correspondance with the data plotted in Figures 10, 13, and 14. The order of magnitude of the difference

between the "centerline" ($\frac{X}{d} = 0$) and the "near-cathode" ($X/d > 0$) velocities - about .5 ft./sec. - and the location of the maximum difference - .1 to .2 inch downstream from the flame surface - are the same both for the idealized model and for the experimental observation. The calculated lateral velocities (Fig. 34) too, are similar in kind to those observed experimentally. Figure 18 shows that, on the anode side of the centerline of the flow ($X/d < 0$), a particle goes for some distance downstream of the flame until it passes the anode, and then is suddenly accelerated laterally, while a particle on the cathode side of the flow has, at the same height, a much higher lateral velocity. The calculated X velocities in Figure 34 exhibit the same sort of behavior, and, again, the orders of magnitude are the same.

Comparisons of the case when the Lorentz force is <u>against</u> the direction of the flow are not expected to be as good, as the flow expands to fill the test section downstream of the flame, so that interferance by the tube walls will significantly alter the flow. Despite this, Figure 35 shows that the decelerations of V_y on the anode side are greater than those along the center line, as might be inferred from the data of Figure 12.

Similarly, as shown in Figure 16, the flow far downstream of the flame has no lateral velocity, probably because of the constraint imposed by the walls of the test

section. In the absence of this constraint, the behavior exhibited in Figure 36 might be expected, where it is the particles near the cathode side of the test section whose lateral accelerations are delayed, while particles near the anode side of the test section are predicted to be immediately accelerated laterally.

Interpretation of Results

It must be noted that the analysis presented in this chapter predicts lateral accelerations because the Lorentz forces, normal to the curved lines of current flow, contain components in the X direction. This being the case, the X accelerations observed in the experiments are accounted for on the basis that the electric currents do not flow strictly in the X direction.

What is significant about this is the fact that, in the present experiments, the electric current does not prefer to concentrate in the highly ionized reaction zone of the flame. If this were the case, the current flow would all be in the X direction, and accelerations would be confined mostly to the Y direction, with only very slight lateral components. However, in the measurements with Lorentz forces with the direction of flow described in Chapter 3, the vary large lateral velocities .38 inches downstream of the flow indicate that there are very large lateral components of Lorentz force acting on the gas.

The fact that current flow (and therefore Joulean

heating) is downstream of the flame, in the burnt gases, was discussed in Chapter 4 as one good reason why the flame's burning velocity should not be affected in the experiments of this thesis.

A question which cannot be answered definitively is just where in the flame's luminous zone the insulating boundary occurs. The spatial resolution of the $\vec{E}$ field probes was of the order of 1 mm., which could not resolve the structure of the luminous zone - itself of the order of 1 mm. thick. Consequently, it is possible that some fraction of the current passed through the luminous zone in the experiments of this thesis. The amount of current passing through the luminous zone can be estimated by assuming that the density of current flow through the luminous zone equals the calculated current density parallel to the downstream edge of the insulating boundary. Then, the total current through the 1 mm. thick luminous zone would be approximately 7% of the total current, or 0.35 milliamperes. Consequently, the particular location of the insulating boundary within the luminous zone is not too relevant, since, in any event, the current (and the associated Joulean heating) in the luminous zone would be only a small fraction of the total current (and associated Joulean heating) through the flame gases.

SUMMARY

This chapter has analyzed the electric current and the Lorentz forces arising from an application of a magnetic

field to the electric current. The situation studied was one having the following features in common with the experimental work performed in this thesis; fixed terminal points of the electric current flow in the gas, discontimuity of conductivity at the flame surface, the presence of a Hall effect, and a flow of gases without contact with confining walls.

When values of magnetic field intensity, Hall parameter, mass flow rate, flame burning velocity, flame position (insulating boundary position), and electrode separation characteristic of the experimental situation were used to define the corresponding parameters in the analytical model, the predicted behavior, both of the electric field and of the gas flow field, showed a striking similarity to the observed behavior, suggesting that the analytical model contained the major features of the physical situation.

A very important piece of data from this analysis was a demonstration of the fact that the current flow on which Lorentz forces are acting to stabilize a flame or to destabilize it passes through the burnt gases, rather than concentrating in the reaction zone.

CHAPTER VI

CONCLUSIONS AND SUGGESTIONS FOR FURTHER WORK

THE CONCLUSIONS OF THE THESIS

The Problem and Data

In briefest sense, this thesis is a demonstration that the stability of a flame can be altered by Lorentz forces, which alter the flow field of the flame gases, but not the burning velocity of the flame.

The basic problem was posed in Chapter 2 by experimental evidence showing that a flame's stability could be affected by the application of a magnetic field to the flame gases, when the products of combustion were carrying an electric current. In order to determine what was causing this change in stability, the effects of an electric current (of 5 ma.) and a magnetic field (of .12-.14 Tesla) on a flame in a total mass flow of 15.83×10^{-6} kg./sec., with a fuel/air ratio of .0309 was studied in more detail in Chapters 3, 4, and 5. It had been shown in Chapter 2 that Lorentz forces could blow the flame off (Lorentz force with flow direction) and could stabilize this flame against blowoff when the total mass flow rate was increased (Lorentz force against flow direction). The use of the stabilized flame, which was not blown off, in the remainder of the thesis was justified under the assumption that the mechanism

of interaction of the electric and magnetic fields with the flow - observed when the flame was not blown off - was also at play under conditions when the flame was blown off.

In Chapter 3, the flow patterns of the burnt gases were observed, and the changes of flow patterns with Lorentz forces were interpreted as showing that the burning velocity was unchanged by Lorentz forces, while the flow downstream of the flame was being accelerated or decelerated by Lorentz forces.

In Chapter 4, several possible effects of electric and magnetic fields on the transport of charged species in a flame were discussed, and were found to be negligable. Another approach, taken by earlier studies of magnetohydrodynamic effects on the structure and propagation of flames, was appraised and found inapplicable to the situation experimentally studied in this thesis.

Chapter 5 presented an analysis of a two-dimensional current field which had an electrode separation, Hall parameter, and flame location which were the same as those used experimentally. Measurements of the electric field were very close to the calculated electric fields, showing that the experimental electric current field could be expected to be described by the calculated current field. After this, the changes in an idealized flow field due to the Lorentz forces arising from these current patterns were calculated. In these calculations, the idealization was that the changes were due exclusively due to the application of

Lorentz forces to the flow field (without viscosity or pressure gradients). These changes in flow field showed the asymmetries and other features which had been observed experimentally in Chapter 3. The significance of these current patterns lay in the fact that the current mostly flows downstream of the flame, and so affects the stability of the flame by acting on the burnt gases rather than on the flame itself.

Summing Up

Taken together, these facts give the picture that the effect which Lorentz forces have on a flame's stability is simply one of obstructing or accelerating the flow of burnt gas. Obstruction of the flow of burnt gas was proposed by Putnam[47] as a universal technique of flame stabilization, irrespective of how this obstruction was achieved. While Putnam discussed no means of destabilization of a flame by forces accelerating the flow, this possibility is a straightforward extrapolation of his conclusions.

Just why and how such a deceleration of flow stabilizes the flame is, itself, a deeper and more fundamental question which lay outside the scope of the present thesis. The simple explanation that the deceleration of the flow allows an equilibrium to be achieved between the flow velocity and the burning velocity holds only for laminar flames, and must, itself, be augmented by considerations of the stability of the equilibrium, while the more complex problem of flame holding

in turbulent streams (which was not achieved in the present thesis) is best viewed from the qualitative criteria of Gammon[16].

SUGGESTIONS FOR FUTURE WORK

Several questions have been raised in the course of this thesis, which could be investigated further.

The extrapolation of the conclusions and methods of this thesis to the problem of flame holding in an aeronautical or industrial combustor is a very great one. In these combustors, flow velocities are very much greater than the burning velocity, the flow is highly turbulent, and it would be impractical to apply Lorentz forces over the entire cross-section of the flow. It would be highly desirable that both the current flow through the gas and the spatial extent of the magnetic field be small, and that the power consumption of the apparatus not be excessive. (In the present thesis, a 1 kw., 12 kv. D.C. power supply and a 40 kw. magnet were used to stabilize a flame releasing approximately 40 watts - hardly an economical proposition!)

The restricted volume of current flow and low electrode voltages are characteristics of the arc mode of electric discharge. Thus, a very worthwhile problem would be a study of the properties and capabilities of an arc in a turbulent flame for stabilizing the flame by Lorentz forces. A preliminary study of this could be performed by studying

the stabilization of laminar flames by an arc, which could be done in the apparatus used in the present thesis.

A possible mechanism for the alteration of the flame's structure by magnetic fields, pointed out in Chapter 4, lies in the alteration of the diffusion of charged molecular species by a magnetic field. While this was certainly unlikely in the experiments reported in Chapters 2 and 3, it would become a possibility if the ionic Hall parameter were raised to the order of unity. This could be done if the flame burned at a pressure of 1-2 mm. Hg absolute, and a magnetic field intensity of the order of .7 to 1.0 Tesla were applied (both conditions being achievable in the apparatus described in Appendix 1). If any visual changes were observed, it would then be possible to check the change in flame structure by microprobe sampling[14], or even by Langmuir probes (if an adequate theory of Langmuir probes in a magnetic field were ever devised).

The effect of an electric discharge on the chemical reactions in the flame would be of interest in its own right. Since an electric discharge can catalyze chemical reactions, it might be conjectured that a discharge, acting alone, might alter the chemical reactions and structure of the flame. This can only be conjectured, as the whole topic of catalysis by electric discharges is a vast field of unknowns. If this were studied, infrared and microwave spectroscopy, and microprobe sampling would be the most useful techniques for study of the molecular species formed, their distribution,

and the alteration of this distribution with magnetic fields.

Another matter for study, more directly related to the main themes of the present thesis, is the distribution of Joulean heating downstream of the flame. This could be studied either by use of thermocouples traverses, or by a spectral line-reversal technique. What would be of interest would be the distribution of this Joulean heating relative to the zones of chemical heat release of the flame. The knowledge of this would provide further justification for the contentions of Chapter 5 that the Joulean heating of the products of combustion would not affect the reaction zone of the flame.

These previously cited problems are directly connected with extant problems of combustion research - flame stabilization, flame structure, or the chemical kinetics of flames. Two other questions suggested themselves during the course of the present research which would be of interest in themselves, though somewhat removed from any present programs of research in combustion.

The first question is suggested by the fact that, when a flame is stabilized - with no current flowing - <u>coplanar</u> with the electrodes, it does not <u>remain</u> coplanar when the electric current is switched on, but moves <u>upstream</u> of the electrodes. Just why this occurs is difficult to answer. It is possible that current passing near the reaction zone, when the flame is coplanar with the electrodes, heats the

reaction zone enough to raise the burning velocity, causing the flame to move upstream to an equilibrium position where this Joulean heating is not so significant. Alternatively, the distortion of the electric field by the insulating flame surface would give electrostatic forces acting on the flame surface.

The second problem was suggested by observations that a thin, filimentary discharge passing between needle-point electrodes behaved much like a tiny bluff body in the flow when acted on by Lorentz forces against the direction of flow. The question of interest is just how far this bluff body behavior would go. Would a stagnant region of fluid be formed downstream of the discharge? Would a vortex street form? What sort (if any) of boundary layers would form? Would there be a transition to turbulence in this boundary layer before the main stream became turbulent?

However, before undertaking any future work on the studies outlined above, the whole idea of using hydrocarbon oxidation flames might well be reconsidered. While gaseous hydrocarbon fuels are cheap, readily available, and can be obtained in very high-purity forms for chemical studies, they also cause difficulties. The products of combustion, if lean, are strong oxidizers, so that any metals introduced into the flame as an electrode or a probe must either be strongly cooled, and so quench the flame, or must be made of noble metals and be allowed to get hot, consequently annealing

and/or warping. A rich hydrogen-air flame, if it could be stabilized in a flat shape, would neither have the oxidizing character of a lean hydrocarbon-air flame, nor the sooty and wrinkled character of a rich one. Consequently, it would be possible to use refractory metals such as Tungsten, Tantalum, etc. for the construction of electrodes, probes, and thermocouples, thereby avoiding the difficulties brought about by the poor mechanical properties of the noble metals at high temperatures. The increased experimental convenience might well outweigh the difficulties of making such an apparatus safe.

APPENDIX 1

DESCRIPTION OF APPARATUS

In the execution of this work, an apparatus of unfamiliar design and characteristics was required. This appendix describes the specialized items, and features of standard equipment well-suited to the present work.

Basic Configuration

In order to study separately the effects of flame gas flow field, electric current distribution, Lorentz force, and flame structure in a problem where all of these might be important, it is desirable that each of these be as simple as possible, and, if possible, indepently variable.

The configuration depicted in Figures 37 and 42 was intended to do this. The use of an Edgerton-Powling flat flame burner[34,46], symmetric about a center line, assured that the inlet flow to the test section would be uniform. In order to assure that there would be no spurious current paths in the apparatus between the electrodes, the matrix of the burner was constructed of a bundle of 3 mm. o.d. fused quartz tubes, cemented together at the bottom with alundum cement, and held within a Vycor outer sleeve of 28 mm. o.d. and 25 mm. length. Earlier versions of the burner[35] had been made of Pyrex melting point capillary tubes pressed into a Pyrex outer sleeve, and fused together by heating in a furnace at 1450°F for 75 minutes. If the

end of the matrix was sawed off on a Carborundum wheel, a very flat and smooth burner surface was obtained. The quartz burner, though inferior to the Pyrex burner because of its greater area blockage and larger passages, lasted for 2-1/2 years (including one uninterrupted run of 26 hours) while Pyrex burners would last approximately 1 hour. Despite this, at lower pressures the Pyrex burners could probably be used, as at these lower pressures heat loads would not be as great as they were at 86 mm. pressure.

Another form of burner design which was attempted consisted of a piece of aluminum oxide honeycomb ("Thermacomb") which was obtained from the Minnesota Mining and Manufacturing Company. While this burner was potentially superior to the quartz burner insofar as aerodynamic properties were concerned (both its passages and its fractional area blocked by the honeycomb cell walls were smaller than those of the quartz matrix), its brilliant white color would have given troubles with particle track pictures.

To assemble the apparatus, the $\mathbb{S}\,\frac{40}{50}$ inner standard taper joint containing the burner and electrodes was inserted into the outer $\mathbb{S}\,\frac{40}{50}$ taper joint of the upper half of the test section, shown in Figures 38 and 41. A $\mathbb{S}\,\frac{45}{50}$ outer taper joint, with a 1/16" thick window, fit over the upper taper joint. Similarly, an inner $\mathbb{S}\,\frac{50}{50}$ taper joint with a faceplate bearing four concentric O-rings attached with epoxy to its tubing side was fit into the $\mathbb{S}\,\frac{50}{50}$ taper joint on the side, and

either an auxiliary window or the electric field strength probe (to be described later) was pressed against the faceplate and held tightly when the apparatus was under vacuum. The electrode power supply could then be attached to the electrode lead-outs, fuel-air mixture introduced from the gas supply to the gas inlet, the exhaust connected to the appropriate place, and the apparatus placed between the poles of a magnet for experiments.

Start-up procedure was generally of the sort described in Chapter 2.

Electrodes

The electrode configuration was a very special feature of the apparatus, and permitted a great simplification in evaluation of the data. The fact that a flow of current between two parallel plates does not develop in a uniform manner, but rather often tends to be unstable and concentrates at a very few points on the electrode, and then jumps around as a magnetic field is applied[35] means that the electrodes must be very tiny if the end points (at least) of the current flow are to be well defined.

The wire electrodes were of .005 inch diameter wire, either of pure Rhodium or of an alloy of 60%Pt-40% Rh. These were flame welded onto .040 inch diameter Platinum wires over which "Refrasil" (H. I. Thompson company trademark) braided silica tubing had been stretched, and which had been cemented to the lower end of the burner with General Electric RTV-102

or RTV-60 silicone rubber (Figure 37).

Electrode life was the major factor governing the extent and rapidity of performing an experiment, once it was set up. The major enviromental conditions encountered were heat and oxidation. Since lean, hot products of combustion are strongly oxidizing, the usual refractory metals - Tungsten, Tantalum, Rhenium, etc. could not be used for this application. The noble metal alloys (alloys of Platinum and Rhodium) described earlier were the most suitable materials found, as they retain some strength to the highest temperatures attainable in these experiments, and also resist oxidation.

After roughly 1-3 hours of five milliampere operation, the cathode would burn through and melt. In general, it appeared that failure took place as follows:

1) Heating by ion bombardment would cause thermal expansion of the wire, putting the electrode in compressive stress and putting a kink in the wire.

b) More violent sputtering of the cathode surface in the region of the kink than over the rest of the cathode surface would result, leading to a burnout of the kinked part of the wire.

The use of a 20-microampere ammeter in series with a 100 megohm resistor for a voltmeter (giving 50 kilohms/volt meter resistance instead of the usual 1 kilohm/volt meter resistance of commercial voltmeters) was an aid in maintaining the electrode current constant under varying Hall parameters, by reducing the current path in parallel to the gas discharge.

(For an electrode power supply description, see below.) By minimizing excursions from the 5 milliampere electrode current level when the magnet switched on and off, electrode life was extended.

The use of the braided quartz tubing over the electrode mounts was necessary to prevent discharge current from flowing anywhere but to the wire electrodes.

Electrical Supply

The electrode power supply - Figure 39 - was a strictly convential circuit consisting of a Variac, a step-up transformer, a full-wave bridge, and an LC ladder filter. As can be seen from Figure 39, the circuit was very heavily ballasted and filtered; the 800 kilohm ballast kept the current steady (within 1/2 milliampere) with changes in magnetic field intensity, and allowed a more precise control of the level of current than a power supply with less ballast would have.

Gas Supply

Propane was supplied from a commercial propane cylinder, regulated by a two-stage regulator. Air came from the laboratory air compresser, after first being dried by passing through calcium chloride, and then being pressure-regulated by a Lexington model 121G regulator. Each gas was metered by a Fisher and Porter Tri-Flat Rotameter, propane being metered by a 1/16 inch diameter rotameter with a sapphire float, and air being metered by a 1/8 inch diameter rotameter with a stainless steel float. The propane and air feed pressures in

the rotameters were measured by mercury manometers, with a pressure of 20 inches Hg (guage) used throughout the course of this research. The flowmeters were calibrated by measuring the amount of time required for the measured gas to travel through the flowmeter and displace a given volume of water at atmospheric pressure, the partial volume of the water vapor being subtracted from the total displaced volume of water to give the flow of gas. These calibrations (Figures 43 and 44) were found to be reproducable to within 1.5%.

Magnet

Two magnets were used in the course of this research. All of the data presented in this thesis - with the exception of the "Series B" data of Chapter 3 - were obtained with a magnet which consisted of a pair of 2.6 inch thick coils of no. 6 square copper wire, with an inside diameter of 5.5 inches and an outside diameter of approximately 18.7 inches, each coil having approximately 650 turns. Calibration of the field intensity of the magnet as a function of excitation current showed it to be linear, within the precision of the Rawson rotating-coil fluxmeter used for calibration, producing 0.0042 Tesla/ampere, with a maximum possible current of 187 amperes. The accuracy of the calibration was the combined accuracy of the fluxmeter and the magnet-current ammeter - probably about 4%.

Exhaust System

Burnt products were exhausted through a recrystallized

aluminum oxide tube (obtained from the McDanel Refractory Ceramics Company) attached to the inside of a water-jacketed tube[35], which projected through a "Viton" rubber stopper (no. 9); this latter was pressed into the 45 mm. diameter open end of the upper half of the test section (see Figure 38). Gas then passed from the exhaust line through a heat exchanger, a throttle (or, alternatively, through a no. 8 Cartesian Manostat) and a liquid nitrogen cold trap to a vacuum pump.

Electric Field Measurements

Electric fields were measured by a double probe (Figure 40). This probe was built into a standard inner ball joint ($\$ ^{18}/_{7}$) which matched an $\$ ^{18}/_{7}$ outer ball joint so that, when mounted, rotary motions of the probe were possible. The outer ball joint was attached with epoxy to a flat Plexiglass plate. This plate, in turn, pressed against a face plate mounted on the $\$ \frac{50}{50}$ taper joint in the upper half of the test section provided for this purpose (Figure 38). The probe could be slid laterally and rotated to measure the electric field strength while the system was under vacuum, with no increase in leak rate.

It was necessary to use instruments of high input resistance, and very high resistance to ground, to measure the electric field. For the measurements actually reported in Chapter 5, an RCA WV-84C battery-operated microammeter was used, which drew 10^{-8} amperes at full scale. In order to

check the effect of electrical loading on the measured electric field direction, an electrometer amplifier, identical to Robinson's (Ref. 49) was constructed and used as a preamplifier for the RCA meter, the preamplifier drawing approximately 10^{-12} amperes. A few checks in the vicinity of the electrodes and the flame surface showed no discrepency between the field directions measured with the RCA meter and those measured with the preamplifier, so that the RCA meter, which was less trouble to use, was employed for all measurements reported in Chapter 5.

As is usual in electrostatic measurements, it was necessary to completely shield all components of the circuitry and to avoid any leakages whatever to ground, either from the circuitry or from the shield. All the shields were connected together, and all circuit components were mounted on polystyrene sheets, while all wires (with their shields) were supported in polystyrene tubes.

The experimental procedure adopted, of keeping the probe out of the flame (to one side of the burner, below the level of the electrodes), bringing it into the flame gases when making a measurement, photographing its position, and immediately withdrawing it, was necessitated by the fact that the probe wires warped when heated, so that time in the flame gases had to be minimized. The accuracy of measuring angles and positions in this manner was not great; measurements of the angles on the pictures by independant workers differed by

as much as 10°, while it seems likely that the precision of locating the probe does not exceed the separation of the probe wires - .03 - .04 inch.

Temperature Measurements

The temperature of the burnt gases (mentioned in Chapter 2) was measured by a .0005 inch diameter 6%Rh-Pt vs. 30%Rh-Pt thermocouple with the hot junction flame-welded in the form of a cross. The calculated error due to radiation[37] heat loss from the thermocouple under the conditions encountered in this thesis was approximately 20°C. The thermocouple itself was mounted in the same manner as the electric field probe described above, with each Pt-40%Rh wire replaced by one leg of the thermocouple. Also, in the thermocouple, the .0005" diameter wires protruding from the end of the quartz tube were flame welded together at the tips, to form the hot junction of the thermocouple.

Particle-Track Measurements

As mentioned in Chapter 3, the particle-track technique measures flow velocities and directions by illuminating particles of dust carried along with the gas flow, and photographing the particle locations, at successive times. A schematic diagram of the technique is given in Figure 4. The final version of the setup, arrived at after some trial and error, used an Edgerton, Germeshausen, and Grier FX-2 or FX-1 flash tube, powered by an Edgerton, Germeshausen and Grier model 501 stroboscope power supply. The stroboscope's

driving signal came from an audio-frequency square wave generator. The actual frequency of the driving signal from this generator was set by measuring the output waveform on an oscilloscope, so that the flashing frequency could be set as accurately as the oscilloscope allowed - approximately 3% of the measured value.

The camera used was a Speed Graphic with a focal plane shutter; this latter was especially useful as, at the magnifications used, the velocity of the shutter across the film was comparable to the velocity of the particle image, allowing long tracks to be obtained without overexposing the very brilliant flame or electrodes.

The lens used was made up of the elements from an f/2.8, 100 mm. focal length Schneider Xenar. The two elements were cemented together (without the shutter between) and the combination was cemented onto a lens board for the Speed Graphic. This arrangement gave a lens of small outside diameter, with no ferromagnetic parts, which could be inserted far into the magnet and, with the maximum bellows extension of the camera, used to produce an image 2.86 x life size. The film used was Polaroid type 410 with an ASA equivalent speed of 10000, in a roll film back attached to the Speed Graphic.

The accuracy of the particle track technique is analyzed in Appendix 4.

APPENDIX 2

DESCRIPTION OF COMPUTER PROGRAMS

Two blocks of machine calculations were performed in the course of this thesis. The programs, written in the MAD and FAP languages, are listed at the end of this appendix.

Flame Structure Calculations

The first program, listed on the pages marked STRUCTURE, performed the flame structure calculations described in Appendix 7. This program accepted as input variables the Lewis number (LEWS), the dimensionless heat release (QBAR), the dimensionless reaction rate (GBAR), ratio of magnetic to gas pressure (PIBO), dimensionless activation energy (ACTE), ratio of specific heats (CPCV), number of steps used in the integration of the equations (FJUMP), either the dimensionless electric field (EPSL) or the constraint that the dimensionless electric field equal the induced electric field at the upstream conducting boundary of the flame ($INDUCED$), unburnt gas reactant mass fraction (CSBO), length of the conducting zone (LCOND) or the constraint that the magnetic Reynold's number be infinite ($INFINITE$), the location of the center of the conducting zone (LCNTR), and the dimensionless conductivity (SIGMA) - approximately 0.1 of the magnetic Prandtl number. Output consisted of the dimensionless burning velocity - or the Mach number of the burning velocity - (MEW), the induced electric

field (MEW=PIBO) at the end of each iteration, and the flame structure, burning velocity, and induced electric field for the final iteration.

As the iterative technique outlined in Appendix 7 was found to be unstable for large values of PIBO when an infinite length of interaction between the fluid and the magnetic field was assumed, an alternate method of integration was used when the first method diverged (an event clearly marked by a call to the floating point overflow dispatcher - $(FPT) - or to the error dispatcher - $LDUMP). In this case, an integration using very coarse integration steps often converged; each step of the integration could then be subdivided into two steps, using the last iteration with the coarse step as the initial flame structure for the finer steps, interpolating for the intermediate points. This procedure was continued until a mesh of the desired fineness was reached. (It would have been simpler to have two separate programs for each procedure, using the second when the first was found to fail; however, the technique actually used maximized the output per run at a time when service at the M.I.T. Computation Center was slow.)

Solutions were obtained for several values of all the input variables, and for a large number of values of PIBO, SIGMA, LCOND, LCNTR, and QBAR to support the conclusion that, when electric currents are passed through the flame structure which are of the order of 5-25 milliamperes, there is no

effect on the burning velocity of the flame when a magnetic field is applied, irrespective of the position of the conducting zone within the flame's structure.

Current Field and Gas Particle Accelerations

The programs listed on the pages marked PATTERNS were written to evaluate the formulae in Chapter 5. The field of electric currents was calculated at a number of points within a region of interest, which began at the flame surface and had a height (HITE) specified as an input variable, and which extended for a specified width (SPAN) from the centerline (also specified as a program input). The height was divided into a number of rows (ROWS), and the width into a number of columns (KMS), with the chosen points at the intersection of the rows and columns. The programs accepted as inputs the ratio of electrode separation to cathode diameter - a/r'' -, the ratio of electrode separation to anode diameter - a/r' -, the distance of the flame below the electrodes as a fraction of the electrode separation - $Y_F/2$ -, the Hall parameter, the gas velocity at the downstream edge of the flame surface, the electrode separation (in meters), the magnetic field (in Tesla), the thickness of the column of gas - t -, the number of rows in the region of interest, and the number of columns in the region of interest.

Output consisted of normalized current densities (JX, JY), angles of current flow (JANGLE), and stream functions (SF) at each intersection of a row and column, and

fluid particle trajectories starting at the intersection of each column with the flame surface.

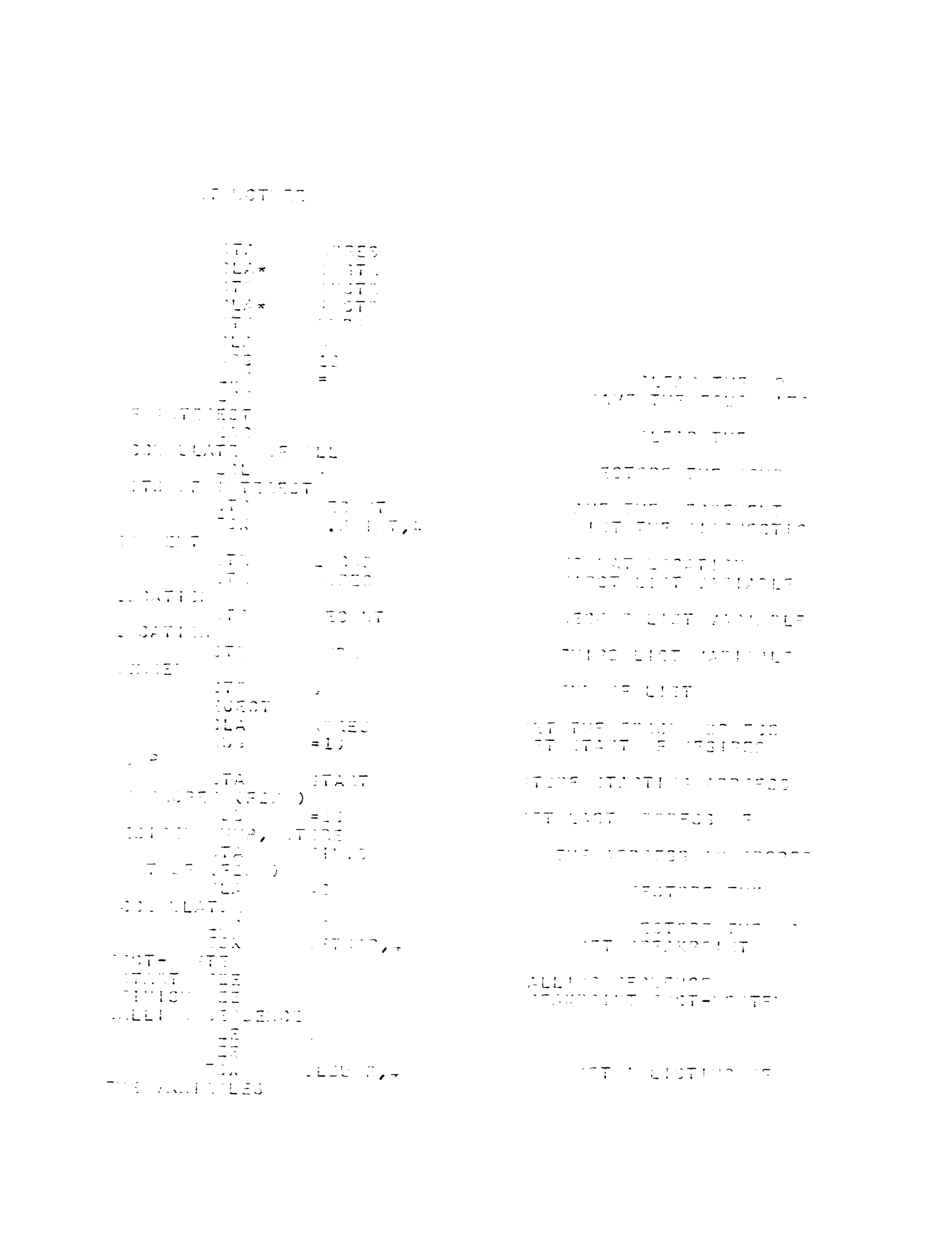

```
      ...STRUCTURE

                  ...CIT        1,3  ,...13                        F...AT
                  ...CIT        1,A...  ...                        F...AT
                   ...CIT       1,E  ...FE...                      F...AT
                   ...CIT       1,...  .  ...                      F...AT
                   ...CIT       1,  ...,...                        F...AT
                   ...CIT       1,...E   F                         F...AT
                   ...CIT       1,FL...  ...                       F...AT
                  ...CIT        1,  ...E...                        F...AT
                   ...CIT       1,  3,...                          F...AT
                   ...CIT       1,F...  ,                          F...AT
                   ...CIT       1,L  L...OA                        F...AT
                   ...CIT       1,  ...  ...TA                     F...AT
                   ...CIT       1,FL...  I                         F...AT
                   ...CIT       1,T  ...E...                       F...AT
                   ...CIT       1,  ...  ...I                      F...AT
                   ...CIT       1,L...ATI...                       F...AT
  ...E...          ...CIT       1,...3  ...F                       F...AT
                  ...CIT        1,...  .  )                        F...AT
                   ...CIT       1,/E...FL...                       F...AT
    ...E          ...CIT        1,(11                              F...AT
    ...           ...CIT        1,ALL                    ...P...  T...E ...LL
    ...E
                   ...CIT       1,...  ...

*                 ...
                   EXTE...AL F...OTI...
     ...TER...  ...  T...E ...TA ...E...IES ...EAFT...  ...  T...E I...TEG...ATI...S T...
    ...TAI... T...E
                   ...APHILES OF ...ONCE...TRATI... ...D TE...PERATURE
    ...ANTITI... T...E
                   TE...PERATURE DISTRIBUTI..., ...D T...E ...NETIC
    ...IELD.  ...TA
                   ...ICALCULATED ...E...  ...CH CALCULATI...  ...F T...E
    T...ETA ...OFILE,
                   ...URVED TO FIT THE ...ED...ANT T...ETA(1)= 1.0
    ...NDARY CONDITIO...
                   DIMENSION
    ...APPA(304),...ELTO(304),...ELTT(304),T...ETA(304),...ETTA(3
    ...04),...EYEE(304),...ELT(304),GA...MA(304),...PEED(304),T...T...(304),...
    ...M...A(304),...TAMA1(304),...TAMA2(304),...T...(100),...C...(100),...C...
    ...3...(100)
                   ...OMMON ...ATA
    ...APPA,...ELTO,...ELTT,T...ETA,...ETTA,...EYEE,...ELT,GA...
    ...A,...PEED,...UTI...,LE...S,...AM,...MAS,...I...,...ASTE,...P...V,...S...,...T...PS,...T...
```

```
.T*OSTOLE

      ,, E, T,,.E,,T,,/,E, ,KAPA,,EPS,,TI E3,3,I,,3,2,,3,3,3,,,  ,LO1
     3   ,,,EPSL,TOL  ,,IO,  ,,,,  ,,T,,,  ,FUN,P,FLI E
       ,,IVALE.OE (,PSIL, 3,  (I)),(,PSID,PSI,(I))
       ,TE,,  3, P,,E,,,  ,,,
       ,TE,,  ,
       ,,LE,,,  ,,  ,T ,,  ,,, I
       ,TE,,,EL  ,,STI,,,(I)
       ,,T,Y TO  ,,T,,.
       ,,STI,,  ,,T,,
   ,,A(I)*(,,ETTA(I)/2,,ELT(I)* E ,+EPSL)*(I,3  -
       ,,EPS,)
       ,,,  ,,,  ,,STI
       ,,T,,/T,,  ,,O,,L.
       ,,MEGLTA,,  ,,EL.
       ,,,  ,,,  ,,OSL,,  ,,  =  I,,I,  .,,.I
       ,,=  ,,  ,,O,,I
        ELTS(J,,,PS)=
,,,,,(J,,,PS).,,I.,,)*((,,T,,STI(L)+T,,ETA(J,,,PS))/2
       ,
,,,.,,.,)*((,,,EVTS(L)+,,EVTE(J,,,PS))/2.,).,,.,)*((EL,,ELT(L)+L
 ELT(J,,,PS))/2.,)/ E,*  ,,*,,,.(,,OSTI*(I.,-I.,/(T,,ETA(J,,,PS)+T
       ,,ETA(L))))
       ,,,LI=
,,E,*,,APPA(J,,,PS)-(T,,ETA(J,,,PS).,,.,S)*,ELTS(J,,,PS))/T
       ,  ,,
         E,,E/,  .,,I,,. ELTS(J,,,PS).,E. I.,-IO
        ,,,I=  ,,,,,A(J,,,PS)/ ELTS(J,,,PS)
        ,,E,,,ISE
        ,,,,I=  E,/,,,,
       ,,,,,F J,,,LITI  ,,L
       ,,,,,  ,,OS=L,,,,  = J,,,PS-I,-I,  .I.I
         ,,I  =  ,,,  ,,
         E,E,E  ,,,  J.  ELTS(  ).I,,  I.,-IO,,,,,I=
,,  ,,A(  )/,ELTS(  )
          ,,I=  ,,,,I+.J*,,KAPA*(T,,,  I+,,,,,S)
 ,OS,I,      ,ELTS(  )=
,( E,*(,,APPA(  )-,,APPA(L))-,,CA,*,,S,,I))=  .,/(T,,ETA(  )
       ,  .,.,.,S)+.,*,ELTS(  )
        ELTS(L)=  ,,.
 ,OSL      ,,KIOSTA  ,,I,,.
       ,,,STI,,,  ,,ETA,,,
       ,,T,,Y TO  ,,TTOAL.
       ,,,E  =  ,OSIL/LE,,O*,,CA,,
       ,,ETA(1)  =  I.,
         E  =  ,,,A*OST,,
```

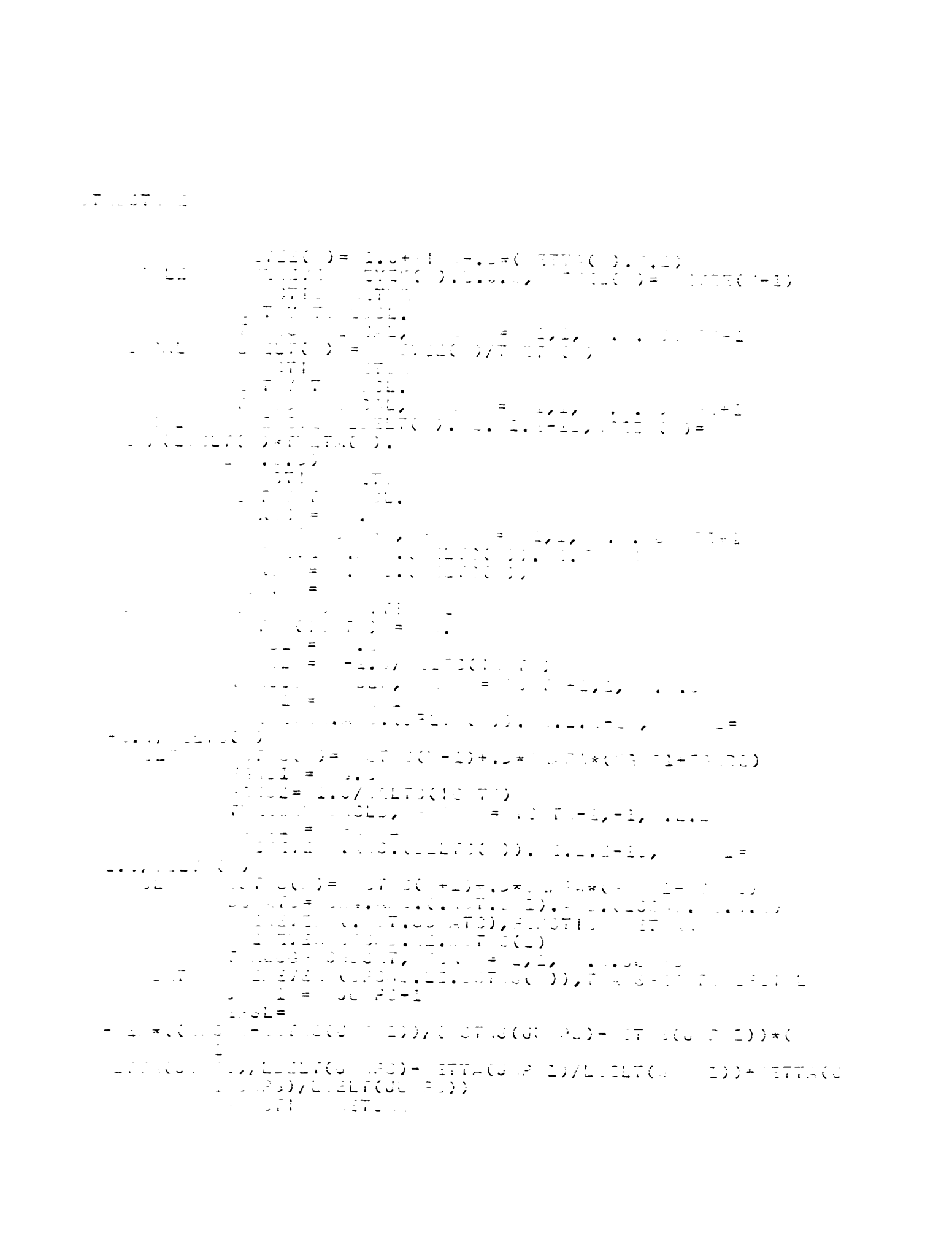

```
```

```
```

```
[illegible]

      [illegible]LINE = [illegible]LI[illegible]ES
      T[illegible] = [illegible]LI[illegible]ES. E. [illegible]
        [illegible]
     [illegible],LE[illegible], [illegible], [illegible], [illegible],ACTE,[illegible], [illegible], [illegible]
        [illegible]
      [illegible] = [illegible]
      [illegible]
      [illegible]
      [illegible], [illegible]
      [illegible]
        [illegible]
        [illegible]
      [illegible]
      [illegible],[illegible],[illegible]
      [illegible]AL
      [illegible]
      [illegible]
[illegible]   [illegible] = [illegible]*[illegible]
      [illegible] = [illegible]
      [illegible] = 1.0/[illegible]
      [illegible], [illegible] L= [illegible]+1,-1, [illegible]
      L1 = L-1
      L[illegible] = L1/2
      L[illegible] = L[illegible]+1
      KAPPA(L) = KAPPA(L[illegible])
      KAPPA(L1) = (KAPPA(L[illegible])+KAPPA(L))/2.[illegible]
      DELTO(L) = DELTO(L[illegible])
      DELTO(L-1) = (DELTO(L[illegible])+DELTO(L))/2.[illegible]
      DELTT(L) = DELTT(L[illegible])
      DELTT(L1) = (DELTT(L[illegible])+DELTT(L))/2.[illegible]
      THETA(L) = THETA(L[illegible])
      THETA(L1) = (THETA(L[illegible])+THETA(L))/2.[illegible]
      [illegible]ITTA(L) = [illegible]ITTA(L[illegible])
      [illegible]ITTA(L1) = ([illegible]ITTA(L[illegible])+[illegible]ITTA(L))/2.[illegible]
      [illegible]YEE(L) = [illegible]EYEE(L[illegible])
      [illegible]YEE(L1) = ([illegible]EYEE(L[illegible])+[illegible]EYEE(L))/2.[illegible]
      [illegible]ELT(L) = [illegible]ELT(L[illegible])
      [illegible]ELT(L1) = ([illegible]ELT(L[illegible])+[illegible]ELT(L))/2.[illegible]
      [illegible]A(L) = [illegible]A(L[illegible])
      [illegible]A(L1) = ([illegible]A(L[illegible])+[illegible]A(L))/2.[illegible]
      SPEED(L) = SPEED(L[illegible])
      SPEED(L1) = (SPEED(L[illegible])+SPEED(L))/2.[illegible]
      [illegible](L) = [illegible](L[illegible])
      [illegible](L1) = ([illegible](L[illegible])+[illegible](L))/2.[illegible]
      [illegible]A(L) = [illegible]A(L[illegible])
      [illegible]A(L1) = ([illegible]A(L[illegible])+[illegible]A(L))/2.[illegible]
      [illegible](L) = [illegible](L[illegible])
```

```
```

```
[illegible]

            TRANSFER TO [illegible]
              WHENEVER
  [illegible].1.2[illegible]. [illegible].[illegible].2.[illegible])[illegible]
            [illegible] (1) = [illegible]
            EXECUTE [illegible].
            PRINT FORMAT [illegible], [illegible], [illegible]
            TRANSFER TO [illegible]
              WHENEVER [illegible].[illegible].[illegible].[illegible]
            PRINT FORMAT [illegible]
            END OF CONDITIONAL
[illegible] EXECUTE [illegible].
[illegible] EXECUTE [illegible].
            EXECUTE [illegible].(1)
            [illegible] = [illegible].[illegible]*[illegible]
             WHENEVER [illegible]
             EXECUTE [illegible].
             TRANSFER TO [illegible]
            END OF CONDITIONAL
             WHENEVER [illegible] (0.1 [illegible]), TRANSFER TO
[illegible]
            EXECUTE [illegible].
            TRANSFER TO [illegible]
            ENTRY TO [illegible].
             WHENEVER [illegible]
[illegible] PRINT FORMAT [illegible]
            EPS = [illegible]
            [illegible] = 1.
            [illegible] = [illegible]
            EXECUTE [illegible].
            TRANSFER TO [illegible]
            [illegible]
            [illegible] = [illegible]
            [illegible] = [illegible]
            [illegible] = 1.0/[illegible]
            EPS = [illegible]* EPS
            [illegible] = 1.
            [illegible] = 1.
            TRANSFER TO [illegible]
            END OF CONDITIONAL
[illegible] PRINT FORMAT [illegible],[illegible], [illegible]
            WHENEVER [illegible], PRINT FORMAT [illegible],EPSL
[illegible] WHENEVER [illegible], EXECUTE [illegible].
            EXECUTE [illegible].
            [illegible]
*           [illegible]
[illegible]
            [illegible] FUNCTION
```

```
```

```
```

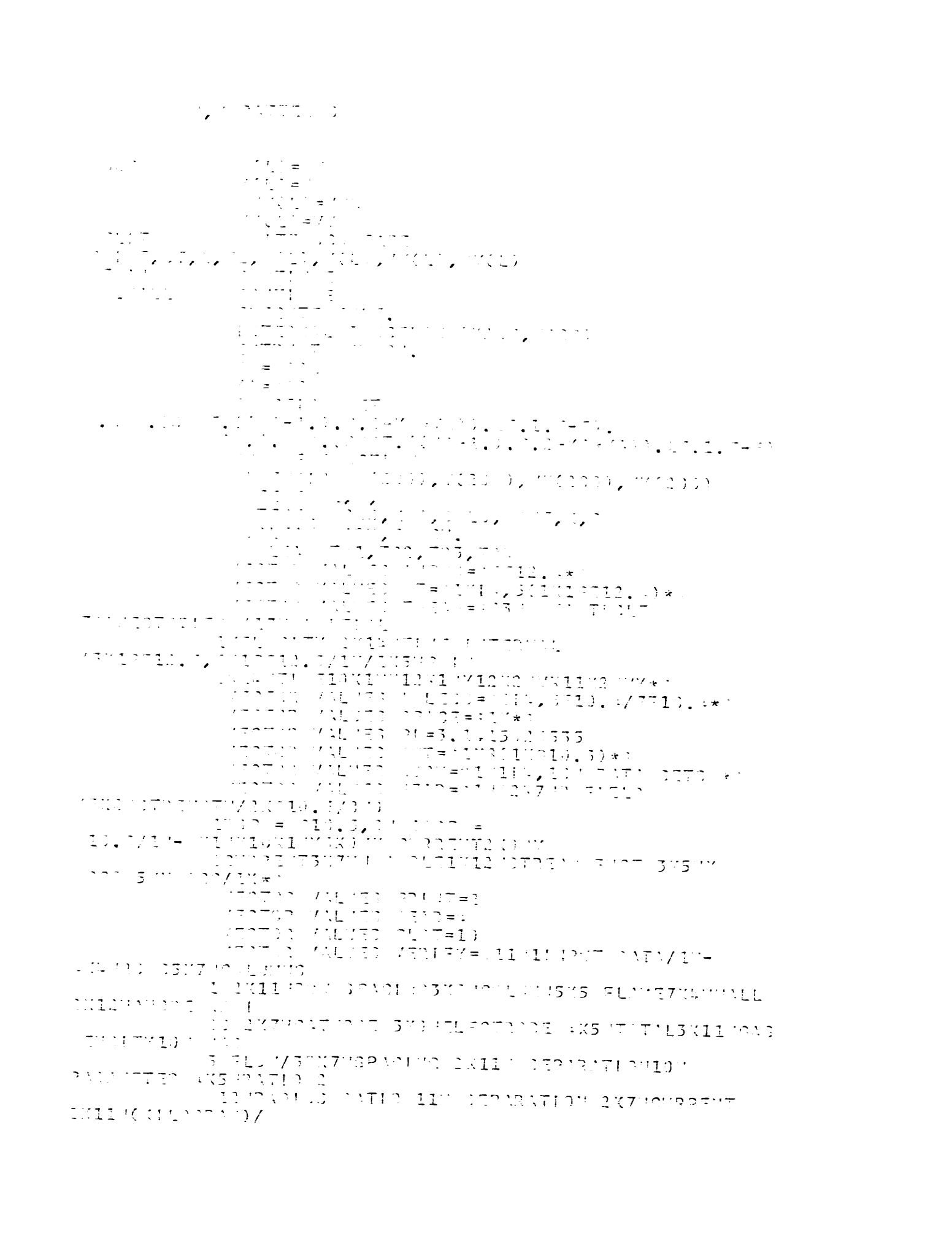

```
```

```
      I/O PATTERNS


            ATA=ARG1
            ETA=ARG2
            PHI=0.
            TRANSFER TO SET
            ENTRY TO ASSET.
            ATA=ARG1
            ETA=ARG2
            PHI=-PI/2.
  SET       W1=SIN.(ATA)*SIN.(ETA)
            ZW = COS.(ETA)*COS.(ATA)-1.
            W2=((ATA.G.PI).AND.(ATA.LT.2.*PI))
.AN.((ATA.G.PI).AND.(ZW.
           L E. 0.))
            W2=((ATA.L.PI).AND.(ATA.GE.1.))
.OR.((ATA.L.PI).AND.(ZW.LE.
           0.))
            W1=ETA.GE.0.
            WHENEVER .NOT.(ZW) .GE. 1.E-38
            PHI = ATAN.(W1/ZW)
            TRANSFER TO SET
            END OF DEFINITION
            WHENEVER .NOT.W1 .AND. W2)
.OR.
(. NOT.W1).AND.W2
            FUNCTION RETURN (1.5*PI+PHI)
            WHENEVER (. NOT.
W1).AND.W2).OR.(W1.AND.W2)
            FUNCTION RETURN (PI/2. + PHI)
            END OF DEFINITION
  SET       W3=PHI .GT. 0.
            WHENEVER ETA .G. 0., FUNCTION RETURN PHI
            WHENEVER PHI .NE. W2 .AND. W3
            FUNCTION RETURN (ANGLE + PI + PHI)
            WHENEVER W1 .AND. W2 .AND.(.NOT.W3)
            FUNCTION RETURN (ANGLE +2.*PI - PHI)
            WHENEVER W1 .AND. W2 .AND.(.NOT.W3)
            FUNCTION RETURN (ANGLE+PI+PHI)
            WHENEVER W1 .AND. W2 .AND. W3
            FUNCTION RETURN (ANGLE+PHI)
            WHENEVER (.NOT.W1).AND.W2 .AND. W3
            FUNCTION RETURN (ANGLE+PHI)
            WHENEVER (.NOT. W1).AND.W2 .AND.(.NOT.
W3)
            FUNCTION RETURN (ANGLE+PI+PHI)
            WHENEVER (.NOT. W1).AND.(W2).AND.W3
            FUNCTION RETURN (ANGLE+PI+PHI)
            WHENEVER (.NOT.W1).AND.W4.AND.(.NOT.W3)
            FUNCTION RETURN (ANGLE+2.*PI+PHI)
            ATTENTION
            PRINT FORMAT 100,ETA,ATA,ANGLE/PI*180.
            WHENEVER ERR
            END OF DEFINITION
            SUBPLEN W1,W2,W3,W4
            VECTOR VALUES DEF=(1/1-TRUE) W1 ETA,,= ETA.*,
```

```
     1,X PATTERNS


          1 5HY= F14.3,10HINITIAL ETA= F14.3*G
           VECTOR VALUES ZOOF=G33'-ERROR IN TRER', ZETA=
F14.3,5HETA= F
           14.3, MAXCLT= F14.3,3H DEGREES*G
           VECTOR VALUES PI=3.1415926535
           END OF FUNCTION
  SPHS     C  THIS SUBROUTINE WILL CALCULATES CURRENT
DENSITY
           SUBROUTINE SPHSUB(ARG1,ARG2)
           ENTRY TO SPHSUB.
           ZOOF=ARG1
           ZOOP = ARG2
           FUNCTION RETURN
           ENTRY TO SPHSUB.
           XALL = ARG1
           FUNCTION RETURN
           ENTRY TO ZDET.
           ZETA = ARG2
           ETA = ARG1
           SUM2=.5
           ZOOF=ZOOP-ZOOP
           THROUGH A001,FOR I=1,1, I.G. 200
           ZPS=
A001*(1.-2.*EXPT.(2.*I*ZOOF)+EXPT.(4.*I*ZOOF))+(1.+2.*EXP
          1 .(2.*I*ZOOF)+EXPT.(4.*I*ZOOF))
           ZEOS=
-EXPT.(I*(ZETA+ZOSP-2.*ZOOP))*(I*I*(1.-EXPT.(2.*I*(ZOSP
          I
ZOOP)))-(1.+EXPT.(2.*I*(ZOSP-ZOOP))))+EXPT.(I*(ZOSP-ZETA))*
          I
I*I*(1.-EXPT.(2.*I*(ZOSP-ZOOP)))+(1.+EXPT.(2.*I*(ZOSP-ZOOP)
          3 ))
           ZPSI=
2.*I*EXPT.(I*(ZETA+ZOSP-2.*ZOOP))*(1.-EXPT.(2.*I*(ZOSP-
          1 ETA)))
           TERM=
(-1).P.I)/EPS*(SIN.(I*ETA)*ZPSI+COS.(I*ETA)*ZEOS)
           SUM2=SUM2+TERM
  A001     REMEMBER .ABS.(TERM/SUM2) .L. 1.E-4,TRANSFER
TO SUM1
  SUM1     FUNCTION RETURN
COSH.(ZETA)-COS.(ETA))/PI*SUM2
           ENTRY TO ZDET.
           ETA = ARG1
           ZETA = ARG2
           SUM3= 1/2.
           ZOOF=ZOSP-ZOOP
           THROUGH A002,FOR I=1,1, I.G. 200
           ZPS=
A002*(1.-2.*EXPT.(2.*I*ZOOF)+EXPT.(4.*I*ZOOF))+(1.+2.*EXP
          1 .(2.*I*ZOOF)+EXPT.(4.*I*ZOOF))
           ZEOS=
2.*I*EXPT.(I*(ZETA+ZOSP-2.*ZOOP))*(1.+EXPT.(2.*I*(ZOSP-
```

```
J, / PATTERNS

            1 ETA-2.*ZOSP)))
              TEMP=
EXPT.(I*(ZETA+ZOSP-2.*ZOSP))*(I*I*(1.-EXPT.(2.*I*(ZOSP-
            1
ZOSP)))-(1.+EXPT.(2.*I*(ZOSP-ZOSP))))+EXPT.(I*(ZOSP-ZETA))*(I
            1
*(1.-EXPT.(2.*I*(ZOSP-ZOSP)))+(1.+EXPT.(2.*I*(ZOSP-ZOSP)))
              TEMP=
((-1).**I)/TEMP*(SIN.(I*ETA)*COSH(COS.(I*ETA)*SINH
              SUM=SUM+TEMP
 1000         WHENEVER .ABS.(TEMP/SUM).L.1.E-6, TRANSFER TO
+1000
 +1002        FUNCTION RETURN
 TEMP=(ZETA)-LOG.(ETA))/PI*SUM
              INTERNAL FUNCTION (COS)
              ENTRY TO EXPT.
              X=COS
              WHENEVER ABS.X .L. -10.123
              FUNCTION RETURN EXP.(1.23)
              OTHERWISE
              FUNCTION RETURN X.
              END OF CONDITIONAL
              END OF FUNCTION
              INTEGER I
              DIMENSION VALUE(ALL,)
              RESERVE VALUES PI=3.1415926535
              END OF FUNCTION
   INIS       THIS IS A SUBROUTINE WITH TWO ENTRIES
            ! ANGLE, GIVES THE ANGLE OF THE CURRENT FIELD,
            ! AND MAG, GIVES THE ABSOLUTE STRENGTH OF THE
            ! CURRENT DENSITY.  BOTH OF THESE ARE IN
ENTER
            ! POINT IF THE X,Y PLANE.  THE CALLS ARE
            !       ANGLE=ANGLE.(X,Y)
            !       MAG=MAG.(X,Y)
            !  IF EQUIVALENT ACCURACY IN ARITHMETIC
EXPRESSION
              ENTERNAL FUNCTION (X,Y)
              ENTRY TO ANGLE.
              I=X
              J=Y
              AMI=M(I,J)
              AMJ=M(I,J)
              WHENEVER AMI .E. 1.
              ANGLE=ATAN.(AMJ/AMI)
              OTHERWISE WHENEVER AMJ .E. 1.
              ANGLE=(1.-SIN.(AMJ))/AMJ*PI/2.
              OTHERWISE
              ANGLE=PI/2.
              END OF CONDITIONAL
              WHENEVER AMI .L. 1.,ANGLE=ANGLE+PI
              FUNCTION RETURN ANGLE
              ENTRY TO MAG.
```

```
      !,/ PATTERNS

                  X=X(
                  Y=Y(
                  FUNCTION RETURN
     1*T.(AA.(X,Y).*.2+AY.(X,Y).*.2)
                  /EXTRA /ALWAYS PI=3.14159265359
                  END IF SUBROUTINE
     *ERR          ! ! INTRINSIC *ILMY *AYXIAR: THE *ATTRACTIO
     2*IC SUBROUTINE
                  ! ! TYPICAL INTEGER
                  ENTRY *IL FLOATING (X***)
                  ENTRY TO ZERO.
                  *** = 0.0*
                  *ITERATE .OR.(*.EQ.0.0).L. 30.***
                  FLOATING RETURN 2./(EXP.(***)+EXP.(-***))
                  *ITER *ISE
                  FLOATING RETURN 0.
                  END IF *ATTRACTIVE *IL
                  ENTRY TO ZERO.
                  *** = 0.0*
                  FLOATING RETURN *EXP.(***)+EXP.(-***/2.
                  ENTRY TO ZERO.
                  *** = 0.0*
                  FLOATING RETURN (EXP.(***)-EXP.(-***))/2.
                  ENTRY TO ZERO.
                  *** = 0.0*
                  *ITERATE .AND.(***).L. 30.123
                  FLOATING RETURN 2./(EXP.(***)-EXP.(-***))
                  *ITER *ISE
                  FLOATING RETURN 1.
                  END IF *ATTRACTIVE *IL
                  ENTRY TO ZERO.
                  *** = 0.0*
                  *ITERATE .AND.(***) .L. 30.123
                  FLOATING RETURN
     .EXP.(***)-EXP.(-***))/(EXP.(***)+EXP.(-***)
                  *F *ITERATE *** .LT. -30.123
                  FLOATING RETURN -1.
                  *F *ITERATE *** .GE. 30.123
                  FLOATING RETURN 1.
                  END IF *ATTRACTIVE *IL
                  ENTRY TO ZERO.
                  *** = 0.0*
                  *ITERATE .AND.(***) .L. 30.123
                  FLOATING RETURN
     EXP.(***)-EXP.(-***))/(EXP.(***)+EXP.(-***)
                  *F *ITERATE *** .LT. -30.123
                  FLOATING RETURN -1.
                  *F *ITERATE *** .GT. 30.123
                  FLOATING RETURN 1.
                  END IF *ATTRACTIVE *IL
                  ENTRY TO ZERO.
                  *** = 0.0*
                  *I=INT.(A**X**-1.)
```

```
      1,/ PATTERNS

            FUNCTION RETURN ASINH.(SIN)
            ENTRY TO ASIN.
            ARG = SIN
            FUNCTION RETURN ATAN.(ARG)
            ENTRY TO ACOS.
            ARG = SIN
            FUNCTION RETURN ASIN.(1./ARG)
            ENTRY TO ATAN2.
            ARG = SIN
            FUNCTION RETURN ATAN.(ARG/SQRT.(1.-ARG*ARG))
            ENTRY TO SINH.
            ARG = ARG
            WHENEVER ARG.L.0.
             ARG=-1.
            OTHERWISE ARG.G.0.
             ARG=1.
            END OF CONDITIONAL
            PRINT RESULTS ARG
            EXECUTE BUILT.
            END OF CONDITIONAL
            FUNCTION RETURN
(ARG*ASINH.(1./ABS.(ARG*ARG-1.)))
            ENTRY TO COSH.
            ARG = ARG
            ARG=1./SQRT.(ARG*ARG-1.)
            FUNCTION RETURN ASINH.(ARG)
            INTERNAL FUNCTION (ARG2)
            ENTRY TO ASINH.
            ARG2=ARG2
            WHENEVER ARG2 .GE. 1-256.)
             ARG = (ARG2+SQRT.(ARG2*ARG2+1.))
            OTHERWISE
            ARG = 1.
            COEF = 1.
            ARG2=.333.(ARG2)
            TERM = ARG2
            THROUGH NEXT,FOR I=1,1,
(I.L.300).IF.(TERM.G.1.E-7.)
            TERM = TERM*(ARG2*ARG2)
            COEF = (1-2*I+1)*COEF/(2*I)
  NEXT      ARG=ARG+TERM*COEF
            END OF CONDITIONAL
            FUNCTION RETURN LOG.(ARG)
            END OF FUNCTION
            INTEGER I
            VECTOR VALUES PI = 3.14159265358
            END OF FUNCTION
  SANTA     R  ROUTINE TO DISTRIBUTE PARAMETERS TO THE
             ORKING SUBROUTINES.  IT IS CALLED BY A CALL
IF
            R   THE FORM
            R EXECUTE SANTA.(A,B,C,.....,Z)
            R WHERE THE PARAMETERS ARE THOSE TO BE
SUBSEQUENTLY
```

```
1,7 PATTERNS


      ! DISTRIBUTED TO THE VECTOR SUBROUTINES
      EXTERNAL FUNCTION (YE,ZDSP,ZDSP,WALL,DSEE)
      ENTRY TO INITA.
      YE=^TYE.(YE,YE)
      EXECUTE ST1PUR.(ZDSP,ZDSP)
      EXECUTE ST2PUR.(WALL,WALL)
      FUNCTION RETURN
      END OF FUNCTION
C     ! THIS INITIAL ROUTINE TURNS ENTRIES -UX.,UY.,
      ^TYE. THE FIRST TWO ^TYE, RESPECTIVELY, THE
C
C     ! DESCRIBES AN ELECTRIC CURRENT PATTERN
C
C     ! MULTIPLY BY MAGNITUDE OF CURRENT YE.  THE
C
C     ! MULTIPLE CURRENT PATTERNS ARE THUS DESCRIB
C
      UNIT. UX. UDT.
      THE ! ITEMS ARE CALLED BY A CALL IN THE MAIN
            UX=UX.(X,Y)
            UY=UY.(X,Y)
            UT=^TYE.(YE,YE)
C     ! NOW IT USED TO INITIATE EXPRESSIONS AS
C     ! ELEMENTS INPUT FUNCTIONS
      EXTERNAL FUNCTION(XJ,YJ)
      ENTRY TO IX.
      X=XJ
      Y=YJ
      ZD=ZETA.(X,Y)
      ET=ETA.(X,Y)
      DDDX=
DDD.(UDZT.(ET,ZD))*(UDET.(ET,ZD))+DDS.(UDZT.(ET,ZD))
     1 *UDZT.(ET,ZD)
      XI=X
      YI=-(2.*.ADS.(YE)+Y)
      ZDI=ZETA.(XI,YI)
      ETI=ETA.(XI,YI)
      IMIDX=
DDS.(UDZT.(ETI,ZDI))*(UDET.(ETI,ZDI))+DDS.(UDZT.(
     1 ETI,ZDI))*UDZT.(ETI,ZDI)
      FUNCTION RETURN (DDDX+IMIDX)
      ENTRY TO IY.
      X=XJ
      Y=YJ
      ZD=ZETA.(X,Y)
      ET=ETA.(X,Y)
      DDDY=
DDL.(UDZT.(ET,ZD))*(UDET.(ET,ZD))+DDL.(UDZT.(ET,ZD))
     1 *UDZT.(ET,ZD)
      YI=X
      YI=-(2.*.ADS.(YE)+Y)
      ZDI=ZETA.(XI,YI)
      ETI=ETA.(XI,YI)
```

```
      1,/ PATTERNS


                  HIMY=
     (SI*.(MODET.(ETI,ZDI))*(MDET.(ETI,ZDI))+SI*.(MODET.(
                 1 ETI,ZDI))*MDET.(ETI,ZDI))
                  SUMSTI=1 'ETMIN' (MDOY-HIMY)
                  WRITE TO 'TYP'.
                  YP=Y'
                  SUMSTI=1 'ETMIN' YP
                  END OF SUMSTI=1
        HITY      THIS IS A SUBROUTINE WITH THE PARAMETERS.  IT
     'ETMIN'
              THE (XX) TRANSPORT OF THE PATIO OF THE FIRST TO
     ---
                  ----, IN THE CONSTANT WINDOWS.  IT IS
     'ILLED' YY
                  . 'ITY' OF THE DAY
                    'HOLE= ETM.(Y,Y)
                    ---- ------ ' ' [TRANSFER EXPRESSIONS TO '
     -- 'ETI' '
                  'ILLED' 'I'ILL'
                  ---------- ---------- ' ',')
                  ---------- ---- ' '.
                  '=.
                  '=1
                  'ETMIN'1 . . . .
                  SUCLI='ETI'.(Y/X)
                  ' 'ETMIN' ' .IT. '.
                    '''LI=Y/2.
                  ------ ---
                  ---------- ---
                  ---------- ---- ).
                  ---- ---------- '.
                  'ETI'1=---- . '' . '.
                  'ETI'2=' . '' . '
                  '------' 'ETI'1 . ' . . 'ETI'2
                  ---------- 'ETMIN' ' ' '.
                  ---- ---------- (. '' . 'ETI'1).' . . 'ETI'2
                  ---------- 'ETMIN' ' 'ETI'
                  ---- ---------- 'ETI'1 . ' . . '' . 'ETI'2)
                  ---------- 'ETMIN' '---- - '!
                  ---- ---------- (. '' . 'ETI'1).' ID.(. '' . 'ETI'2)
                  ---------- 'ETMIN' '---
                  ---- ---------- '''''
                    'LEN' 'ETI'1,'ETI'2
                  ' ' 'IL'=0.54!-'ETI' 'ILLED' 'ITH 'ETI' 'AR'ITERS'
     'EIC', 'ETI' '
                  ------ ---
                  'ETI'2' 'VALUES' '=5.I+13'1.1335
                  --- OF 'UNCTION'
```

APPENDIX 3

ELECTRICITY IN FLAMES - EARLY HISTORY

The references cited in the main text do not comprise a complete history of the subject of electricity and magnetism in flames. However, works earlier than those cited in the text contain no material which could contribute to the technical needs of this thesis, and are included in this appendix as a matter of historical interest.

The study of electricity in flames began with Gilbert[18] who, in 1600, reported that a charged amber rod could deflect the flow of smoke from a smoldering candle. While this effect was probably some manifestation of the Chattock electric wind, Gilbert's own interpretation was in terms of the attraction and flow of an "electric fluid". Penning[44] reports that the Florentine Academy of Experiment had studied the conducting character of flames in 1667, but cites no references. Volta's experiments on "contact electricity" (Ref. 56, p. 399) included experiments in which products of combustion were used to discharge a condensor. Apparently, Volta apparently offered no mechanism for the conduction of the electricity by the flame. Wilson[66] gives a good summary of the state of knowledge concerning electricity in flame gases which existed in the early 20th century, immediately before the hypothesizing of the electron. Wilson's work, however, was not concerned

with the reaction zone's conductivity, but rather studied ionic mobility, electrode sheaths, and seeding of the hot products of combustion.

Thompson[55] mentions a magnet at the University of Genoa with which Bancalari studied the "magnetic properties of flame" in 1848. Just what Bancalari studied was left unmentioned, and Thompson gives no references. Von Engel and Cozens[63] give an analysis in which they show that a flame - free of paramagnetic molecular oxygen - in a nonuniform magnetic field, surrounded by air - which contains paramagnetic molecular oxygen - will be deflected, and cite experiments in which such effects might have been at play.

APPENDIX 4

ERROR ANALYSIS OF PARTICLE-TRACK TECHNIQUE

The particle track technique described in Chapter 4 is subject to several sources of error; thermomechanical diffusion, gravitation, and inertial lag[15]. Of these, only the last is of significance under the conditions used in the course of the present work.

Inertial lag results from the fact that the particles being carried along with an accelerating flow must be accelerated by a viscous drag force; as the existance of this force requires that a difference in velocity between the fluid and the particle exist, it is apparent that the particle cannot faithfully follow the flow of an accelerating fluid. The equation governing this lag is a modified form of Stoke's law giving the relation between particle velocity - U_p - and stream velocity - U_g - (Ref. 28).

$$\frac{4}{3}\pi r_p^3 \rho_p \frac{dU_p}{dT} = 6\pi\mu r_p (U_g - U_p)$$

or

$$U_g - U_p = \frac{2 r_p^2 \rho_p}{9\mu} \frac{dU_p}{dT}$$

In order to estimate the probable error in the measurement of U_g from this lag, it is necessary to have the probability distribution function of r_p and the value of μ ; a maximum error estimate can then be obtained by taking the largest value of dU_p/dT observed, and evaluating $(U_p - U_g)/U_p$ for the particle whose diameter lies above that of 50% of the parti-

cles and the particle whose diameter lies above that of 90% of the particles.

The particle weight distribution function - $f_w(r_p)$ - as a function of radius for the silica "Celite 503" particles used in the present work is available in Reference 28. This may be converted to a number distribution function - $f_N(r_p)$ - by employing the relation between size and mass of a particle of specified density to determine the number of particles of a given size which make up a given mass of particles. The conversion is

$$f_N(r_p) = \frac{C'}{r_p^3} f_w(r_p)$$

where C' is determined by the requirement that the relation

$$\int_0^\infty f_N(r_p)\, dr_p = 1 = C' \int_0^\infty \frac{f_w(r_p)}{r_p^3}\, dr_p$$

must hold (by definition of f_N and f_w) so that

$$f_N(r_p) = f_w(r_p) \Big/ \left[r_p^3 \int_0^\infty \frac{f_w(r_p)}{r_p^3}\, dr_p \right]$$

The data available is in the form of the fraction of particles lying in given weight ranges; however, the shape of $f_w(r_p)$ within these ranges is not given, so that there is a necessity for the assumption of some shape of function. If the weight distribution function - $f_w(r_p)$ - were assumed to be a constant in each size range, then the related number distribution function - $f_N(r_p)$ - would be weighted too heavily to the small size particles: conversely, assumption that the number distribution function were constant in each size interval would mean that the corresponding weight distribution function was too heavily weighted to heavy particles. In an

attempt to strike a balance between these two cases, the distribution functions will be assumed to be impulse functions centered in each size range. Thus, the weight and the number distribution functions will have the same form in each size range.

With this assumption, it is possible to perform the operations outlined above and obtain the number distribution function for the particles as a function of diameter:

range of particle diameters (microns	mass fraction of particles in diameter range	number fraction of particles in diameter range
0-1	0	0
1-2	.005	.005
2-6	.135	.641
6-10	.195	.136
10-20	.290	.149
20-40	.255	.065
40-70	.120	0

It should be noted that approximately 50% of the particles have diameters below 5 microns, and approximately 90% below 17 microns. The error in velocity

$$U_g - U_p = K \frac{dU_p}{dT} \qquad \left(K = \frac{2r_p^2 \rho_p}{9\mu}\right)$$

may be evaluated with a knowledge of K and the observed $\frac{dU_p}{dT}$. In order to evaluate K, it is necessary to know μ; if the variation of μ with temperature is assumed the same as that

for air, Friedman's data[13] on the temperature profile of a flame may be used to evaluate the viscosity at various points in the flame; these become the following:

location	viscosity
burner head	401.4 micropoise
start of luminous zone	490.6 "
end of luminous zone	515.0 "
burnt gas	515.0 "

Consequently, the parameter K becomes, for the 17 micron and 5 micron diameter particles

location	K - 17 micron particle	K- 5 micron particle
burner head	9.05×10^{-4} sec.	7.84×10^{-5} sec.
upstream edge of flame surface	7.40×10^{-4} "	6.4×10^{-5} "
downstream edge of flame surface	7.05×10^{-4} "	6.1×10^{-5} "
burnt gas	7.05×10^{-4} "	6.1×10^{-5} "

The greatest particle acceleration observed was at the upstream edge of the luminous zone, in a case when the Lorentz force was against the flow direction. The observed acceleration was 1100 ft./sec.^{2}, and the local velocity was approximately 3.8 ft./sec.. The errors in velocity for a 5 micron diameter particle and for a 17 micron diameter particle would then be

17 micron diameter particle	0.8 ft./sec.
5 micron diameter particle	0.1 ft./sec.

Usually, downstream of the flame, accelerations were far less than this, being approximately 200 ft./sec.^{2}, so that a 90% certainty can probably be assigned to saying that the viscous drag error of a particle is less than .2 ft./sec., and a 50% certainty to saying that it is less than .03 ft./sec. in the region of interest - e.g., the region downstream of the flame.

The accuracy of the signal generator driving the stroboscope was probably as accurate as the oscilloscope used for calibration - generally assumed by Textronix as 2-3%; the all-electronic stroboscope probably has a negligable random delay after recieving a pulse from the square-wave generator. Thus, the range of the stroboscope error would be about 0.1 ft./sec., in a region where the flow was about 4.0 ft./sec..

Due to the small angle subtended by the field of view, distortion was not detectable when such regularly structured things as chicken wire, rulers, etc. were placed in the field of view.

All of the ranges of error may be summarized as:

inertial lag	0.2 ft./sec.
error in measuring pictures	0.1 ft./sec.
error in stroboscope calibration	0.1 ft./sec.

so that the sum of the ranges of error is 0.4 ft./sec. This was assumed, in the analysis of data, to split up evenly to ± 0.2 ft./sec.

APPENDIX 5

SOME DEMONSTRATIONS ON THE CURRENT PATTERNS

This appendix presents some elementary demonstrations concerning the nature of two-dimensional current patterns (having only x- and y- components) and of the Lorentz force fields arising from these, when a steady and uniform magnetic field is applied in the z-direction.

The current patterns are assumed to arise from the application of a two-dimensional, steady-state electric field to a gas with no net charge, having a constant conductivity and a constant Hall parameter - H . It will be shown that:

1) The current patterns are irrotational.

2) The Lorentz forces arising from these currents are the gradient of a potential.

Irrotationality of the Current Patterns

Application of the generalized Ohm's law to the current arising from an $\vec{E}$ field of two components - E_x and E_y - gives the components of current as

$$J_x = \frac{\sigma}{1+H^2}(E_x + H E_y)$$

$$J_y = \frac{\sigma}{1+H^2}(E_y - H E_x)$$

$$J_z = 0$$

so that $\vec{\nabla} \times \vec{J}$ becomes

$$\vec{\nabla} \times \vec{J} = \frac{\partial J_y}{\partial X} - \frac{\partial J_x}{\partial Y} = \frac{\sigma}{1+H^2}\left(\frac{\partial E_y}{\partial X} - H\frac{\partial E_x}{\partial X} - \frac{\partial E_x}{\partial Y} - H\frac{\partial E_y}{\partial Y}\right)$$

$$= \frac{\sigma}{1+H^2}\left(\vec{\nabla} \times \vec{E} - H \vec{\nabla} \cdot \vec{E}\right)$$

Under the conditions of a steady state electromagnetic field and no net charge in the gas, $\vec{\nabla} \times \vec{E}$ and $\vec{\nabla} \cdot \vec{E}$ are zero, so that the current is rotation-free. This, in conjunction with the solenoidal nature of the electric current, means that the current patterns may be derived from a potential $-\mathcal{H}$ - such that

$$\vec{J} = \vec{\nabla} \mathcal{H}$$

or from a stream function - b - such that

$$\vec{J} = \frac{\partial b}{\partial Y} \vec{i} - \frac{\partial b}{\partial X} \vec{J}$$

where both b and $\mathcal{H}$ obey Laplace's equation.

The Potential Nature of the Lorentz Force Field

Given, as shown before, that

$$\vec{J} = \frac{\partial b}{\partial Y} \vec{i} - \frac{\partial b}{\partial X} \vec{J}$$

and that $\vec{B} = B\vec{k}$ leads to a Lorentz force

$$\vec{J} \times \vec{B} = B\left(\frac{\partial b}{\partial X} \vec{i} + \frac{\partial b}{\partial Y} \vec{J}\right)$$

$$= \nabla(B b)$$

Thus, the Lorentz force, under the stated conditions, is derivable from a potential $-Bb$ - which corresponds to the stream function of the current patterns.

The assumption of a constant magnetic field over the working volume of interest was a good one in the apparatus used in this thesis as, over a portion of the working volume of the air-core magnet of approximately 1. cubic inch (the approximate size of the region observed in the particle-track pictures and in the $\vec{E}$ field measurements) no

measurable variation in magnetic field intensity could be found with a Rawson rotating-coil gaussmeter. Along this line, it should be noted that the air-core magnet was designed so that its mean dimensions corresponded to a Helmholtz pair, in order to enhanche field uniformity.

APPENDIX 6

DETERMINATION OF THE FOURIER SERIES FOR THE PROBLEM IN CHAPTER 5

As stated in Chapter 5, the solution to Laplace's equation in bipolar coordinates may be expressed as a Fourier series

$$\psi = A\xi\eta + B\xi + C\eta + \sum_{N=1}^{\infty} \sin(N\eta)\left(A_N e^{N\xi} + B_N e^{-N\xi}\right) + \cos(N\eta)\left(C_N e^{N\xi} + D_N e^{-N\xi}\right) \qquad \text{(A6-1)}$$

where

$$J_\xi = \frac{1}{h}\frac{\partial \psi}{\partial \xi} \qquad \text{(A6-2a)}$$

$$J_\eta = \frac{1}{h}\frac{\partial \psi}{\partial \eta} \qquad \text{(A6-2b)}$$

$$h \equiv a/(\cosh\xi - \cos\eta) \qquad \text{(A6-2c)}$$

It should be noted that $\eta(X,Y)$ is a multi-valued function; i.e., at a given point in the x,y plane, η has an infinity of values, each separated from its neighbor by 2π. In order that $J_\xi \left(= \frac{1}{h}\frac{\partial \psi}{\partial \xi}\right)$ be single-valued (a physical requirement), A must equal zero. Then the boundary conditions on J_ξ and J_η become: first, that $\vec{J}$ lie at an angle of $\tan^{-1}(H)$ to the normal to the cathode surface $-\xi = \xi''$-

$$\begin{aligned} (J_\eta)_{\xi''} &= H(J_\xi)_{\xi''} \\ \left(\frac{\partial \psi}{\partial \eta}\right)_{\xi''} &= H\left(\frac{\partial \psi}{\partial \xi}\right)_{\xi''} \end{aligned} \qquad \text{(A6-3)}$$

and second, that the current flow from the anode be concentrated at the point on the anode nearest the cathode, or that the current density at the anode $-\xi = \xi'$- is an

impulse function

$$\frac{1}{h}\left(\frac{\partial \psi}{\partial \xi}\right)_{\xi'} = i\ \delta(\eta - \pi) \qquad \text{(A6-4)}$$

(where i is a scaling factor to be determined later). Equations A6-1 and A6-2 imply that J_ξ and J_η are expressed as Fourier series, and the equating of two separate Fourier series (as in A6-3) can only be accomplished if the coefficients of their terms are identical, term by term.

Since

$$\frac{\partial \psi}{\partial \xi} = B + \sum_{N=1}^{\infty} N\left[(\sin N\eta)(A_N e^{N\xi} - B_N e^{-N\xi}) + (\cos N\eta)(C_N e^{N\xi} - D_N e^{-N\xi})\right] \qquad \text{(A6-5)}$$

and

$$\frac{\partial \psi}{\partial \eta} = C + \sum_{N=1}^{\infty} N\left[(\sin N\eta)(-C_N e^{N\xi} - D_N e^{-N\xi}) + (\cos N\eta)(A_N e^{N\xi} + B_N e^{-N\xi})\right] \qquad \text{(A6-6)}$$

and since the constraint of equation A6-3 involves matching A6-5 and A6-6 term by term, the following relations are obtained for the coefficients

$$C = HB \qquad \text{(A6-7)}$$

and

$$A_N(He^{N\xi''}) + B_N(-He^{-N\xi''}) + C_N(e^{N\xi''}) + D_N(e^{-N\xi''}) = 0 \qquad \text{(A6-8)}$$

$$A_N(e^{N\xi''}) + B_N(e^{-N\xi''}) + C_N(-He^{N\xi''}) + D_N(He^{-N\xi''}) = 0 \qquad \text{(A6-9)}$$

At the anode - $\xi = \xi'$ - the Fourier series for $\frac{\partial \psi}{\partial \xi}$ (A6-5) is made to fit the boundary condition - A6-4 - by the usual methods for Fourier series expansions; the coefficient of the

$\sin(N\eta)$ term becomes

$$A_N e^{N\xi'} - B_N e^{-N\xi'} = \frac{1}{N\pi}\int_{-\pi}^{\pi} \frac{\sin(N\eta)\cdot 2i\cdot\delta(\eta-\pi)\,d\eta}{\cosh\xi' - \cos\eta} = 0 \qquad \text{(A6-10)}$$

and the coefficient of the $\cos(N\eta)$ term becomes

$$C_N e^{N\xi'} - D_N e^{-N\xi'} = \frac{1}{N\pi}\int_{-\pi}^{\pi} \frac{\cos(N\eta)2i\cdot\delta(\eta-\pi)\,d\eta}{\cosh\xi' - \cos\eta} = \frac{2i}{N\pi(\cosh\xi'+1)} \qquad \text{(A6-11)}$$

along with the additional condition that

$$B = \frac{1}{2\pi}\int_{-\pi}^{\pi} \frac{2i\,\delta(\eta-\pi)}{\cosh\xi' - \cos\eta}\,d\eta = \frac{2i}{2\pi(\cosh\xi'+1)} \qquad \text{(A6-12)}$$

The set of equations - A6-8 to A6-11 - is a determinate set of four algebraic equations in four unknowns, whose solution is straightforward, though tedious. Similarly, A6-7 and A6-12 allow determination of B and C.

As mentioned before, the coefficient i was to be determined. The constraint

$$I = \oint_{\xi',\xi''} t\,J_\xi\,dS = t\oint_{\xi',\xi''}\left(\frac{\partial\psi}{\partial\xi}\right)d\eta \qquad \text{(A6-13)}$$

that the total current flowing into an electrode of length t must equal the total current passed between the electrodes allows i to be removed from the equations.

The simultaneous solution of A6-7 to A6-13 by elimination of variables eventually gives the working formulas

$$J_\eta = \frac{I}{ta} J_\eta^P$$

$$J_\xi = \frac{I}{ta} J_\xi^P$$

$$C_1 \equiv e^{N(\xi+\xi'-2\xi'')}\left[H^2\cdot\left(1 - e^{2N(\xi'-\xi'')}\right) - \left(1 + e^{2N(\xi'-\xi'')}\right)\right]$$

$$+ e^{N(\xi'-\xi)}\left[H^2\left(1-e^{2N(\xi'-\xi'')}\right)+\left(1+e^{2N(\xi'-\xi'')}\right)\right]$$

$$C_2 \equiv 2H\cdot e^{N(\xi+\xi'-2\xi'')}\left(1+e^{N(2\xi'-4\xi''-2\xi)}\right)$$

$$C_3 \equiv 2H\left(e^{N(\xi+\xi'-2\xi'')}-e^{N(3\xi'-2\xi''-\xi)}\right)$$

$$C_4 \equiv \left[-e^{N(\xi+\xi'-2\xi'')}\left\{H^2\cdot\left(1-e^{2N(\xi'-\xi'')}\right)-\left(1+e^{2N(\xi'-\xi'')}\right)\right\}\right.$$
$$\left.+e^{N(\xi'-\xi)}\left\{H^2\left(1-e^{2N(\xi'-\xi'')}\right)+\left(1+e^{2N(\xi'-\xi'')}\right)\right\}\right]$$

$$\epsilon_N \equiv H^2\left(1-2e^{2N(\xi'-\xi'')}+e^{4N(\xi'-\xi'')}\right)+\left(1+e^{2N(\xi'-\xi'')}\right)$$

$$J_\eta^P = \frac{\cosh\xi-\cos\eta}{\pi}\left\{\frac{H}{2}+\sum_{N=1}^{\infty}\frac{(-1)^N}{\epsilon_N}\left[C_1\sin N\eta+C_2\cos N\eta\right]\right\}$$

$$J_\xi^P = \frac{\cosh\xi-\cos\eta}{\pi}\left\{\frac{1}{2}+\sum_{N=1}^{\infty}\frac{(-1)^N}{\epsilon_N}\left[C_3\sin N\eta+C_4\cos N\eta\right]\right\}$$

APPENDIX 7

SOLUTION OF THE FLAME STRUCTURE EQUATIONS

As pointed out in Chapter 4, the governing equations for flame structure, including electric current and magnetic field terms, may be obtained by the addition of a Joulean heating term and a Lorentz force term - as given (in differential form) by Pai[43] - to the flame structure equations of Toong and Chen[59]. The final form obtained in Chapter 4 is the same as that derived by Toong[58] (though with some changes of notation).

What is basically described by these equations is a chemically reacting, one-dimensional flow, in which the reactants and products have identical molecular weights and specific heats. The production of a unit mass of reactant at constant temperature and pressure requires a flow of heat of q_T per unit mass of reactants. The chemical reaction is treated as a heat and reactant source in the flow of flame gases, yielding a heat flow rate of $K_A q_T$ per unit volume, where K_A is the <u>mass</u> rate of production of reactant per unit volume (algebraically negative in a combustion). Treating the chemical reaction as a heat source immediately means that no chemical term need be included in the enthalpy - h .

An electric field of strength E_y is assumed applied perpendicular to the gas flow direction, and a magnetic

field of intensity B is assumed applied perpendicular to both the electric current and the magnetic field. The electric field must equal $-U_u B_u$ if the magnetic field and electrodes are assumed to be so long as to give a high magnetic Reynolds number $-\sigma\mu_o U B-$ so that the gas flow and magnetic field are coupled. If the condition of a high magnetic Reynolds number is not invoked, then the electric field may be chosen at will. The fact that, in the absence of electrodes no current can flow necessarily means that the conductivity across the channel effectively goes to zero at values of Y where there are no electrodes.

The equations derived in Chapter 4 will be rewritten in this appendix as a coupled system of Volterra integral equations, in which reactant concentration is the independent variable. The reason for choosing concentration rather than the usual choice of temperature[24] as the independent variable is that, in the unrealistic case where the magnetic field is assumed coupled to the gas flow, the final temperature becomes a function of the applied magnetic field, so that the range of the temperature would be unknown. However, on the "burnt" side of a flame, the reactant concentration is known to be zero, irrespective of whether or not a magnetic field is present.

As derived in Chapter 4, the governing equations are

Species Continuity

$$D_c \equiv dC_A/dY \qquad \text{(A7-1)}$$

$$\rho U D_c - \frac{d}{dY}(\rho \mathcal{D} D_c) - K_A = 0 \qquad \text{(A7-2)}$$

Ampere's Circuital Law

$$\frac{dB}{dY} = \sigma \mu_0 (UB + E_u) \qquad \text{(A7-3)}$$

Energy Conservation

$$D_h \equiv dh/dY \qquad D_T \equiv dT/dY \qquad \text{(A7-4)}$$

$$\rho U D_h - \frac{d}{dY}(\lambda D_T) - q_c - \sigma E_u (UB + E_u) = 0 \qquad \text{(A7-5)}$$

Mass Conservation

$$\dot{m} = \rho U \qquad \text{(A7-6)}$$

Static Pressure Balance

$$P + \frac{B^2}{2\mu_0} = P_u + \frac{B_u^2}{2\mu_0} \qquad \text{(A7-7)}$$

Perfect Gas Law

$$dh = C_p(T)\, dT \qquad \text{(A7-8a)}$$

$$\rho = P/RT \qquad \text{(A7-8b)}$$

$$C_p - C_v = R \qquad \text{(A7-8c)}$$

Reaction Rate Law (Arrhenius formulation with concentrations less than 90% of initial reactant concentration, zero for reactant concentrations greater than 90%)

$$K_A = K P^{N-1} C_A^{\,N} T^{\frac{3}{2}-N} \rho\, e^{-E_A/RT} \;;\; \frac{C_A}{C_{A_u}} \leq .9$$

$$K_A = 0 \;;\; \frac{C_A}{C_{A_u}} > .9 \qquad \text{(A7-9)}$$

Heat Release Rate

$$q_c = q_T K_A$$

Transport Properties

$$\sigma = \sigma(P, T, C_A, Y) \qquad \text{(A7-11)}$$

$$\lambda = \lambda(P, T, C_A) \qquad \text{(A7-12)}$$

$$\mathcal{D} = \mathcal{D}(P, T, C_A) \qquad \text{(A7-13)}$$

A necessary and sufficient set of boundary conditions are:

$$(D_T)_u = 0$$
$$(D_c)_u = 0$$
$$(C_A)_u = C_{A_u}$$
$$(T)_u = T_u$$
$$(P)_u = P_u$$
$$(B)_u = B_u$$
$$(U)_u = \dot{m}/\rho_u$$
$$(D_c)_b = 0$$

(It should be noted that these eight boundary conditions for seven equations - A7-1 to A7-7 - are an overdeterminate set, so that only one value of U_u is permissable. Thus, U_u is an "eigenvalue" of the equations and boundary conditions.)

The following characteristic quantities

characteristic velocity - $\bar{V} = \sqrt{\gamma_u R_u T_u}$

characteristic distance - $\bar{X} = \mathcal{D}_u/\bar{V}$

characteristic reaction rates - $\bar{\Gamma} = K\rho_u C_{A_u} P^{N-1} T^{\frac{3}{2}-N} e^{-E_A/RT_u}$

$\bar{q} = \mathcal{D}_u \bar{\Gamma}/(\rho_u C_{A_u} \bar{V})^2$

allow definition of the dimensionless groups

dimensionless magnetic field - $\beta = B/\sqrt{\mu_o P_u}$

dimensionless initial magnetic field - $\pi_B = \beta_u^2/2$

dimensionless heat release - $\bar{q} = q_T/C_{P_u} T_u$

dimensionless electric field - $\mathcal{E} = E_u/(\bar{V}\sqrt{\mu_o P_u})$

dimensionless burning velocity - $\phi = U_u/\bar{V}$

dimensionless reaction rate -

$$\Gamma = K_A / \overline{\Gamma}$$

dimensionless concentration gradient - $\Delta_c = D_c \overline{X} / C_{A_u}$

dimensionless electrical conductivity - $\overline{\sigma} = \frac{\sigma \rho_u^2 \mu_0 P_u}{T_u \lambda_u}$

dimensionless pressure - $\pi = P / P_u$

dimensionless temperature gradient - $\Delta_T = D_T \overline{X} / T_u$

dimensionless density - $\delta = \rho / \rho_u$

dimensionless enthalpy - $\mathcal{I} = h / c_{p_u} T_u$

dimensionless concentration - $\mathcal{C} = C_A / C_{A_u}$

dimensionless temperature - $\Theta = T / T_u$

It is desirable to change the independent variable from Y to C_A. In the flame structure equations, Y occurs only in the differential, so that the transformation is achieved by the substitution

$$dY = dC_A / D_c$$

Doing this with (A7-1) and (A7-2) yields

$$\rho U D_c - D_c \frac{d}{dC_A}(\rho \mathcal{D} D_c) - K_A = 0$$

Use of the initial conditions, and reformulation in terms of dimensionless variables, integrating from the downstream boundary gives

$$(\Delta_c)_m = \frac{\rho_u}{\rho} \cdot \frac{1}{\delta}\left[\phi(\mathcal{C}_m - \mathcal{C}_b) - \overline{q}_b \int_b^m \frac{\Gamma}{\Delta_c} d\mathcal{C}\right] \qquad \text{(A7-14)}$$

or, on integration to the upstream boundary

$$\phi = \left(\overline{q}_b \int_b^u \frac{\Gamma}{\Delta_c} d\mathcal{C}\right) / (\mathcal{C}_u - \mathcal{C}_b) \qquad \text{(A7-15)}$$

Similarly, the chain rule for derivatives and the

dimensionless parameters allow A7-3 and A7-6 to be rewritten as

$$\frac{d\beta}{d\mathcal{O}} = \frac{\phi\, Le_u \gamma_u}{\gamma_u - 1}\,\bar{\sigma} = \frac{(\beta/\delta + \varepsilon/\phi)}{\Delta_c} \qquad \text{(A7-16)}$$

which may be integrated from either the burnt or the unburnt boundary to yield three alternate (though equivalent) forms:

$$\beta_m = \beta_u + \frac{\phi\, Le_u \gamma_u}{\gamma_u - 1}\int_u^m \frac{\bar{\sigma}}{\Delta_c}(\beta/\delta + \varepsilon/\phi)\, d\mathcal{O} \qquad \text{(A7-17a)}$$

$$\beta_m = \beta_b + \frac{\phi\, Le_u \gamma_u}{\gamma_u - 1}\int_b^m \frac{\bar{\sigma}}{\Delta_c}(\beta/\delta + \varepsilon/\phi)\, d\mathcal{O} \qquad \text{(A7-17b)}$$

$$\frac{\gamma_u - 1}{\phi\, Le_u\, \gamma_u}(\beta_m - \beta_b) = \int_b^m \frac{\bar{\sigma}}{\Delta_c}(\beta/\delta + \varepsilon/\phi)\, d\mathcal{O} \qquad \text{(A7-17c)}$$

For the values of electric field used in the experiments of this thesis, β/δ is negligable compared to ε/ϕ, the gas flow is decoupled from the magnetic field, and A7-17a is the form of A7-3 used. If the (unrealistic) condition is imposed that

$$E_u = -U_u B_u = -U_b B_b \;;\; \varepsilon = -\left(\frac{\beta\phi}{\delta}\right)_u = -\left(\frac{\beta\phi}{\delta}\right)_b \qquad \text{(A7-18)}$$

then A7-17b must be used in the equations of flame structure instead of A7-17a in conjunction with A7-18, and permits a strong coupling between the gas flow and magnetic field intensity.

Manipulation of the energy equation, and imposition of the conditions that, as Δ_c goes to zero, $\mathcal{T}$ and Δ_T remain finite (Δ_T going to zero) leads to

$$(\lambda D_T)_m = \int_b^m \dot{m}\,\frac{D_T}{D_c}\, dC_A - \int_b^m \frac{q}{D_c}\, dC_A - \int_b^m \frac{\sigma E_u (UB + E_u)}{D_c}\, dC_A$$

or

$$\Delta_T = \frac{\lambda_u}{\lambda}\Big[\phi(\mathcal{T}_m - \mathcal{T}_b) - \bar{q}\, C_{A_u}\phi(\mathcal{O}_m - \mathcal{O}_b) - \frac{\varepsilon(\gamma_u - 1)}{\gamma_b\, Le_u}(\beta_m - \beta_b) + \bar{q}\, C_{A_u}\,\delta\, D_c\Big] \qquad \text{(A7-19)}$$

The relation

$$d\tau = \left(\frac{d\tau}{dx}\Big/\frac{dc}{dx}\right)\cdot dc$$

leads to

$$\Theta_m = \Theta_b + \int_b^m \frac{\Delta_T}{\Delta_c}\, d\mathcal{J} \qquad \text{(A7-20)}$$

which may now be expanded using the form for Δ_T (A7-18) with the stipulation, from the first law of thermodynamics, that, across the thickness of the flame, the change in the gas' enthalpy must equal the sum of the chemical and Joulean heat input, or:

$$\tau(\Theta_b) = \tau(\Theta_u) - \bar{q}\, C_{A_u}(\mathcal{J}_u - \mathcal{J}_b) - \frac{\varepsilon(\gamma_u - 1)}{\phi\, \gamma_u}(\beta_m - \beta_b) \qquad \text{(A7-21)}$$

An iterative numerical technique, based on Toong and Chen's[59] method, can be used to solve the system of equations. As a <u>first</u> iteration

$$\frac{\Theta}{\pi} = \Theta_u + \bar{q}\, C_{A_u}(\mathcal{J} - \mathcal{J}_u)$$
$$= 1$$
$$\Gamma = \Gamma(\mathcal{J}, \Theta, \pi)$$
$$\beta = \beta_u$$
$$\delta = \pi/\Theta$$
$$\Delta_c = \frac{1}{\delta}\sqrt{{}_b\int^m \bar{q}\,\Gamma\, d\mathcal{J}}$$
$$\Delta_T = \bar{q}\, C_{A_u}\, \Delta_c$$

and, for <u>subsequent</u> iterations, the following equations are looped through until they converge

$$\phi = \left(\bar{q}\int_b^u \Gamma/\Delta_c \cdot d\mathcal{J}\right)\Big/(\mathcal{J}_u - \mathcal{J}_b) \qquad \text{(A7-15)}$$

$$\Delta_c = \frac{\rho_u}{\rho}\cdot\frac{1}{\delta}\cdot\left[\phi(\mathcal{J}_m - \mathcal{J}_b) - \bar{q}\int_b^m \Gamma/\Delta_c\, d\mathcal{J}\right] \qquad \text{(A7-14)}$$

$$\tau(\Theta_b) = \tau(\Theta_u) - \bar{q}\, C_{A_u}(\mathcal{J}_u - \mathcal{J}_b) - \frac{\varepsilon(\gamma_u - 1)}{\phi\,\gamma_u}(\beta_u - \beta_b) \qquad \text{(A7-21)}$$

$$\Theta_m = \Theta_b + \frac{\phi}{Le_u}\int_b^m \frac{d\mathcal{J}}{\Delta_c}\,\frac{\lambda_u}{\lambda}\left\{\left(\tau - \bar{q}\, C_{A_u}\mathcal{J} - \frac{\varepsilon(\gamma_u - 1)}{\phi\,\gamma_u}\beta\right) \qquad \text{(A7-20)}\right.$$
$$\left. -\left(\tau_b - \bar{q}\, C_{A_u}\mathcal{J}_b - \frac{\varepsilon(\gamma_u - 1)}{\phi\,\gamma_u}\beta_b\right)\right\} + \frac{C_{A_u}}{Le_u}\int_b^m \bar{q}\,\frac{\rho\,\lambda_u}{\rho_u\,\lambda}\,\delta\, d\mathcal{J}$$

$$\delta = \frac{\Pi}{\Theta}\,\frac{R_u}{R}$$

$$\beta_m = \beta_u + \frac{\Phi\, Le_u\, \gamma_u}{\gamma_u - 1}\int_u^m \frac{\bar{\sigma}(\beta/\delta + \varepsilon/\phi)}{\Delta_c}\, d\Im \qquad \text{(A7-17a)}$$

or, alternatively, if it was assumed that

$$\varepsilon = \Phi\,\beta_u \qquad \beta_b = \delta_b\,\beta_u \qquad \text{(A7-18)}$$

then A7-17b was used in place of A7-17a, in the form

$$\beta_m = \beta_b + \frac{\Phi\, Le_u\, \gamma_u}{\gamma_u - 1}\int_b^m \frac{\bar{\sigma}(\beta/\delta + \varepsilon/\phi)}{\Delta_c}\, d\Im \qquad \text{(A7-17b)}$$

Further,

$$\Pi = 1 + \Pi_B - \beta^2/2 \qquad \text{(A7-7)}$$

$$\Gamma = \Gamma(\Im, \Pi, \Theta) \;;\; \Im \le .9$$

$$\Gamma = 0 \;;\; \Im > .9$$

$$\gamma/\bar{\gamma} = \int_c^m d\Im/\Delta_c \qquad |(\Delta_c)_c| \gg |(\Delta_c)|$$

$$\bar{\sigma} = \bar{\sigma}(\Pi, \Im, \Theta)$$

In order to make the model as real as possible, the following relations were used

$$\rho/\rho_u = \Theta^{.75}/\delta \qquad \lambda/\lambda_u = \Theta^{.75}$$

$$\tau = \Theta$$

$$\Gamma = \delta\,\Pi^{.8}\,\Im^{1.8}\,\Theta^{-.3}\, e^{-E_A/RT_u}(1 - 1/\Theta) \qquad \Im \le .9$$

$$= 0 \qquad \Im > .9$$

$$R/R_u = C_p/C_{p_u} = \gamma/\gamma_u = Le/Le_u = 1$$

which, when combined, lead to

$$\bar{q} = \frac{K \rho_u R_u^{.8} C_{A_u}^{1.8}\, e^{-E_A/RT_u}}{\gamma_u R_u \bar{T}_u} \qquad \text{(A7-22)}$$

$$\sim \bar{T}_u^{-.25} P_u^{-.2} C_{A_u}^{-1.8}\, e^{-E_A/RT_u}$$

In order to solve the equations, all of the parameters are available in the literature except for K - the reaction rate constant. A semi-empirical technique was used to determine K, which consisted of taking values of C_{A_u} (=.261)

T_u (=300°K), $\bar{q}$ (=-24.9), L_e (=.78), and γ (=1.4) for which Φ was known from published data to equal .00121, and, with these parameters fixed, varying K (by means of varying $\bar{q}$) until a value for $\bar{q}$ (=1.45×10^{-30}) was found for which the computed Φ agreed with the published Φ.

In the course of this search for the correct $\bar{q}$, an observation was made concerning the variation of burning velocity with pressure as predicted by the numerical technique. With all other parameters fixed, Φ varied directly with $\bar{q}^{1/2}$ (Figure 45). In the light of (A7-22), this demands that $\Phi \sim P_u^{-1}$. This law of variation does agree with the published range of variation of experimentally observed burning velocities of laminar propane-air flames with pressure[17]. (It should be noted that the variation of $\bar{q}$ with P_u, and consequently the variation of Φ with P_u follows from the assumed reaction order, which was taken from published data for well-stirred reactors.)

Having fixed $\bar{q}$, it is possible to proceed with calculations of electromagnetic effects on a flame's burning velocity. The computer programs for this are in Appendix 2.

It should be noted that, in the numerical techniques for solutions, all integrations were performed from the burnt side of the flame forward. It is possible to show that the alternate is unstable[26], and this was borne out by experience in trying to solve the equations.

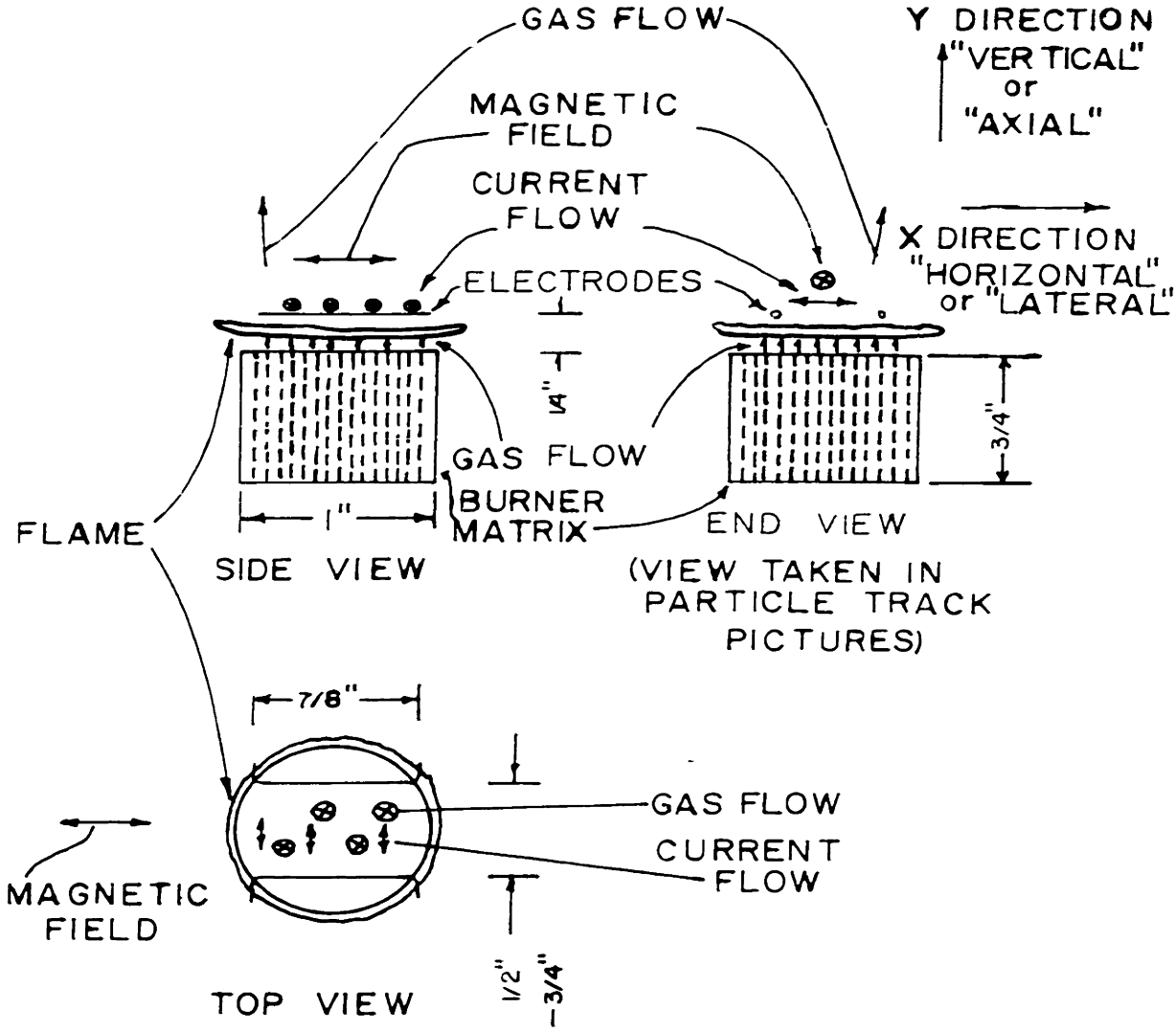

FIG. 1

3 VIEWS, SHOWING RELATIVE POSITIONS AND ORIENTATIONS OF BURNER, GAS FLOW, ELECTRODES, B FIELD, AND CURRENT FLOW

---- LINES OF ELECTRIC CURRENT

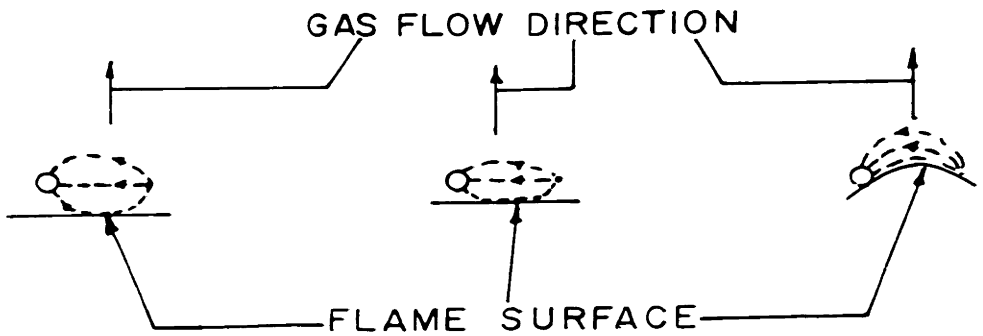

MAGNETIC FIELD=0, OR LORENTZ FORCE IN DIRECTION OF FLOW

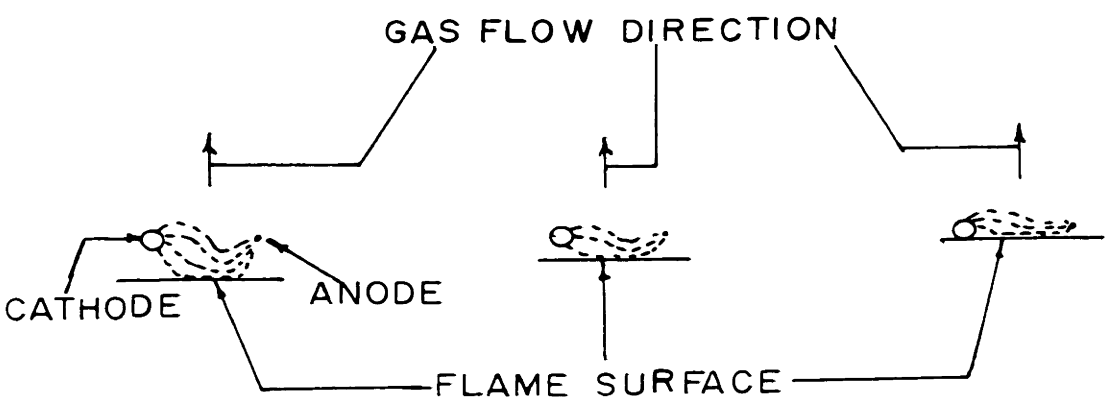

LORENTZ FORCE AGAINST DIRECTION OF FLOW

FIG. 2

OBSERVED CHANGES IN FLAME SHAPE AND POSITION WITH DECREASING FUEL/AIR RATIO

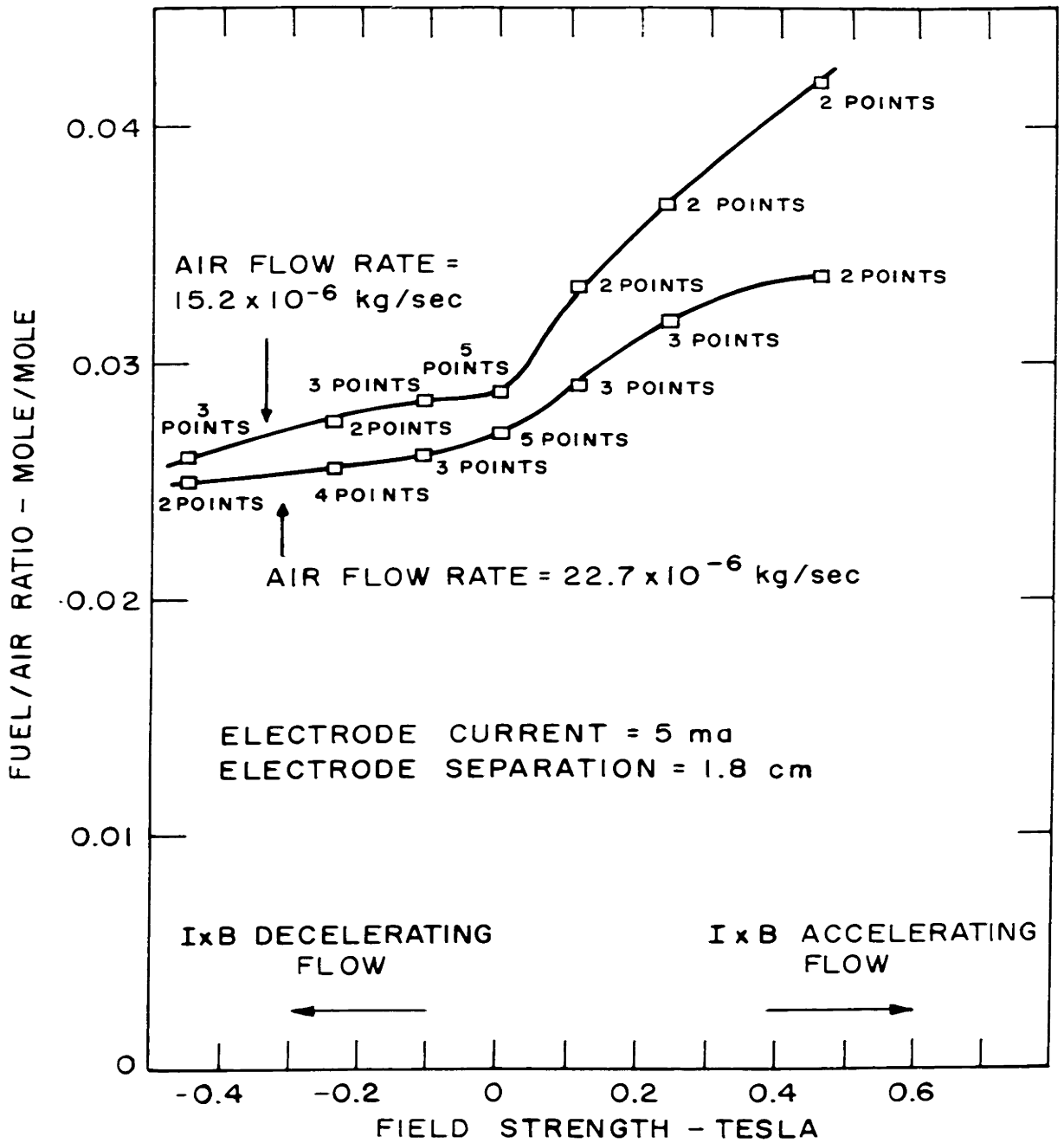

FIG. 3 COMPARISON OF MOLAL FUEL/AIR RATIO AT 5 ma. ELECTRODE CURRENT VS. MAGNETIC FIELD INTENSITY—FOR TWO AIR FLOW RATES

FIG. 4

SCHEMATIC OF PARTICLE TRACK TECHNIQUE

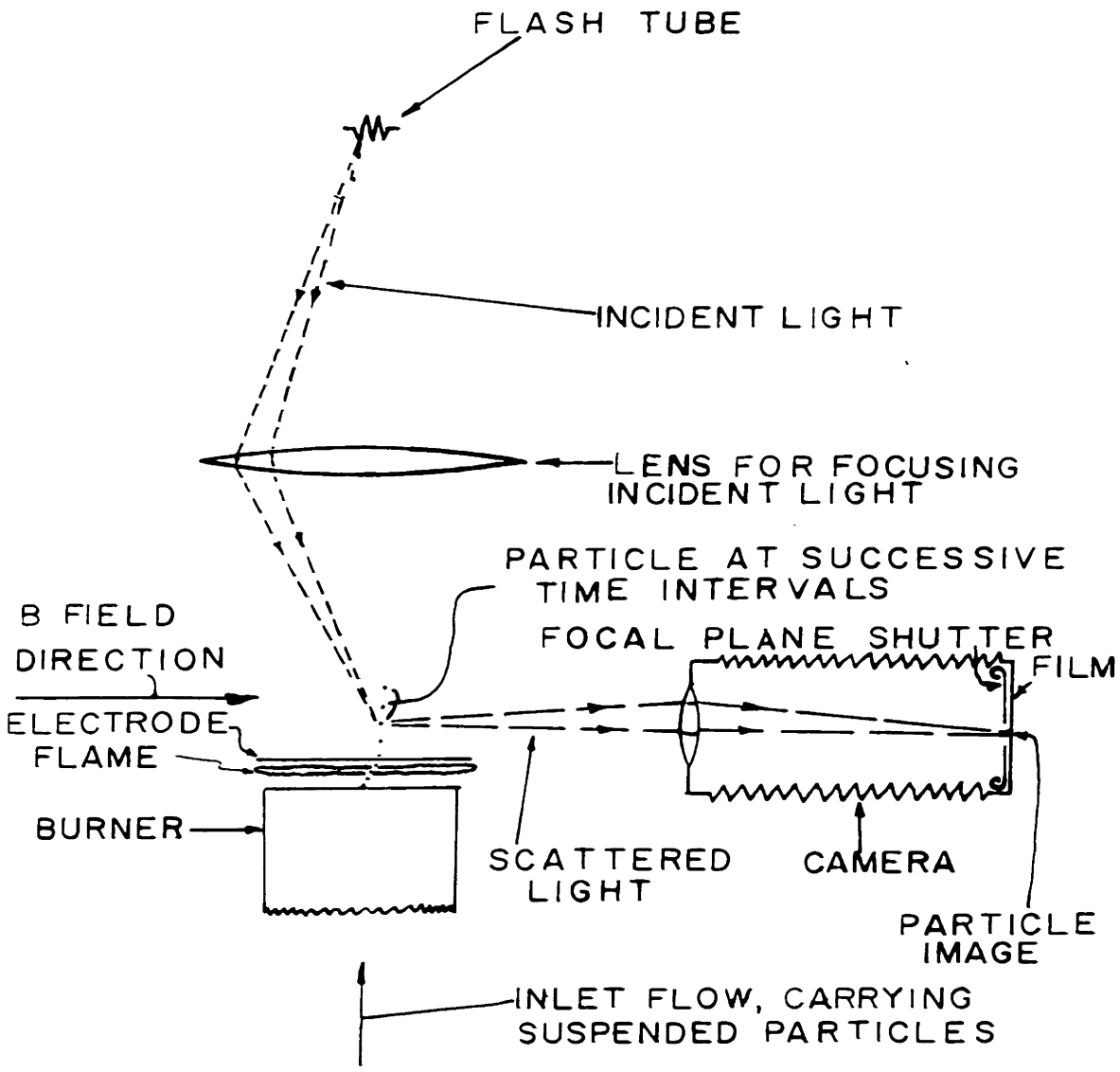

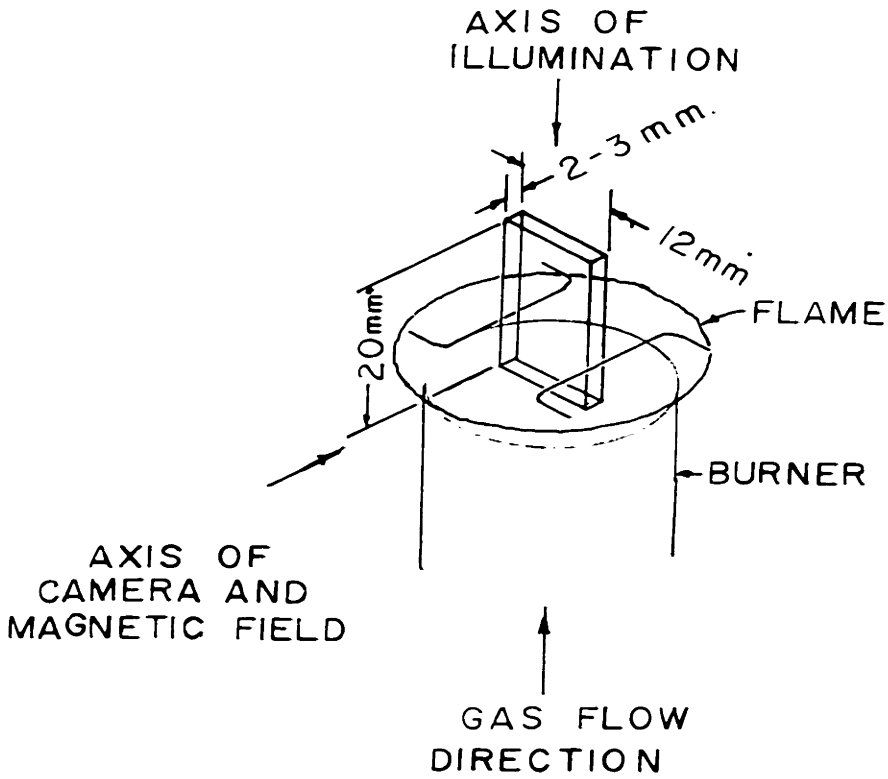

FIG. 5

SCHEMATIC DIAGRAM OF REGION OBSERVED IN PARTICLE TRACK PICTURES

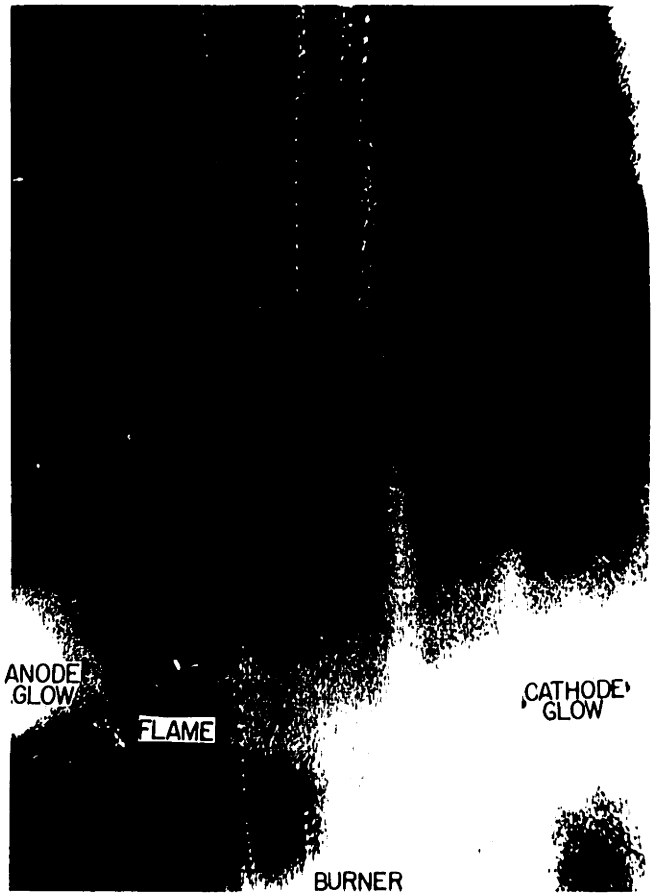

FIG. 7a PARTICLE - TRACK PICTURE, LORENTZ FORCE IN DIRECTION OF FLOW

ANODE ← → CATHODE

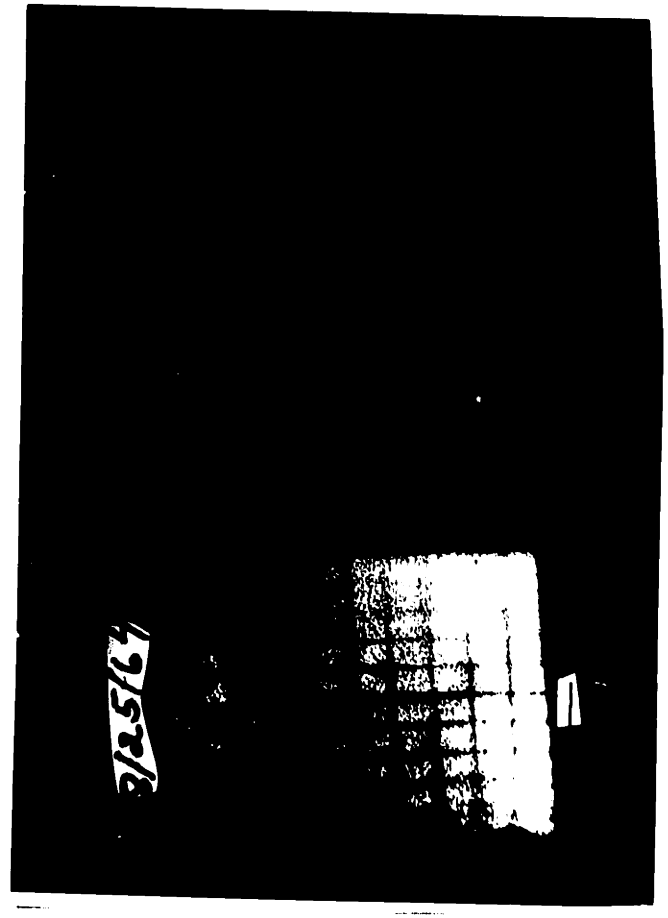

FIG. 6 FOCUSING AND SCALING PICTURE

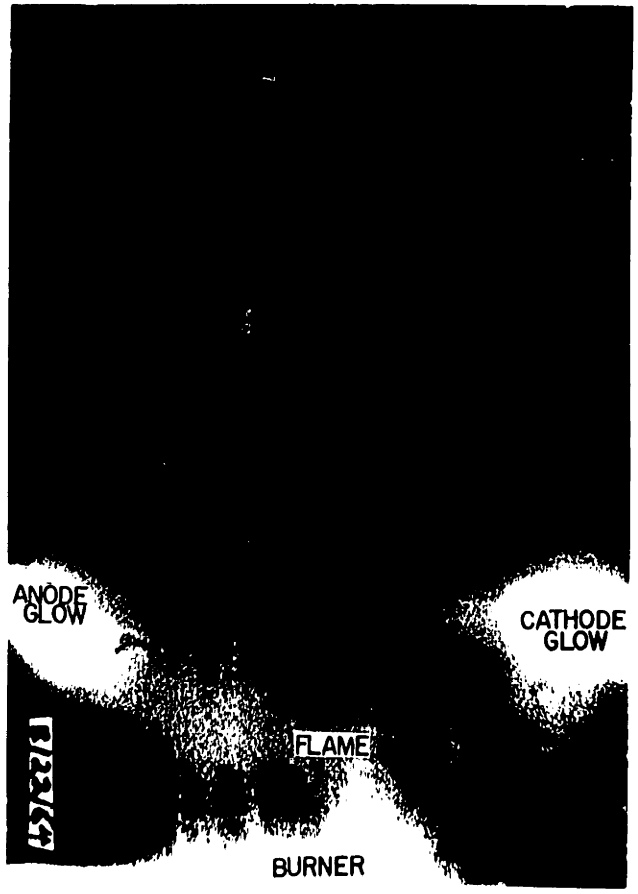

FIG 7b PARTICLE - TRACK PICTURE, LORENTZ FORCE AGAINST DIRECTION OF FLOW

ANODE CATHODE

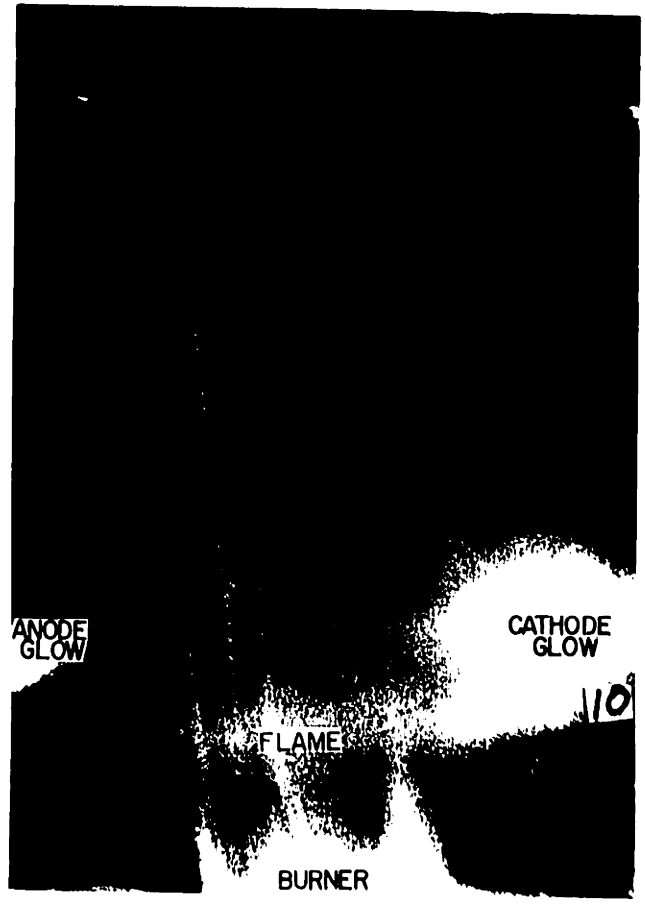

FIG. 7c PARTICLE - TRACK PICTURE, NO LORENTZ FORCE

ANODE CATHODE

FIG. 8a

FEATURES OF PARTICLE TRACK PICTURES

LORENTZ FORCES IN DIRECTION OF FLOW

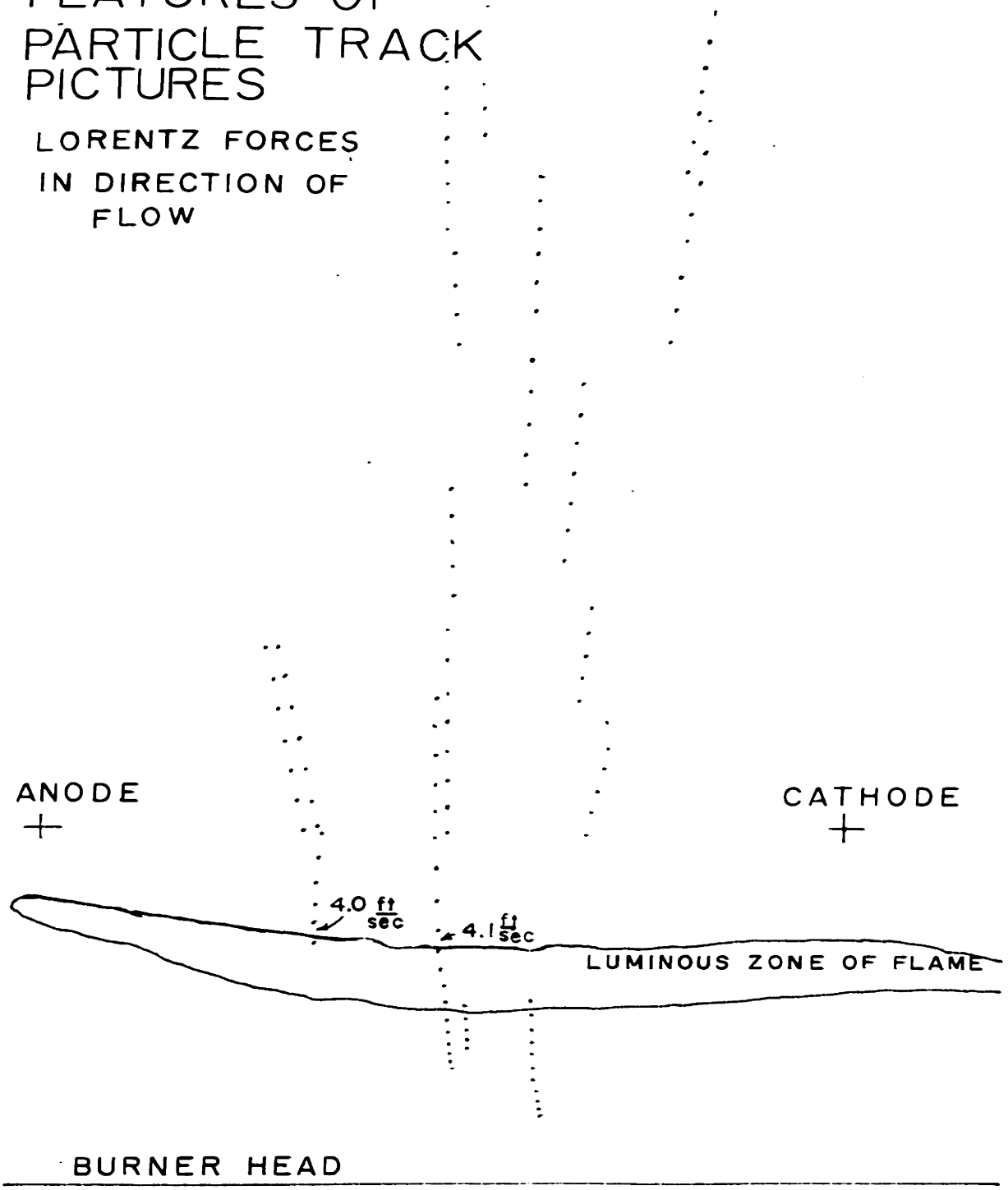

FIG. 8b

FEATURES OF PARTICLE TRACK PICTURES

LORENTZ FORCES AGAINST DIRECTION OF FLOW

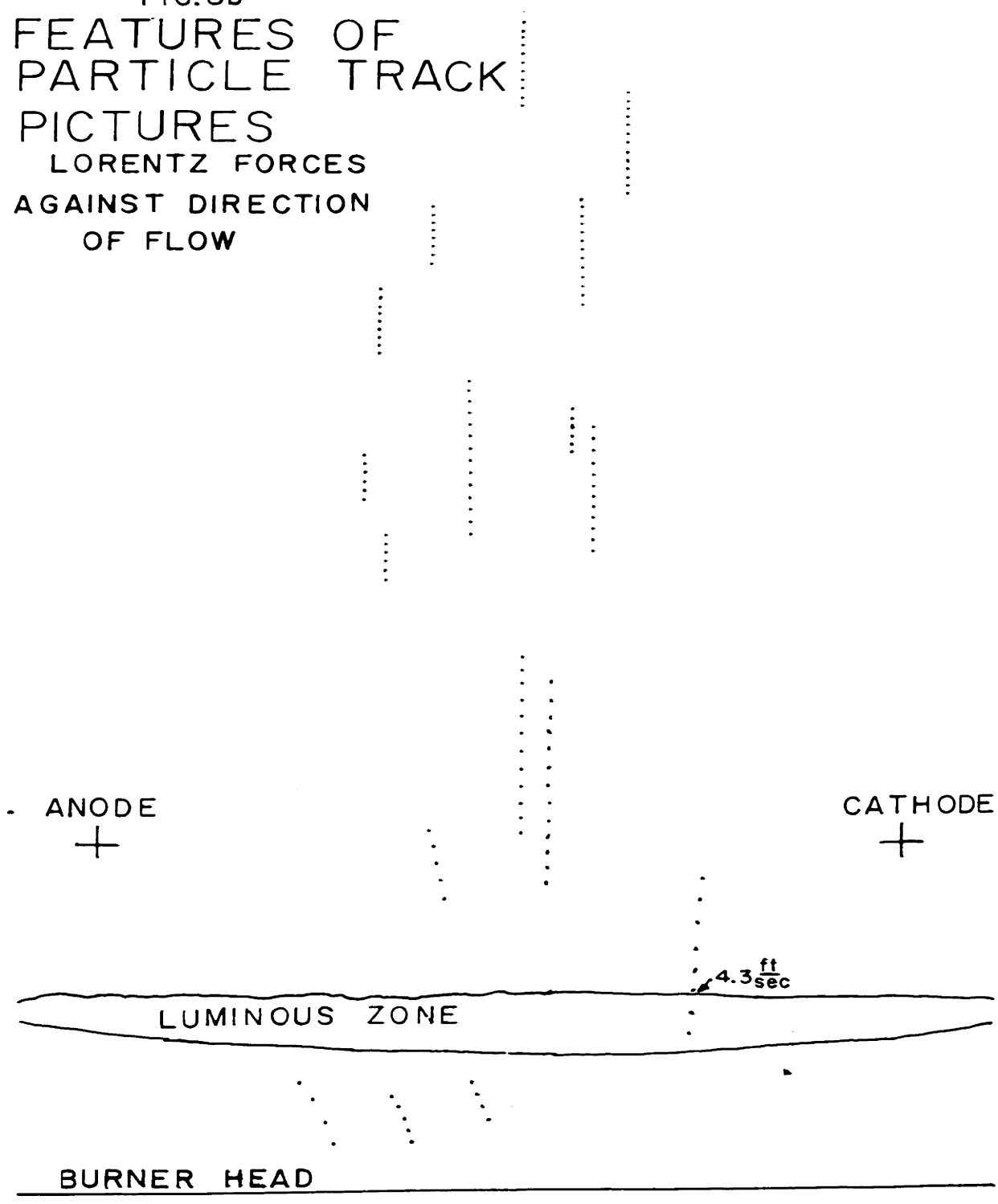

FIG.8c

FEATURES OF PARTICLE TRACK PICTURES

5 ma. ELECTRODE CURRENT, NO MAGNETIC FIELD

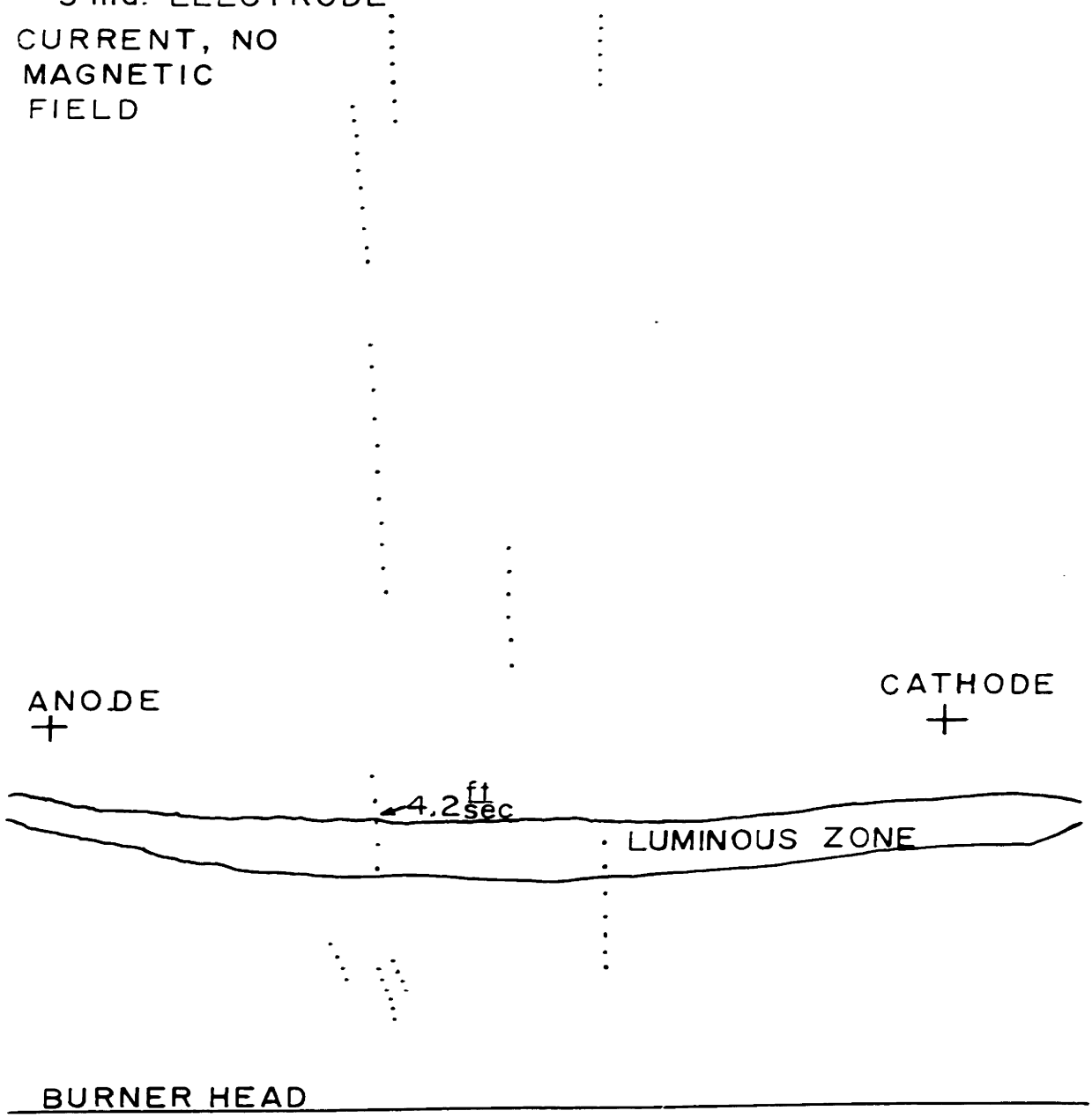

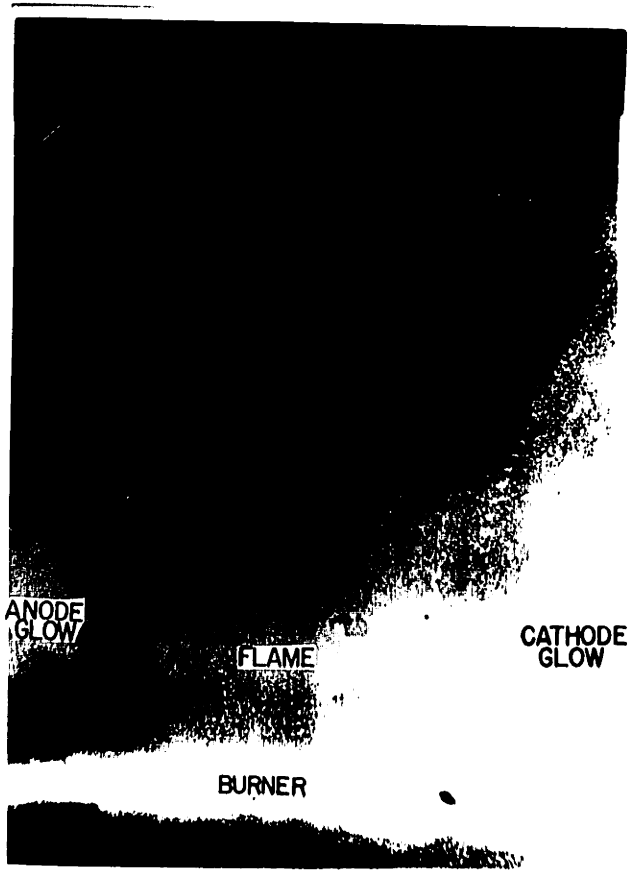

FIG. 9a PARTICLE TRACK PICTURE
LORENTZ FORCE WITH FLOW

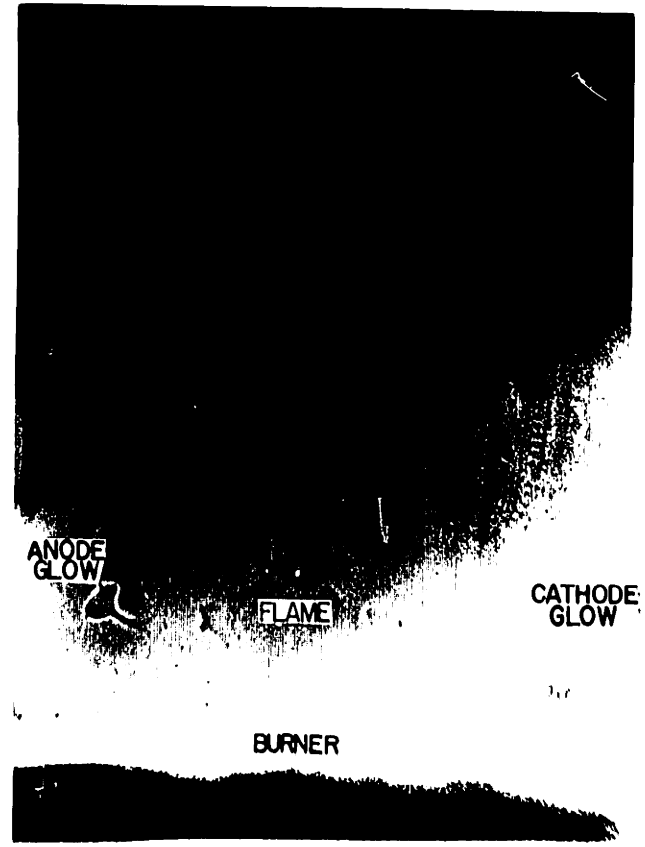

FIG. 9b PARTICLE TRACK PICTURE
I = 5 ma B = 0

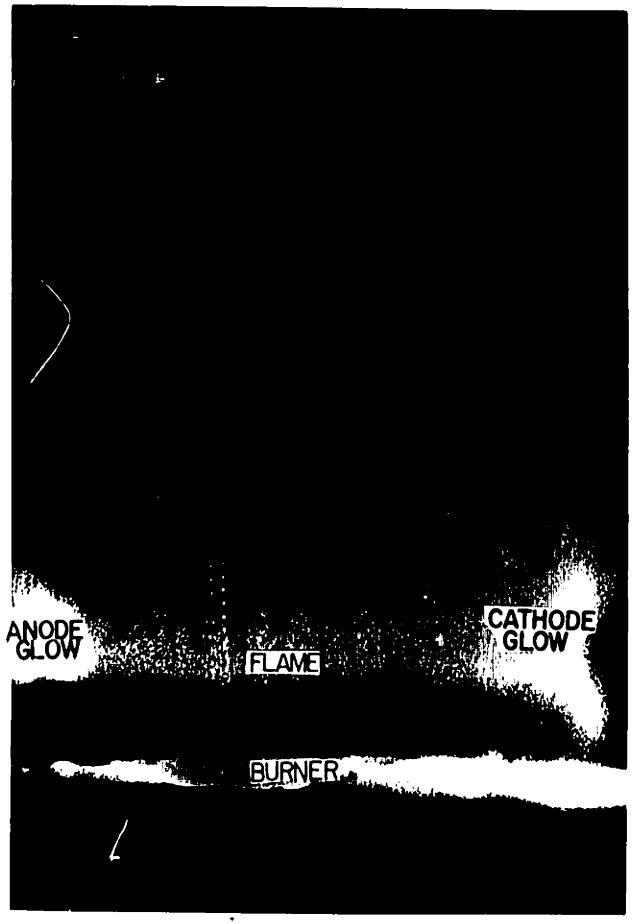

FIG. 9c PARTICLE TRACK PICTURE
LORENTZ FORCE AGAINST
FLOW

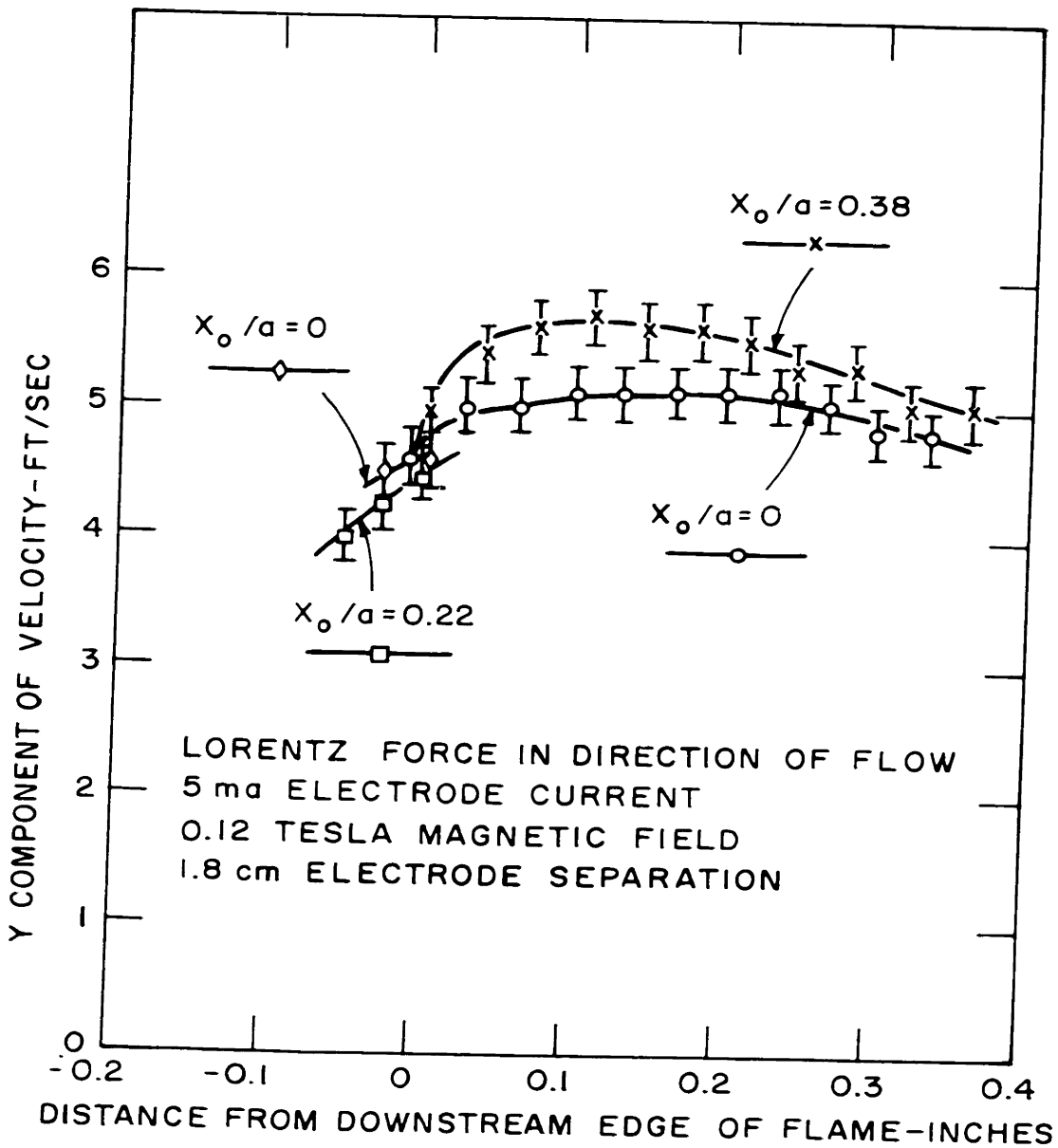

FIG. 10 PLOT OF Y COMPONENT OF VELOCITY AS FUNCTION OF DISTANCE DOWNSTREAM FROM FLAME

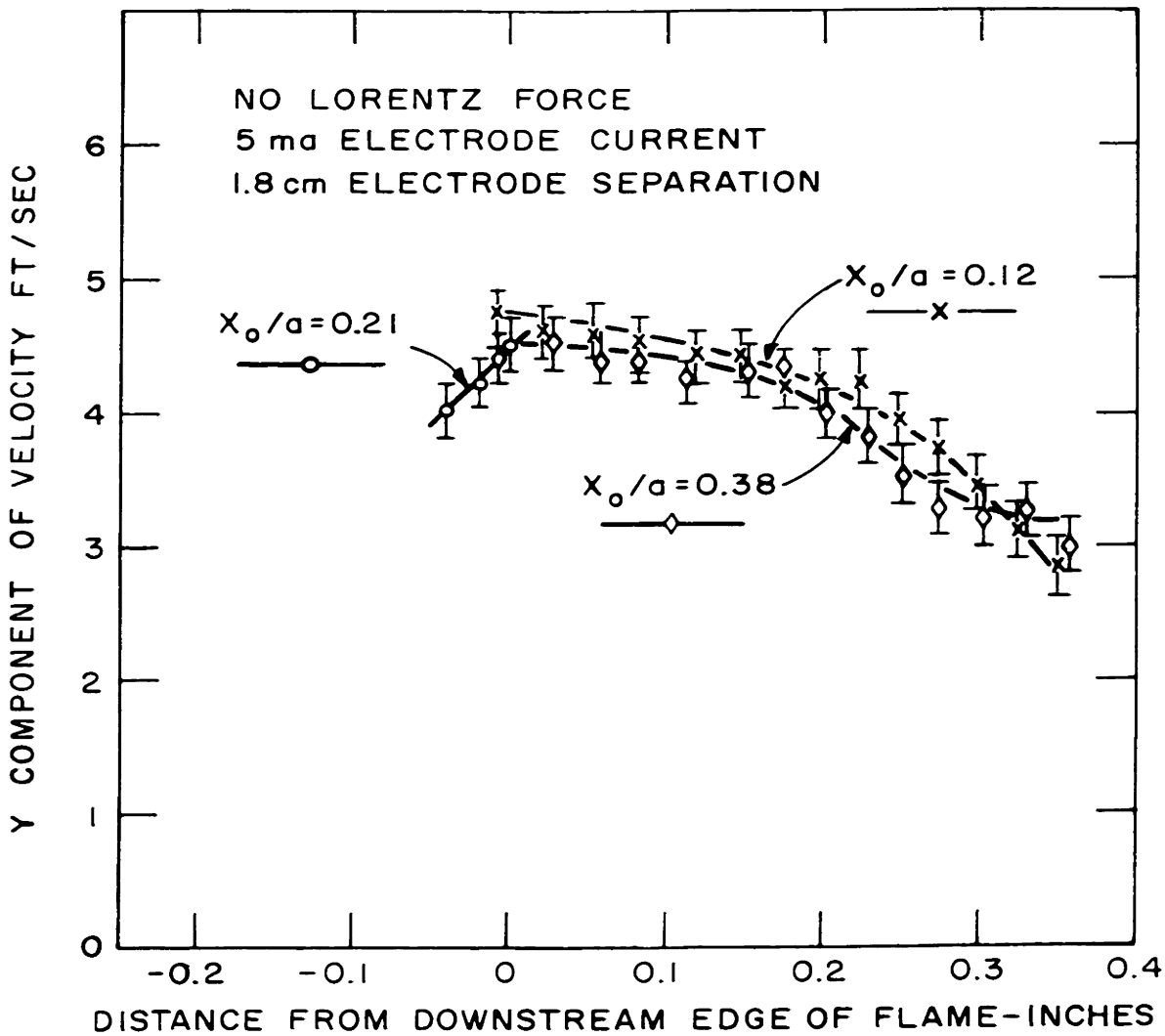

FIG. 11 PLOT OF Y COMPONENT OF VELOCITY AS FUNCTION OF DISTANCE DOWNSTREAM FROM FLAME

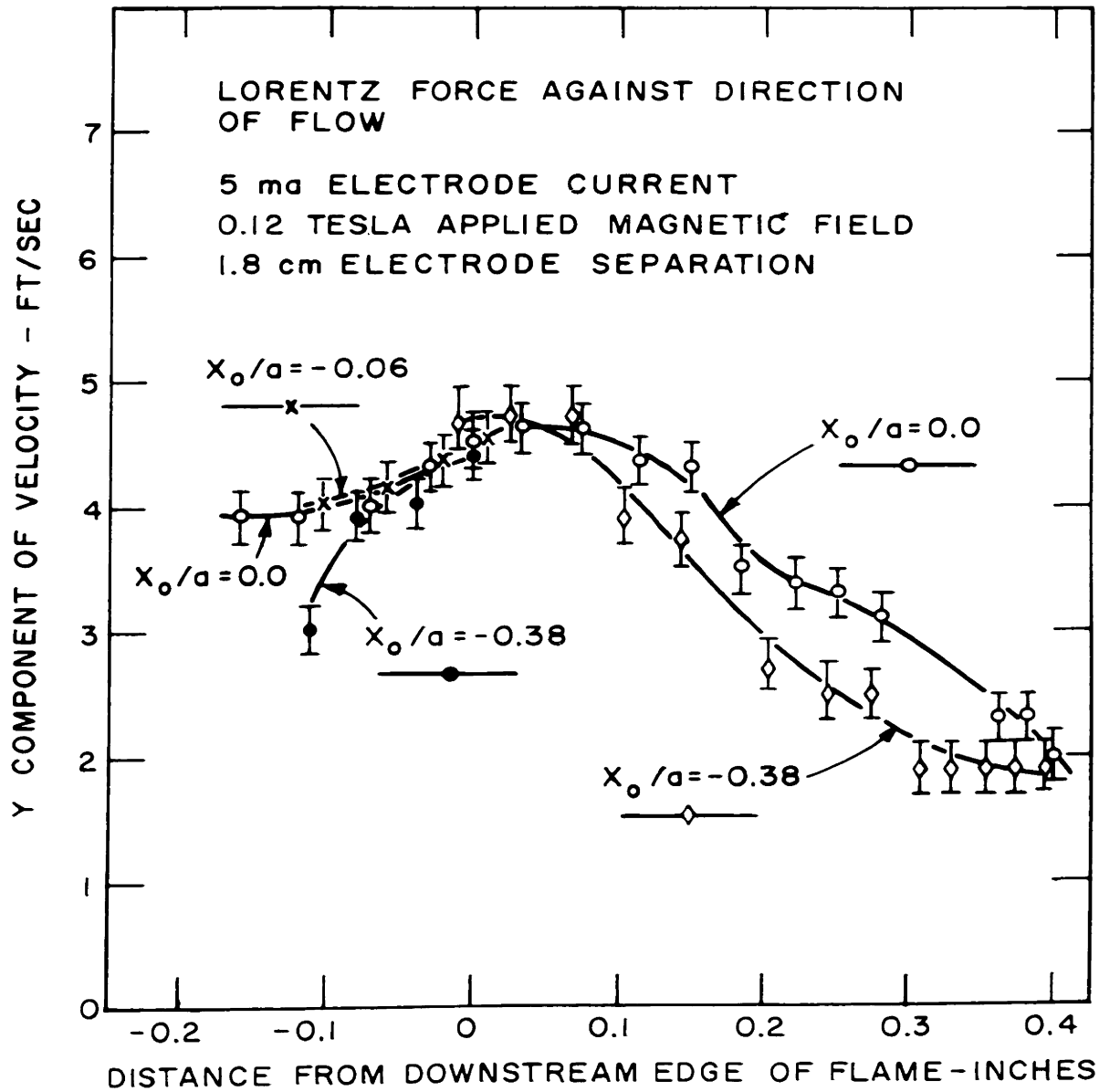

FIG. 12 PLOT OF Y COMPONENT OF VELOCITY AS FUNCTION OF DISTANCE DOWNSTREAM FROM FLAME

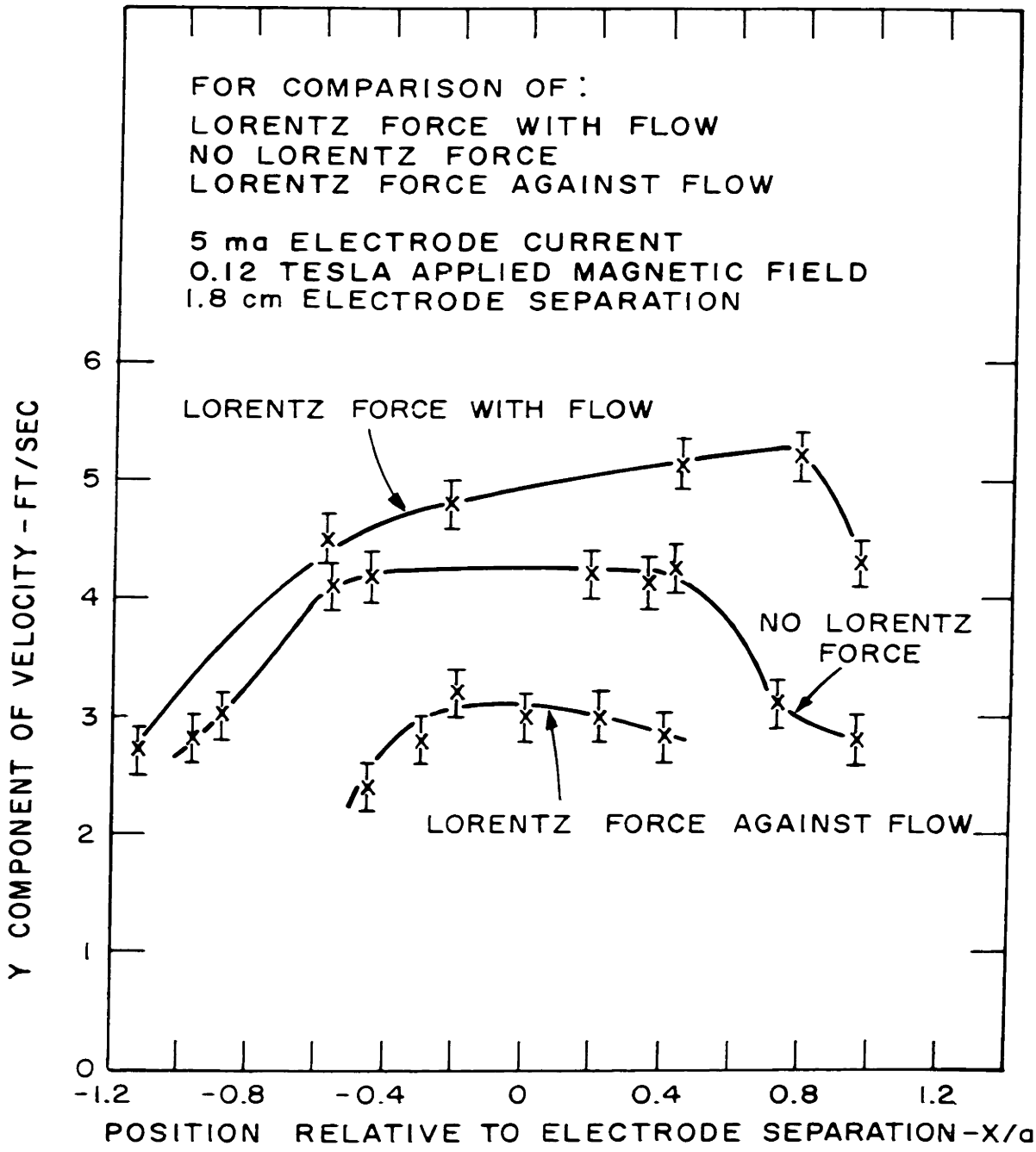

FIG. 13 PLOT OF Y VELOCITY PROFILES
0.19" DOWNSTREAM OF FLAME

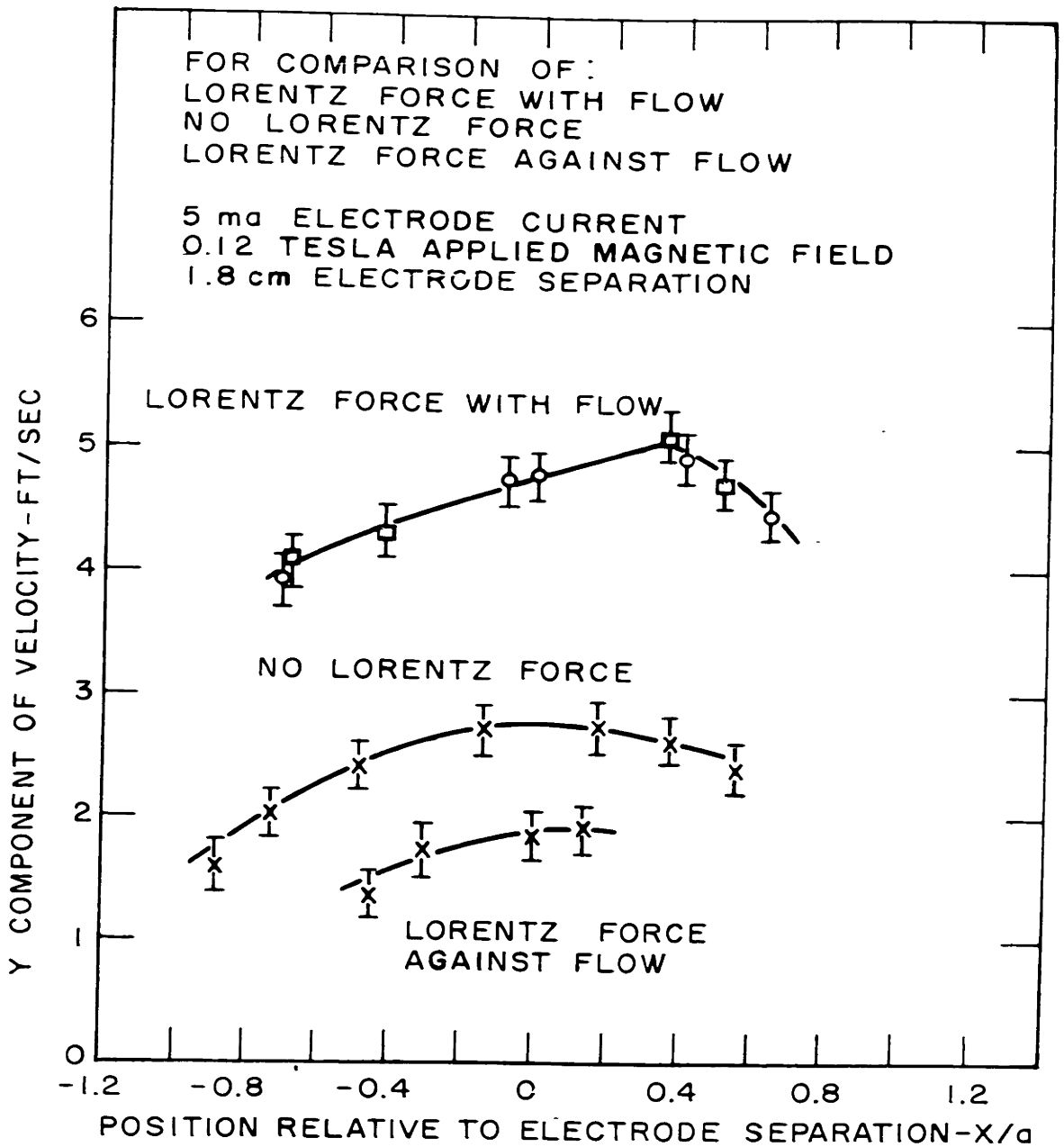

FIG. 14 PLOT OF Y VELOCITY PROFILES
0.38" DOWNSTREAM OF FLAME

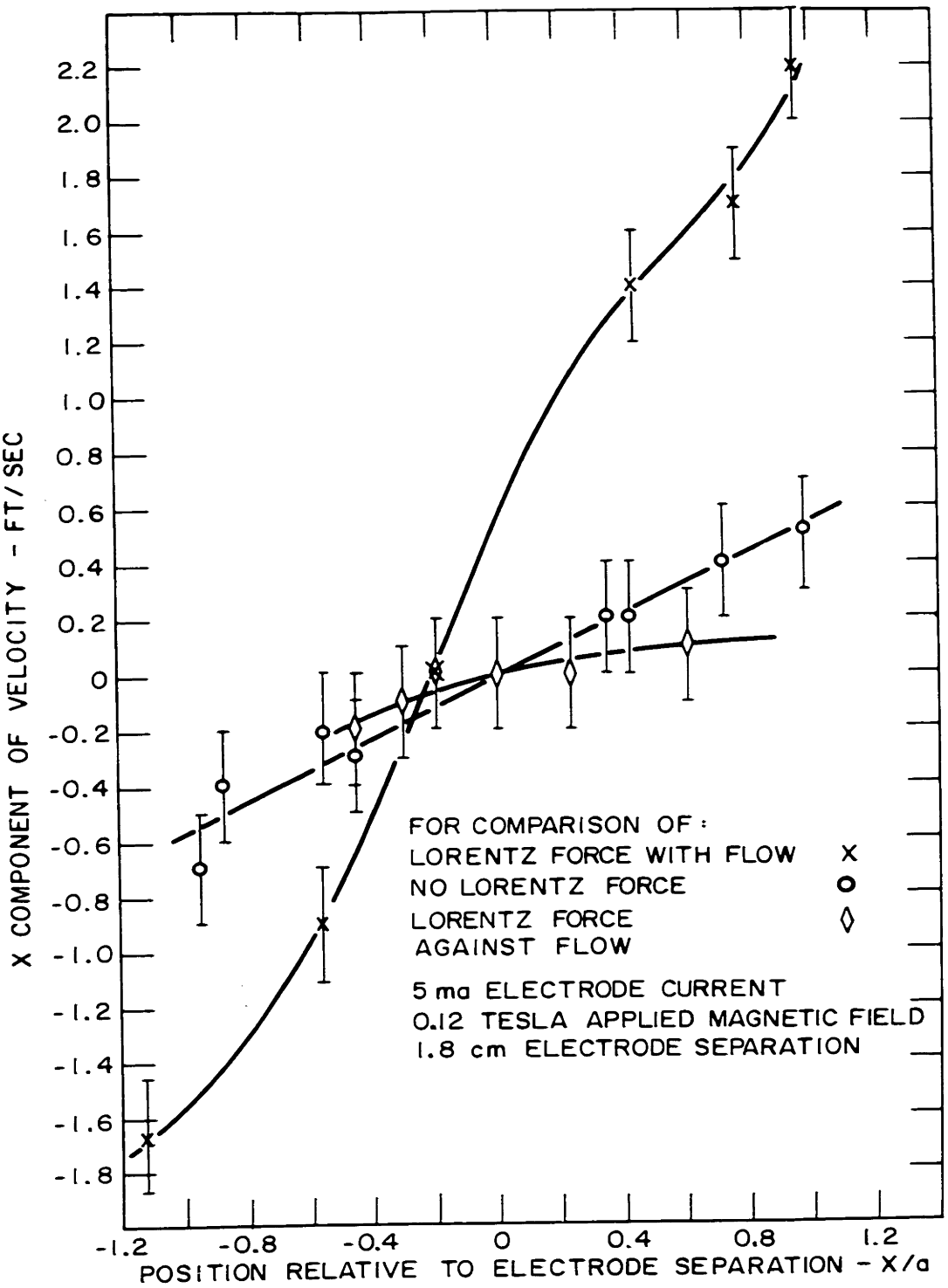

FIG. 15 PLOT OF X COMPONENT OF VELOCITY PROFILES 0.19" DOWNSTREAM OF FLAME

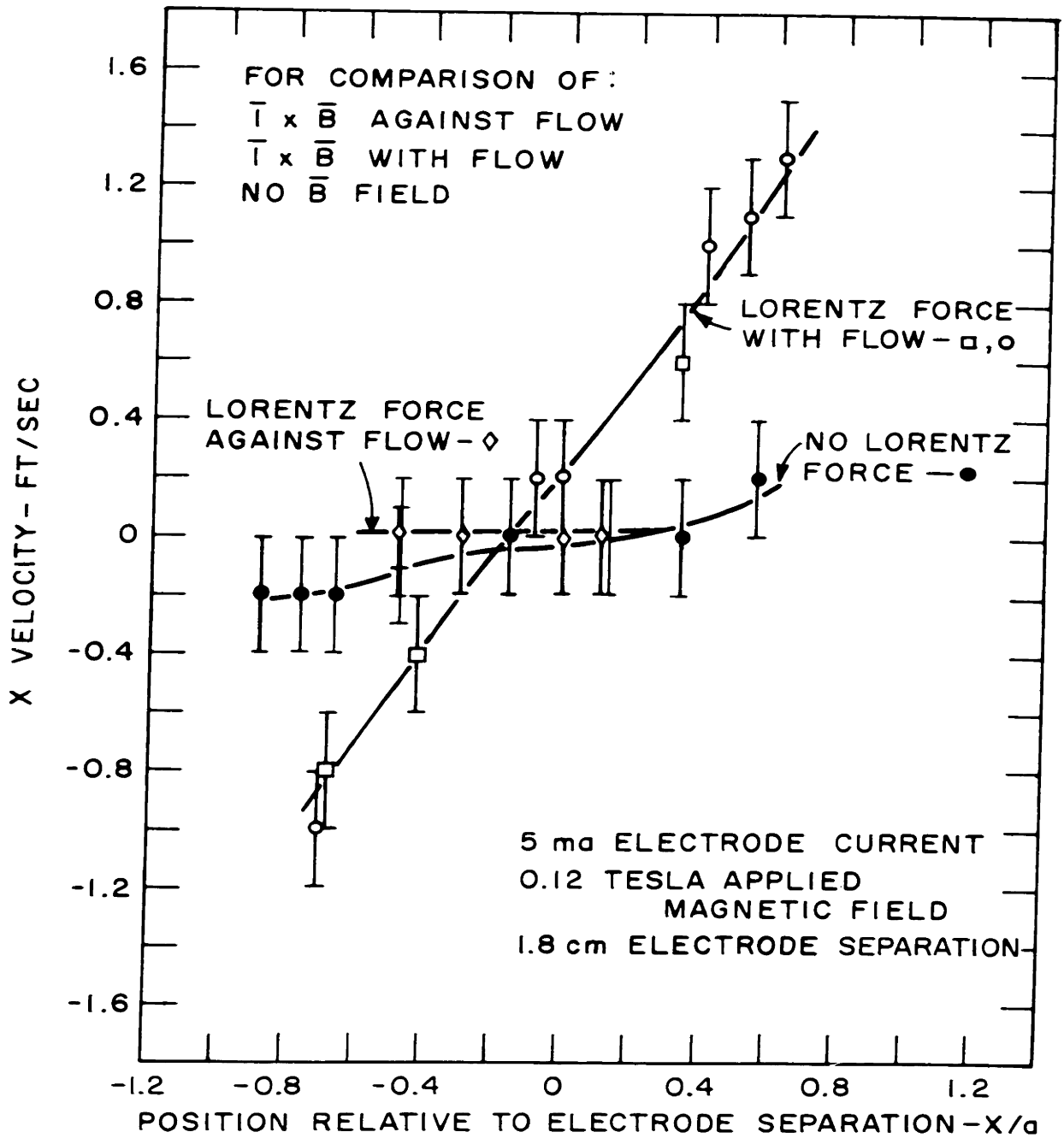

FIG. 16 PLOT OF X VELOCITY PROFILES 0.38" DOWNSTREAM OF FLAME

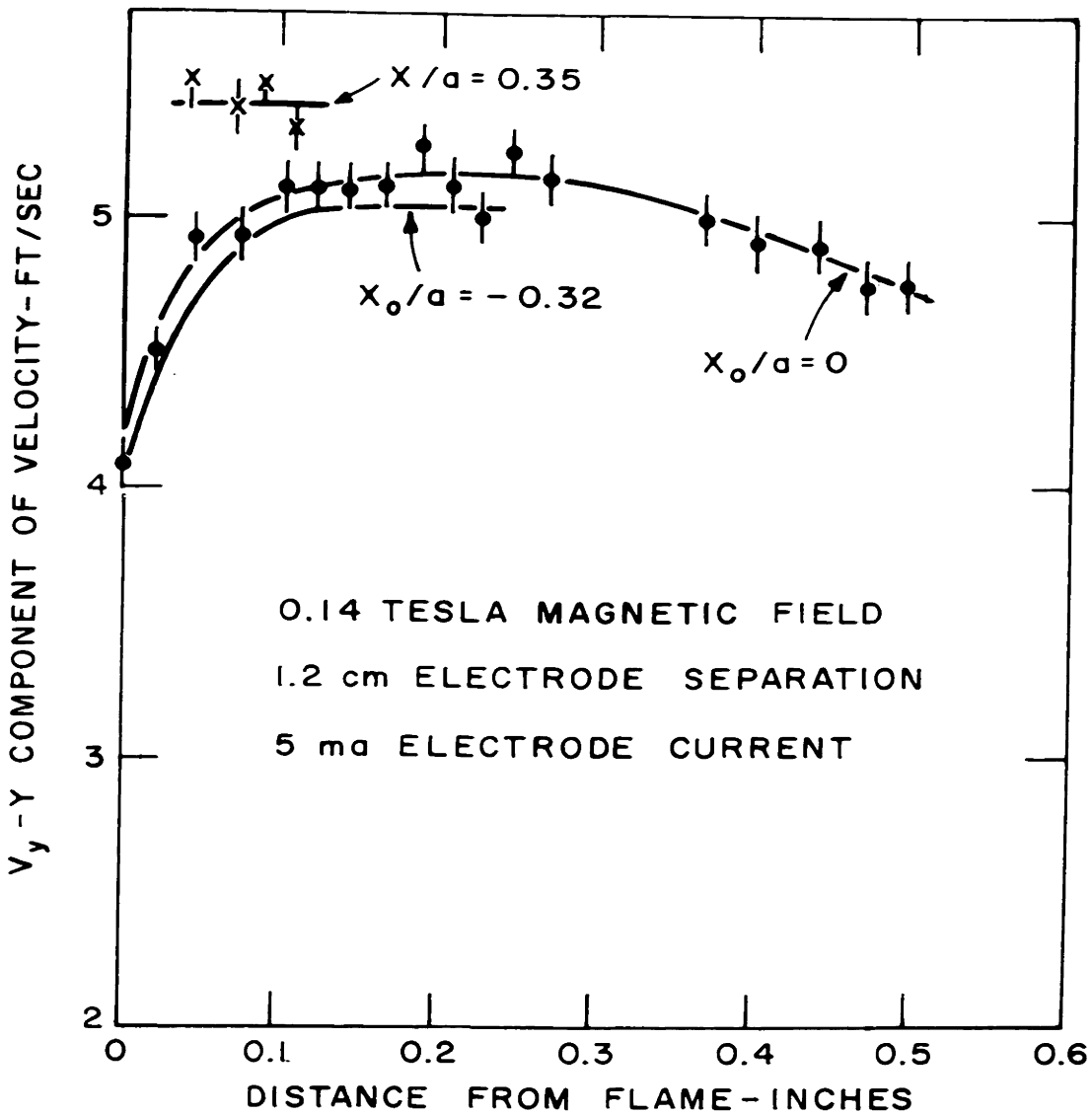

FIG. 17 PLOT OF Y COMPONENTS OF VELOCITY-LORENTZ FORCE WITH FLOW

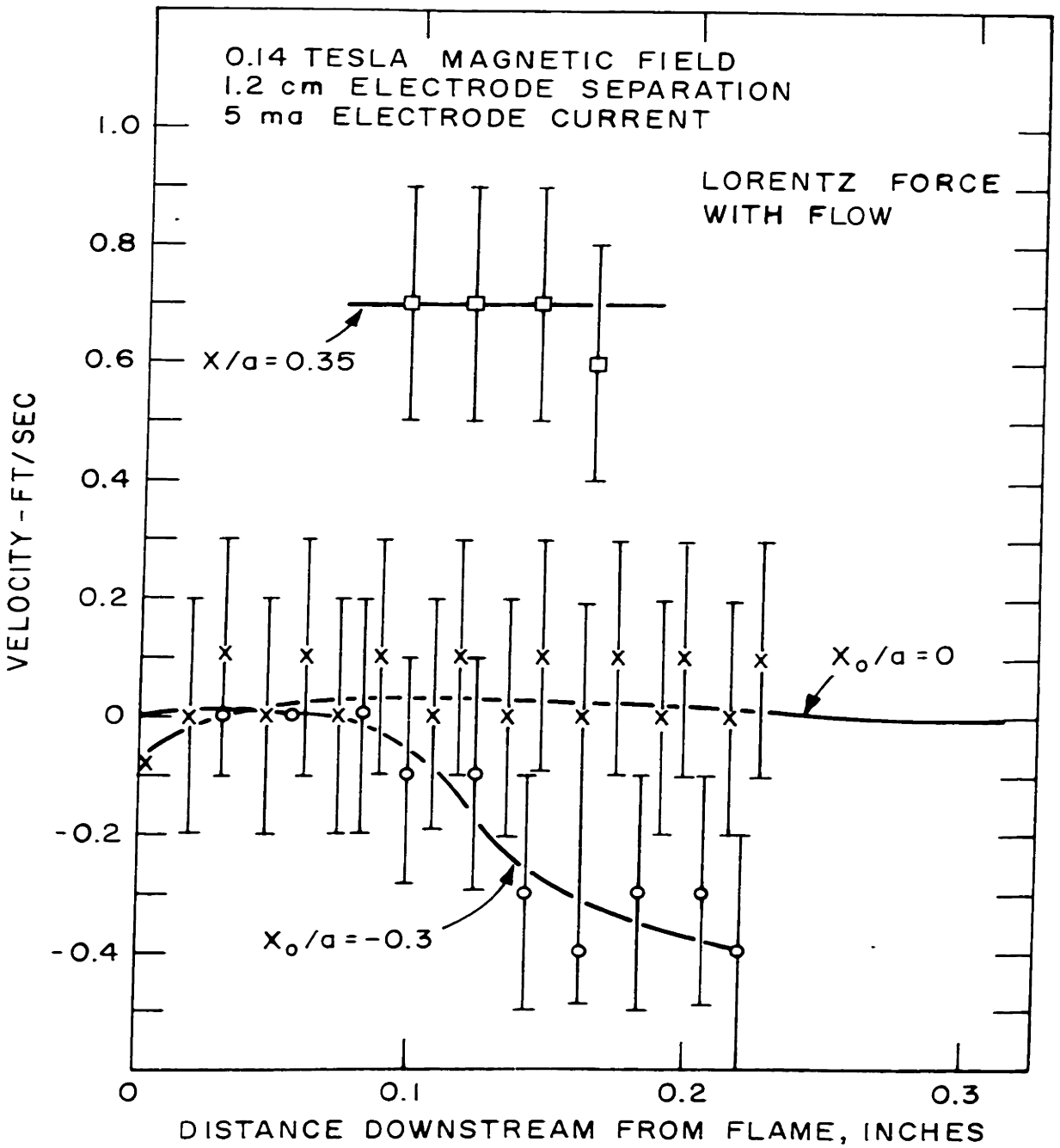

FIG. 18 X COMPONENT OF VELOCITY AS FUNCTION OF DISTANCE FROM FLAME

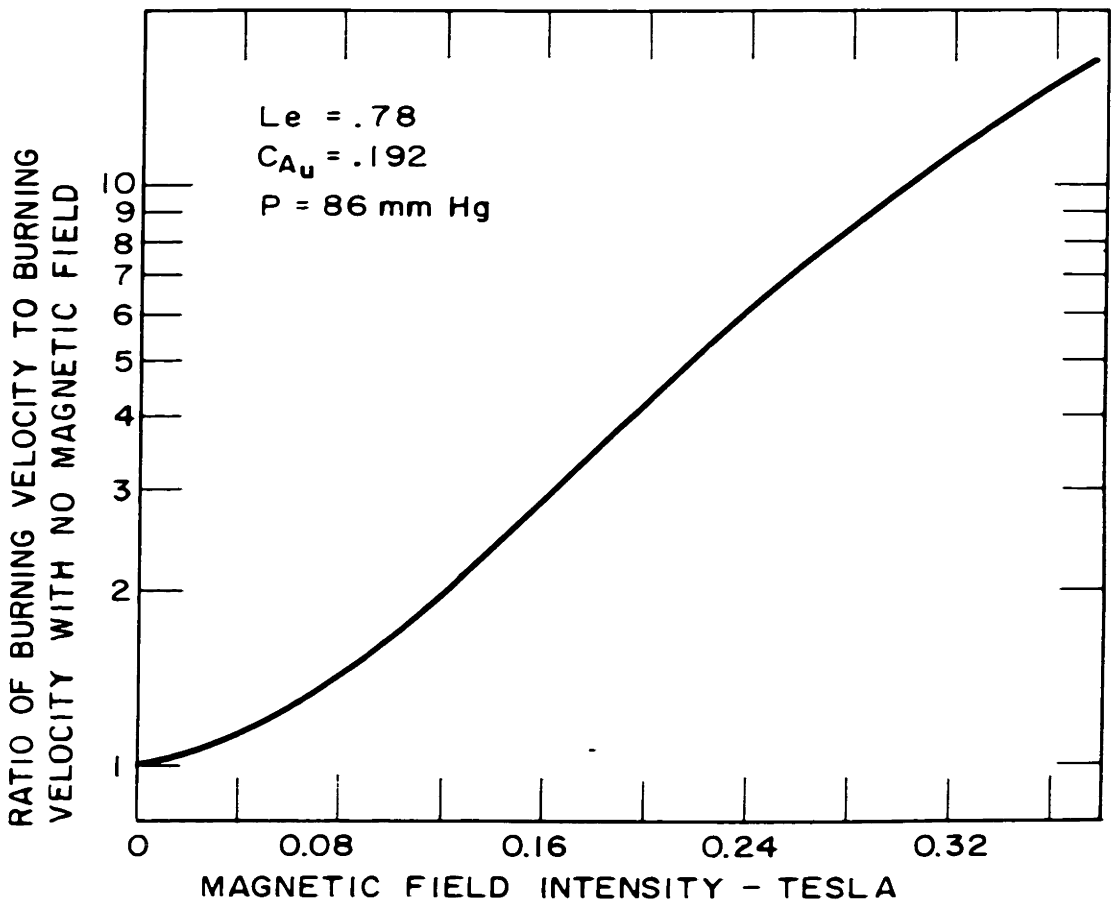

FIG. 20 VARIATION OF BURNING VELOCITY WITH APPLIED MAGNETIC FIELD - CALCULATED ACCORDING TO ANALYTICAL MODEL OF GROSS ET AL

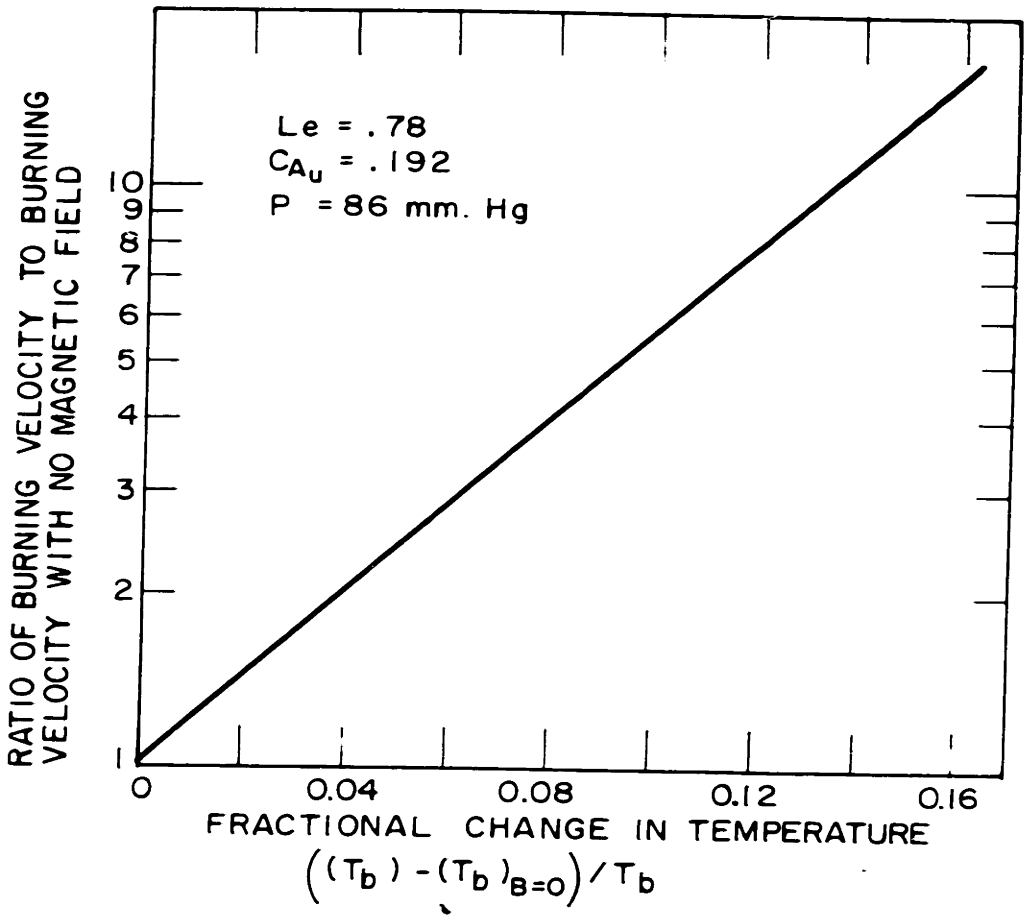

FIG. 21 VARIATION OF BURNING VELOCITY WITH FRACTIONAL CHANGE IN TEMPERATURE AS PREDICTED IN ANALYSES BASED ON CONDITIONS OF GROSS ET AL.

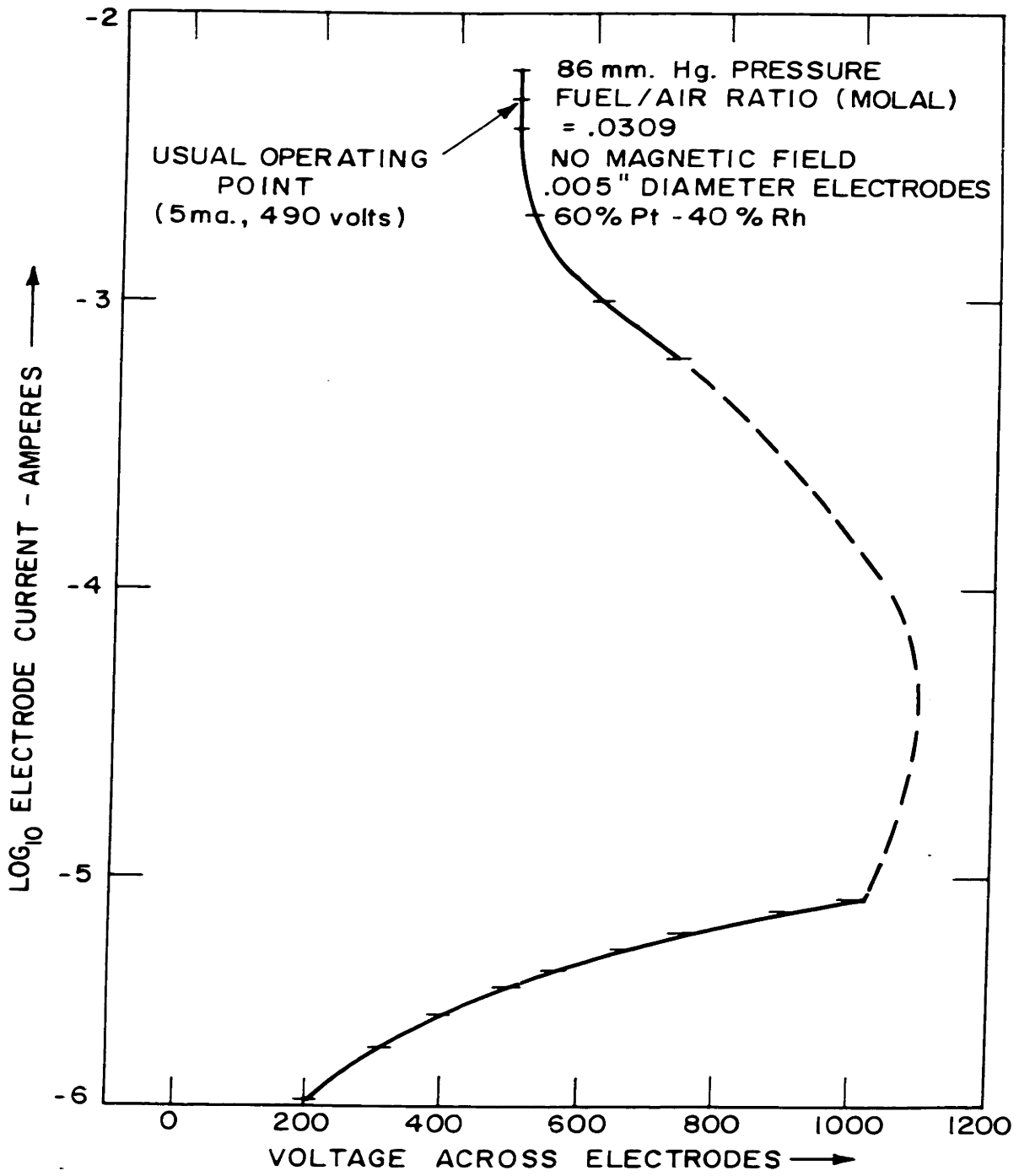

FIG. 22 VOLTAGE VS. CURRENT CURVE ACROSS ELECTRODES

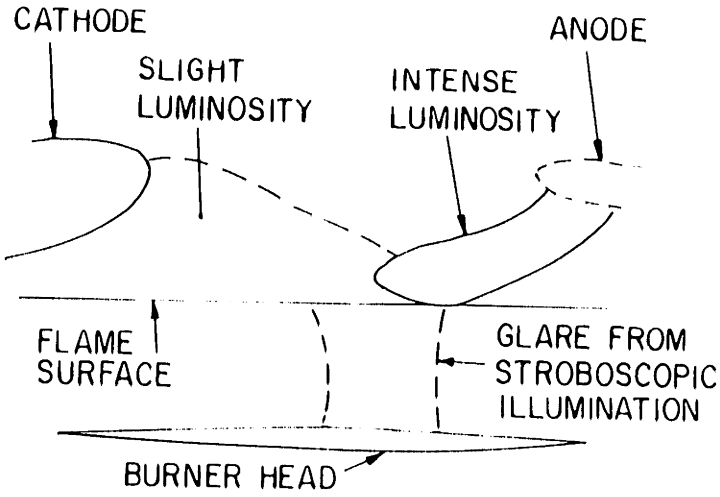

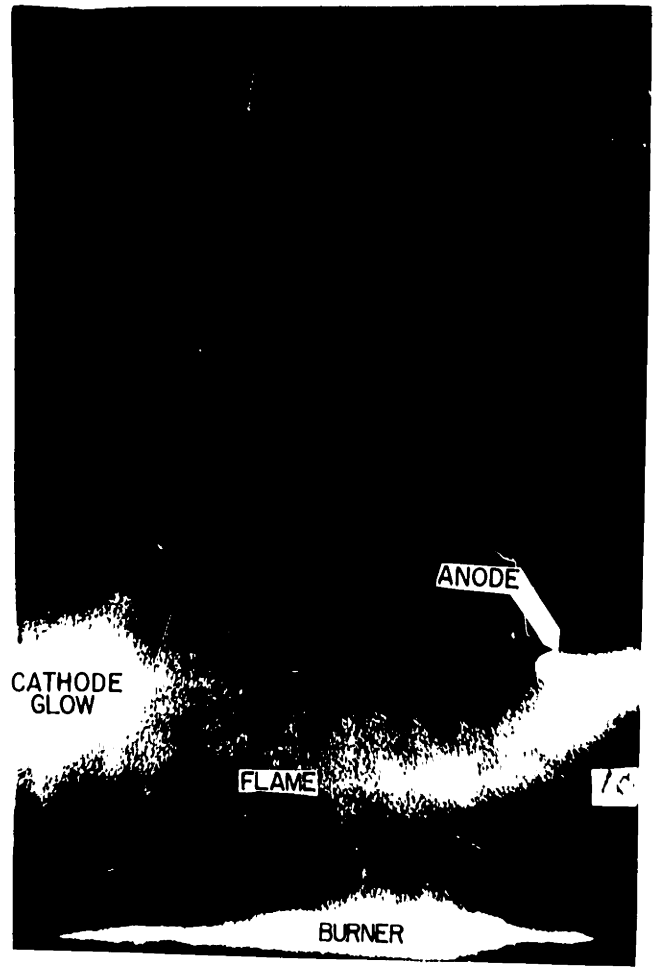

FIG. 23 ILLUSTRATION SHOWING STRATIFICATION OF LUMINOSITY AT FLAME SURFACE (LORENTZ FORCE IS AGAINST FLOW DIRECTION)

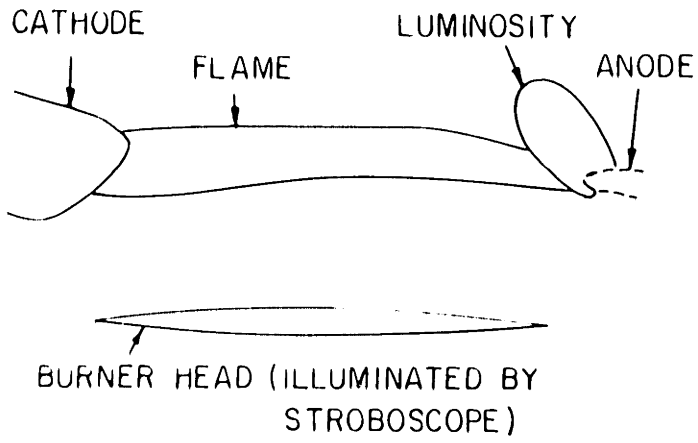

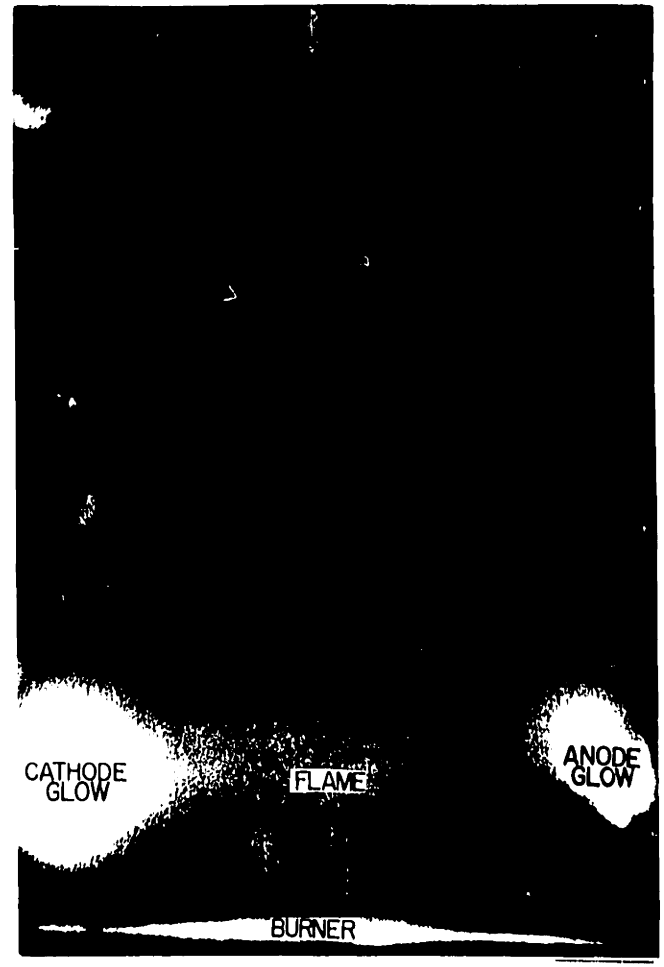

FIG 24 ILLUSTRATION OF TILTING OF LUMINOSITY AT ANODE WHEN LORENTZ FORCE IS IN DIRECTION OF FLOW

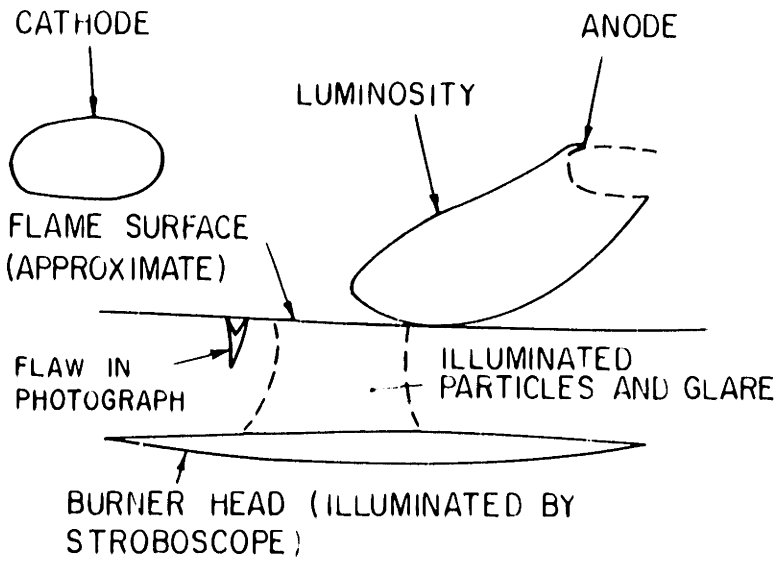

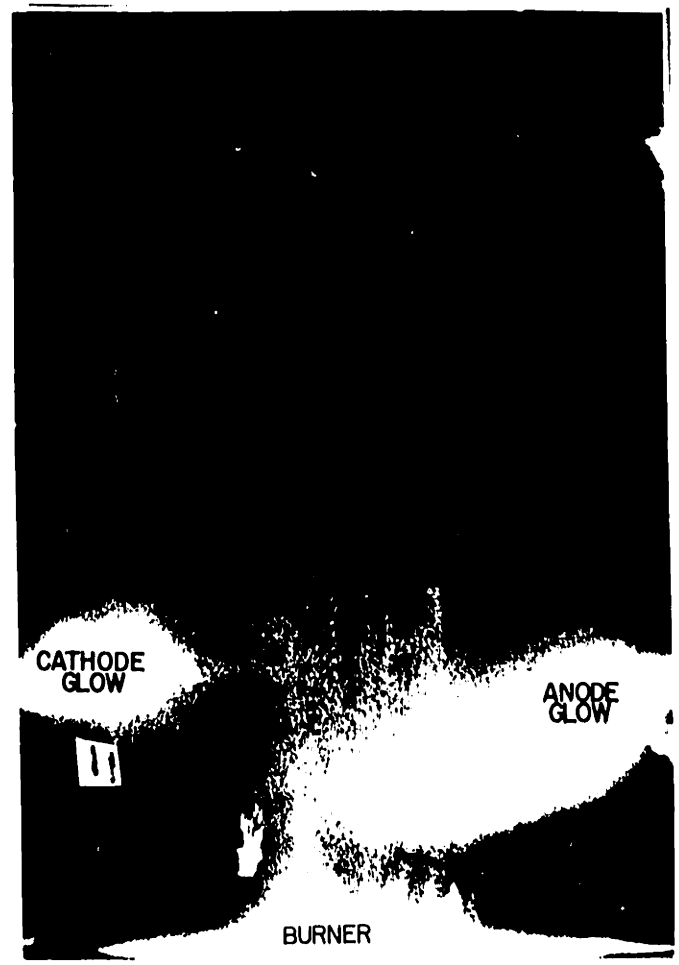

FIG. 25 ILLUSTRATION OF CONCENTRATION OF CURRENT WHEN LORENTZ FORCE IS AGAINST DIRECTION OF FLOW

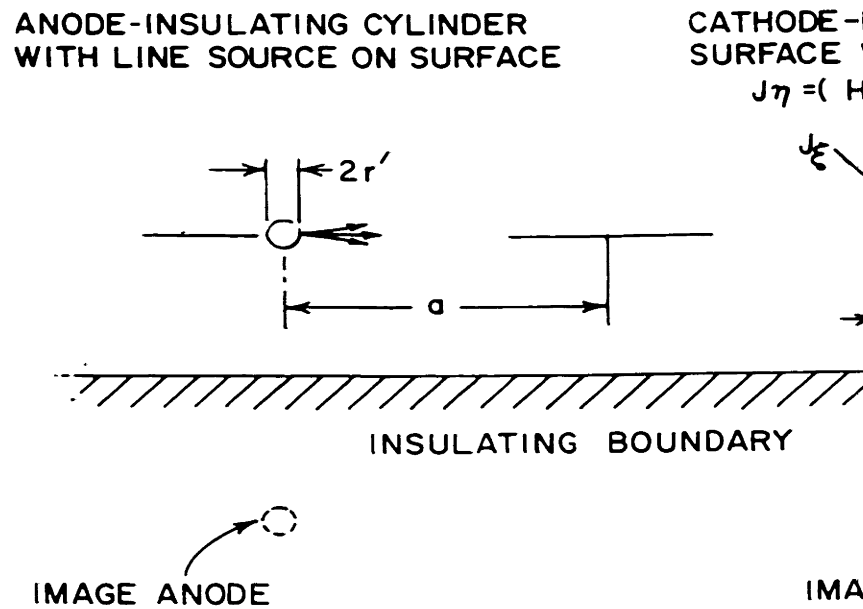

FIG. 26a SOLUTION TREATING DETAIL OF CURRE

ELECTRODE - SOURCE OF E FIELD

$E_r = k/r$

ELECTRODE - SOURCE OF CURRENT + CENTER OF VORTEX OF CURRENT

$$J_r = \frac{\sigma}{(1+H^2)} E_r \quad + \quad J_\theta = H J_r$$

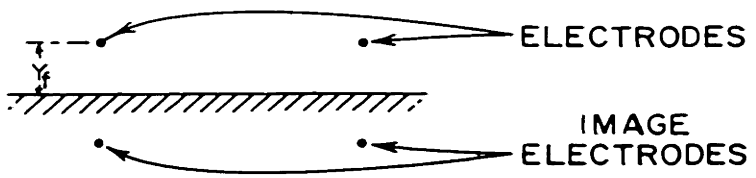

FIG. 26b TREATMENT OF ELECTRODES AS CURRENT SINGULARITIES

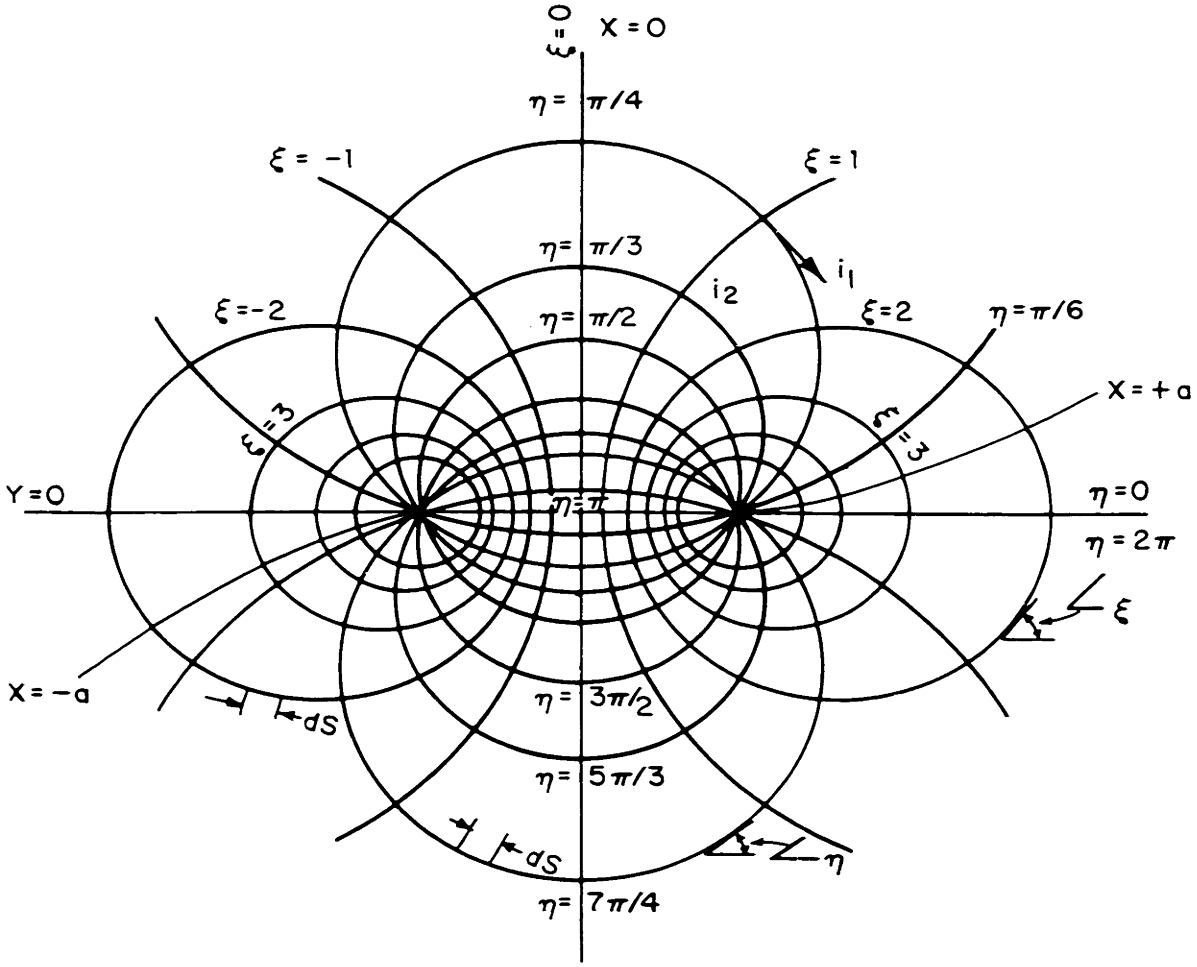

FIG. 26c – BIPOLAR COORDINATES

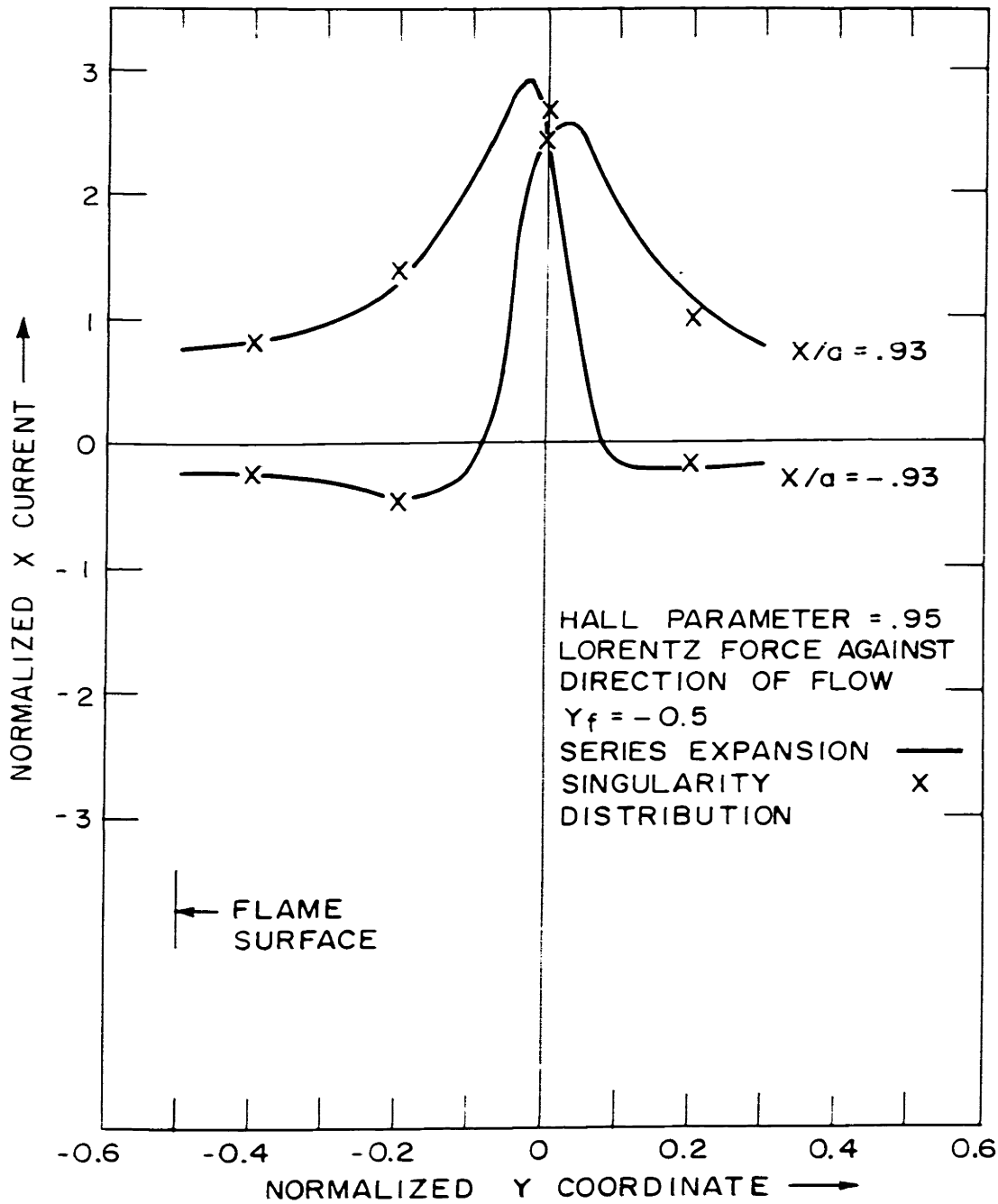

FIG. 27 COMPARISON OF X-COMPONENT OF CURRENT AS CALCULATED BY SERIES EXPANSION AND BY SINGULARITY DISTRIBUTION

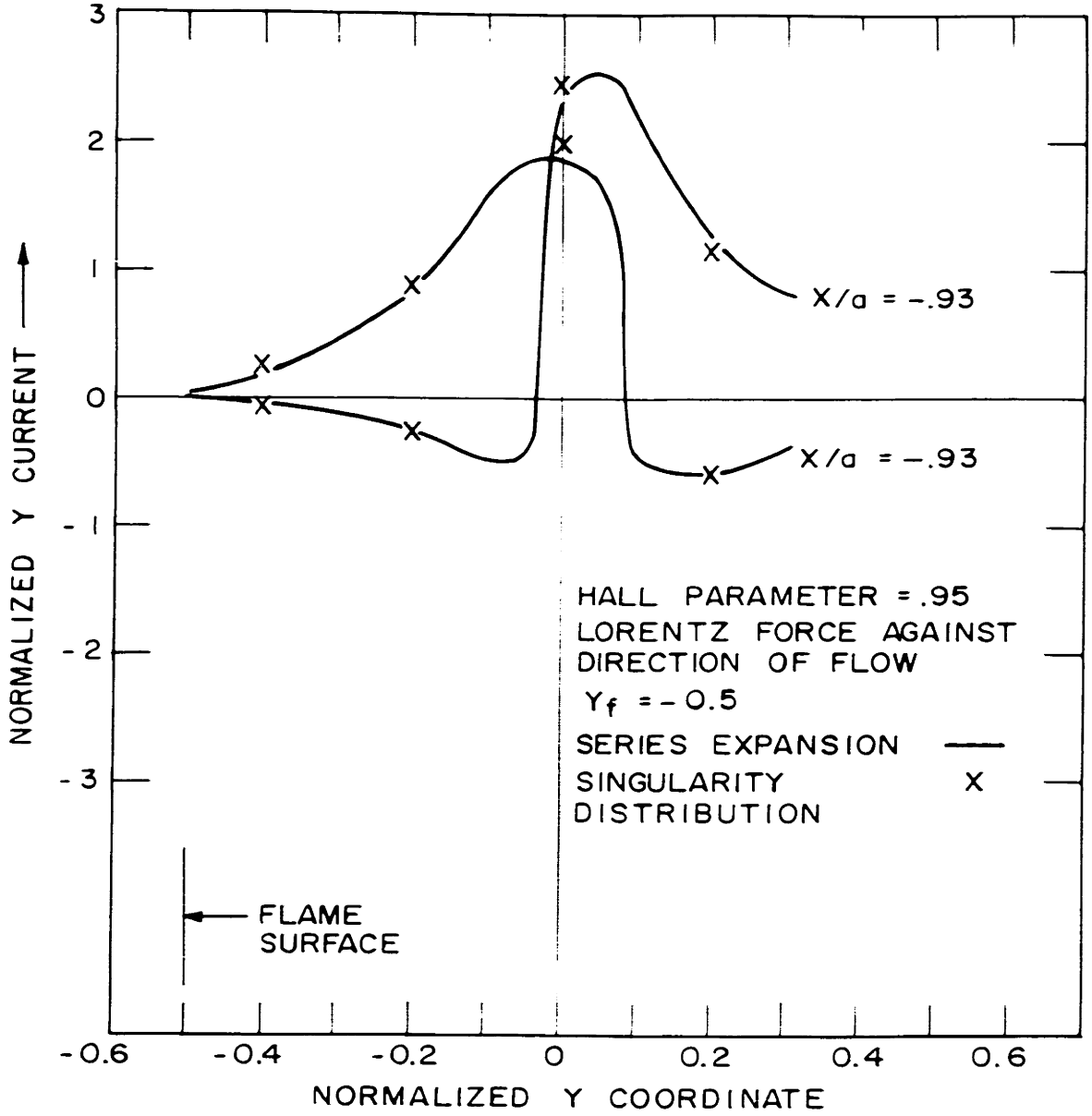

FIG. 28 COMPARISON OF Y-COMPONENT OF CURRENT AS CALCULATED BY SERIES EXPANSION AND BY SINGULARITY DISTRIBUTION

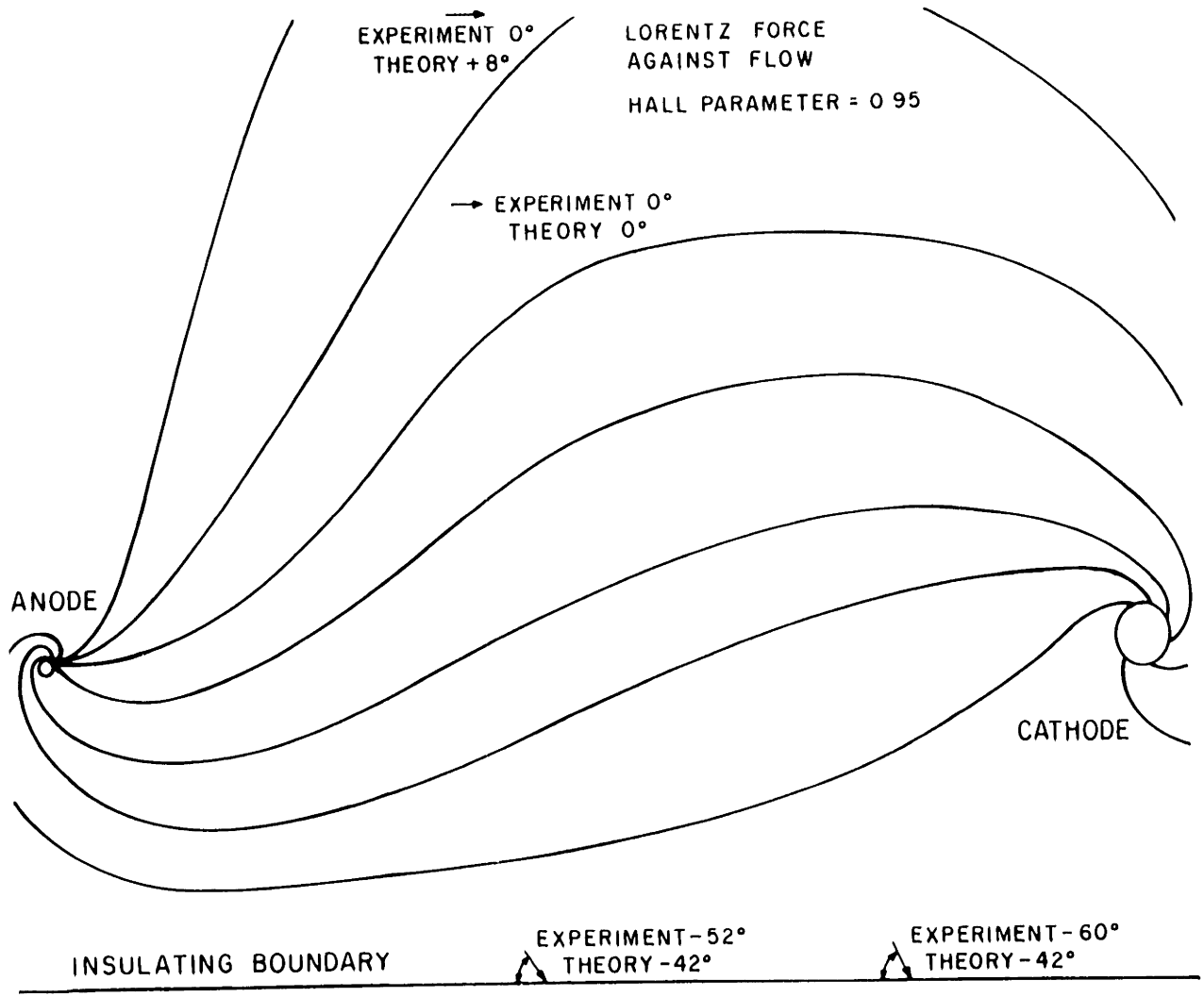

FIG. 29 CALCULATED CURRENT PATTERN - COMPARISON OF THEORETICAL AND EXPERIMENTAL ELECTRIC FIELD

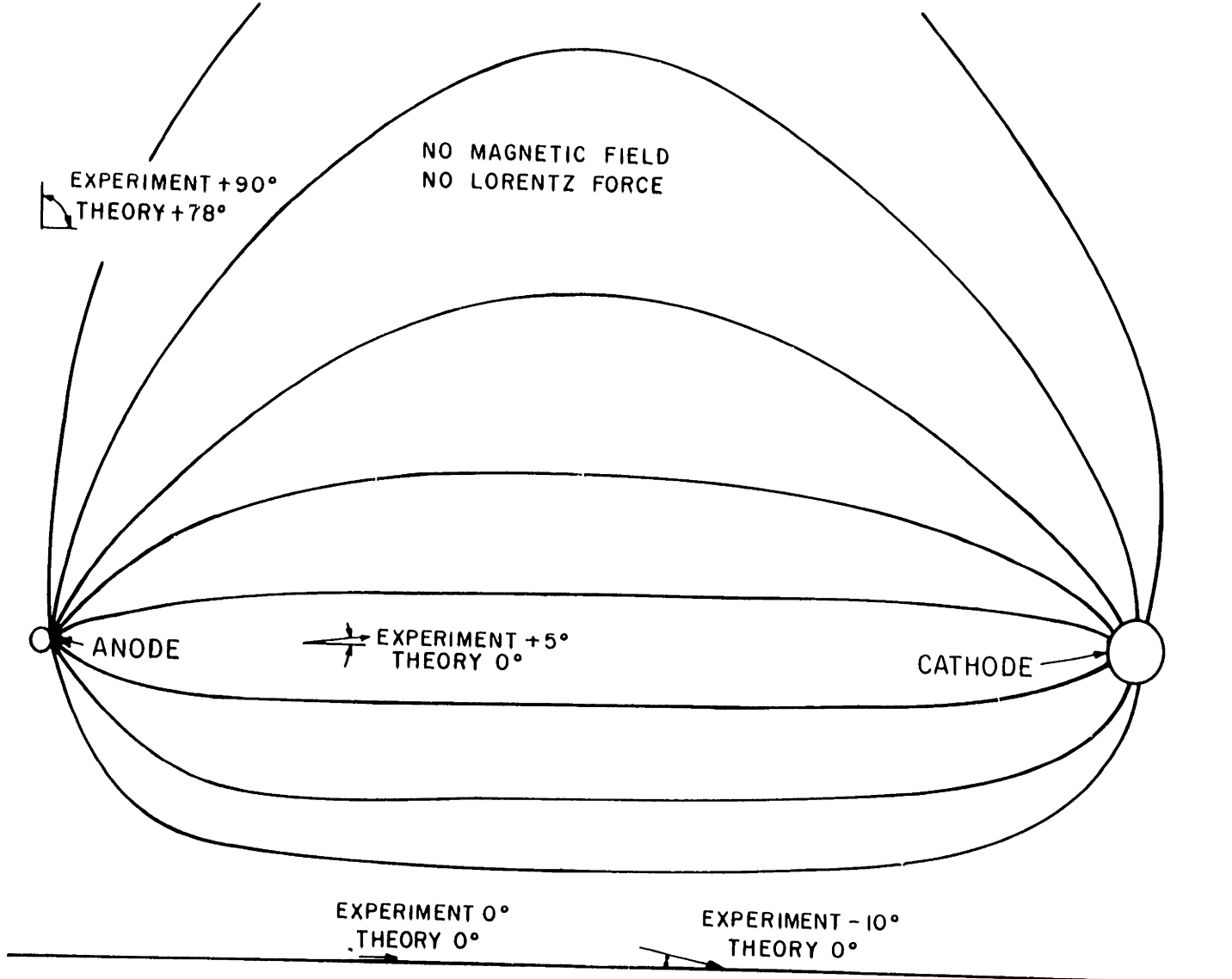

FIG. 30 COMPARISON OF THEORETICAL AND EXPERIMENTAL ELECTRIC FIELD - CALCULATED CURRENT PATTERN

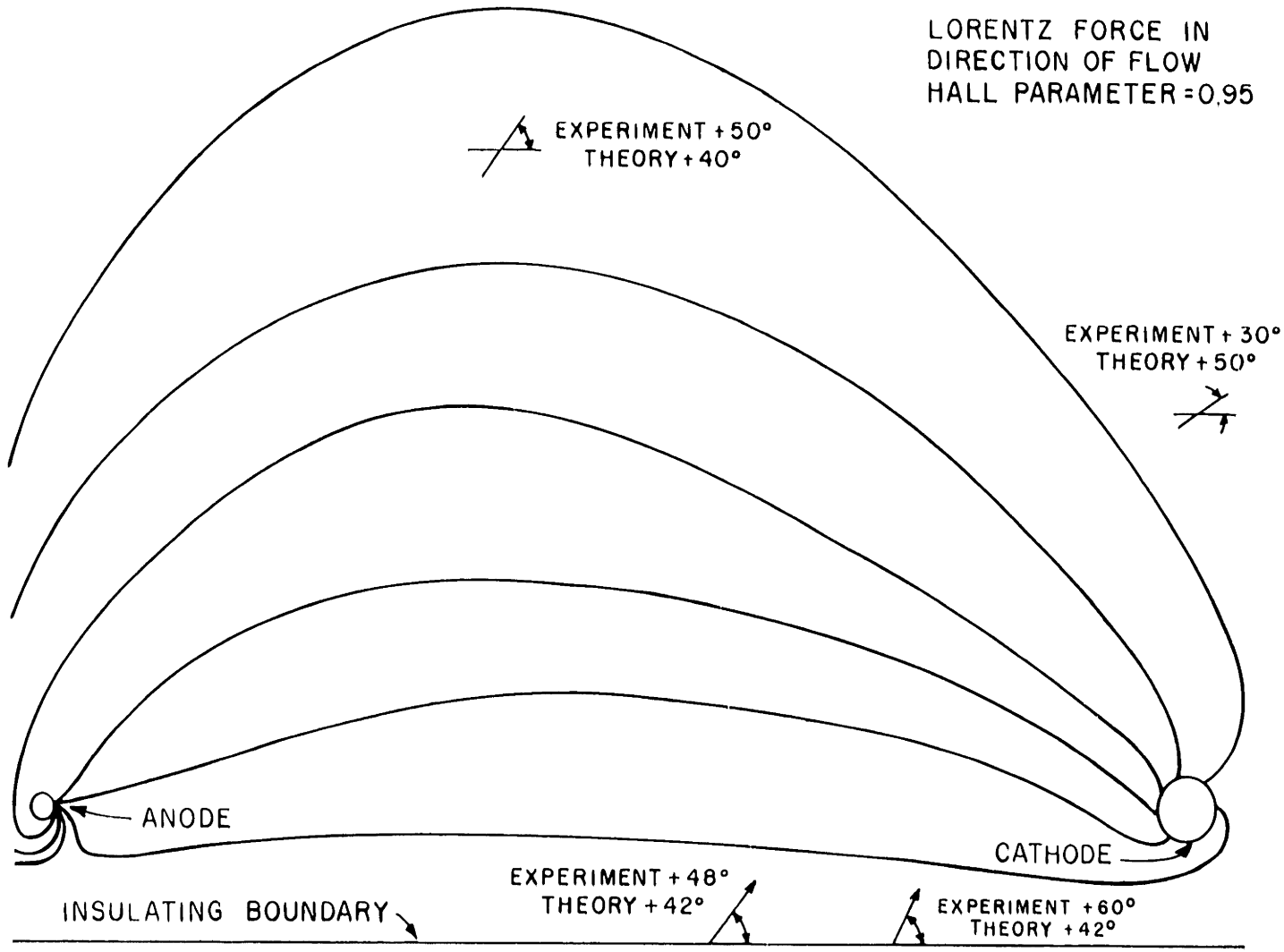

FIG. 31 CALCULATED ELECTRIC CURRENT PATTERN-COMPARISON OF THEORETICAL AND EXPERIMENTAL ELECTRIC FIELD

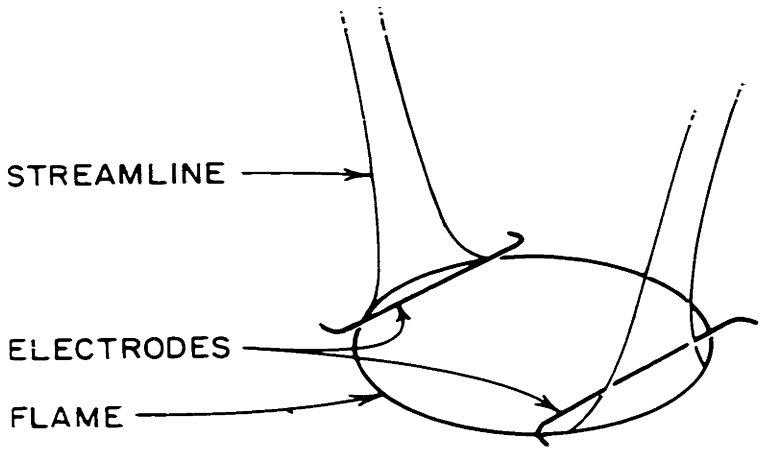

LORENTZ FORCE IN DIRECTION OF FLOW

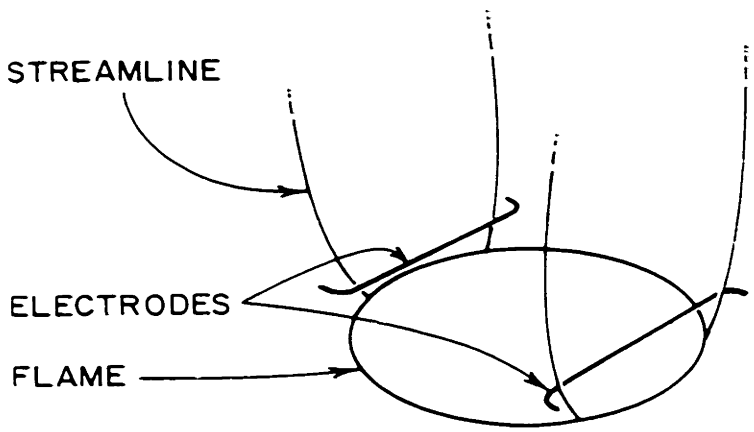

LORENTZ FORCE AGAINST DIRECTION OF FLOW

FIG. 32

FLOW IN CENTRAL STRIP OF GAS FLOW

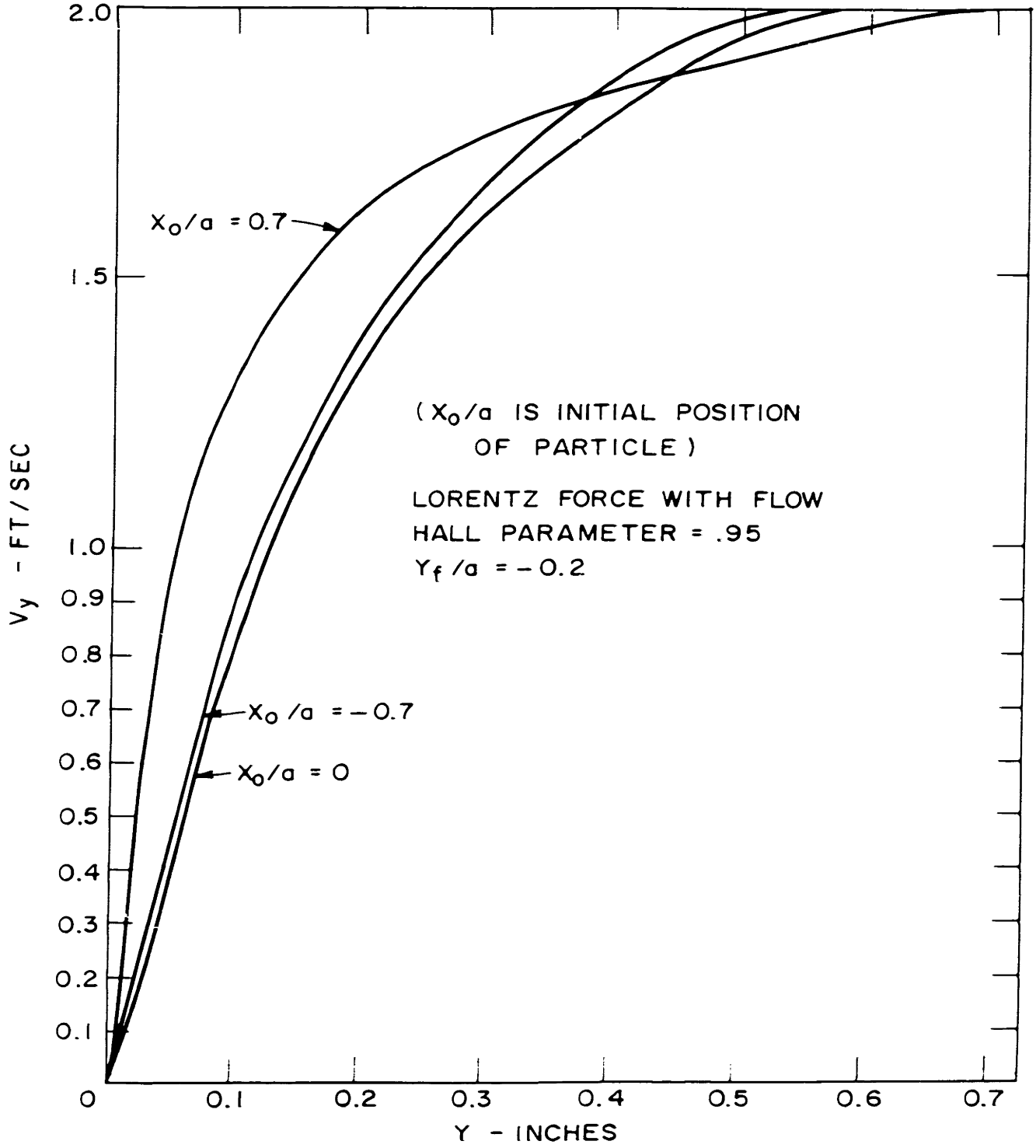

FIG. 33 VELOCITY RISE ABOVE 4.2 FT/SEC VS DISTANCE DOWSTREAM FROM FLAME

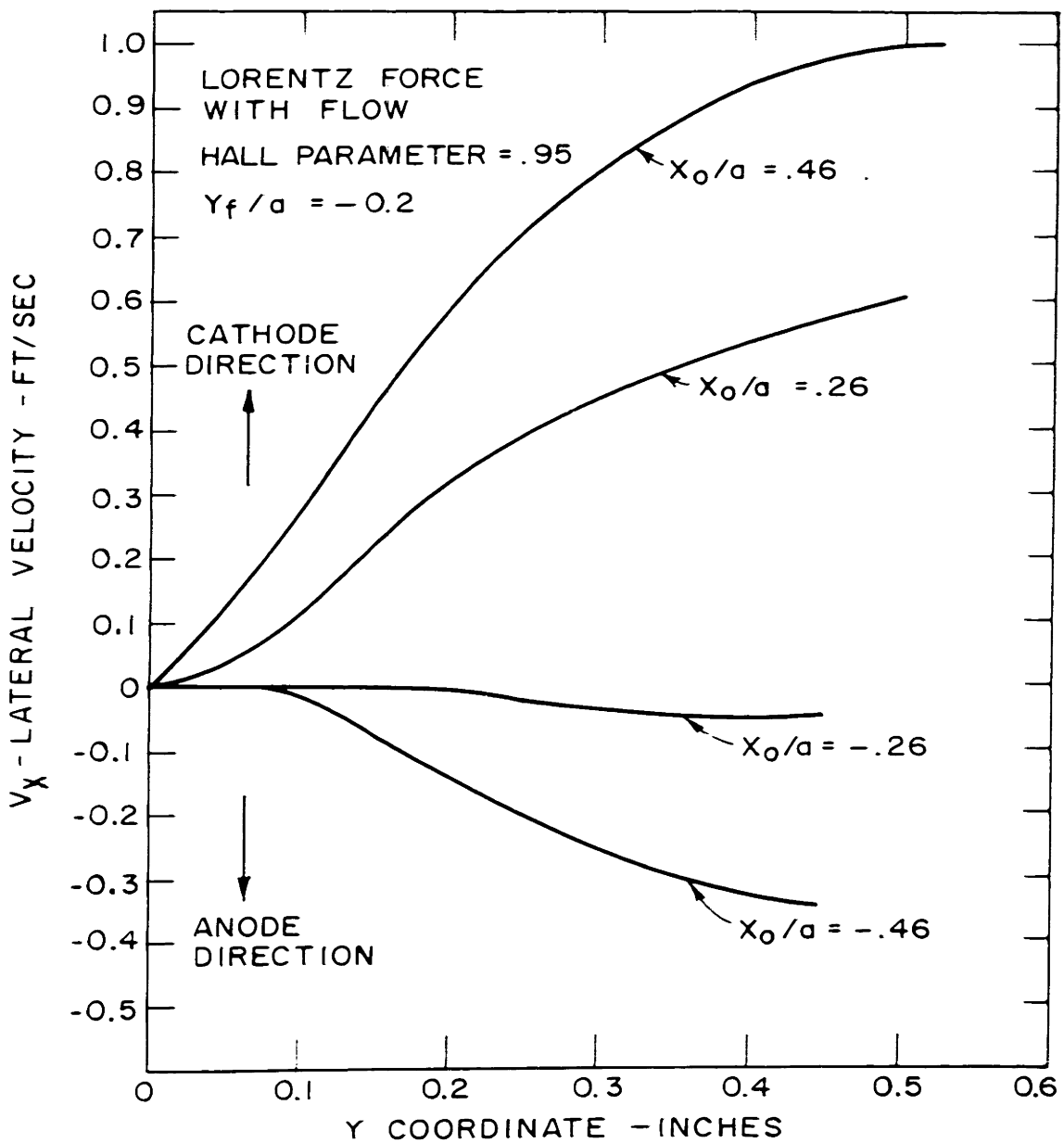

FIG. 34 PLOT OF LATERAL VELOCITY VS DISTANCE DOWNSTREAM FROM FLAME FOR SEVERAL VALUES OF INITIAL POSITION AT FLAME

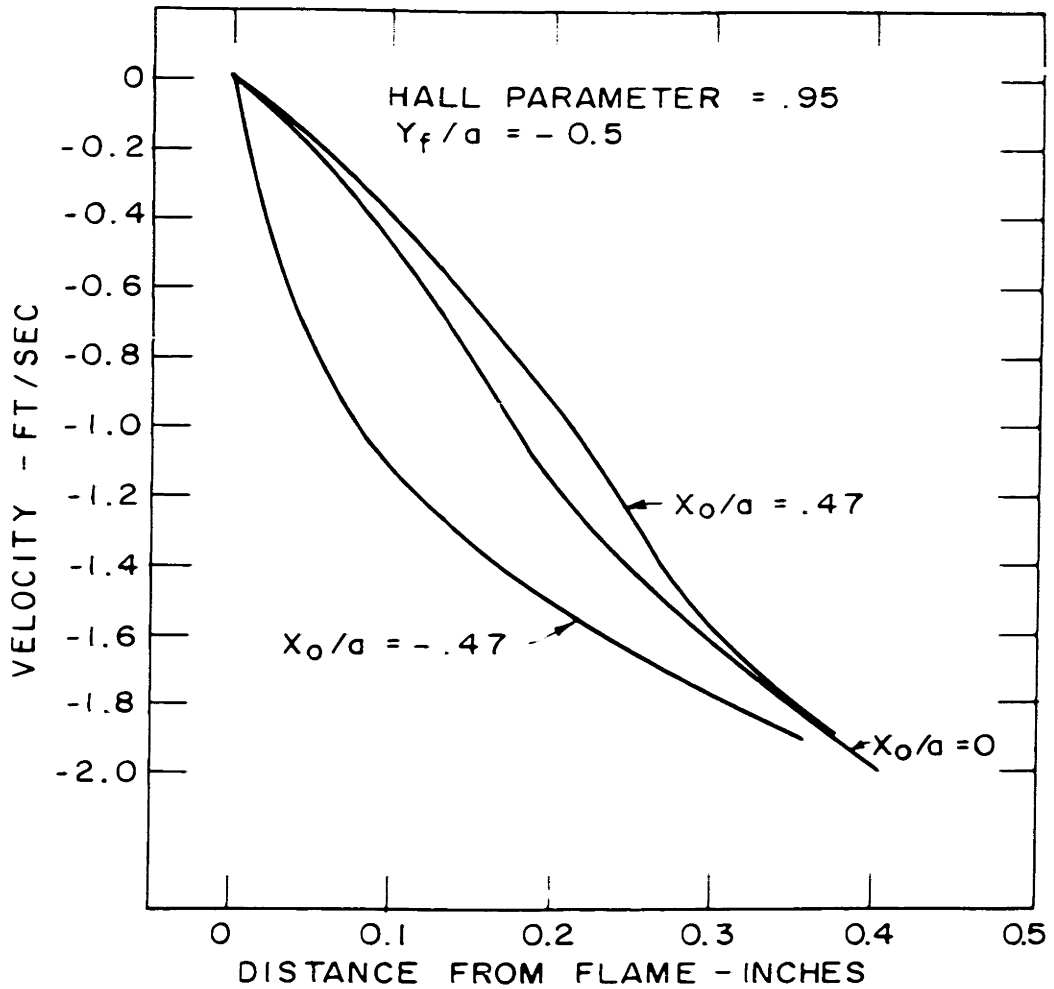

FIG. 35 PLOT OF Y COMPONENT OF VELOCITY CHANGE-LORENTZ FORCE AGAINST FLOW

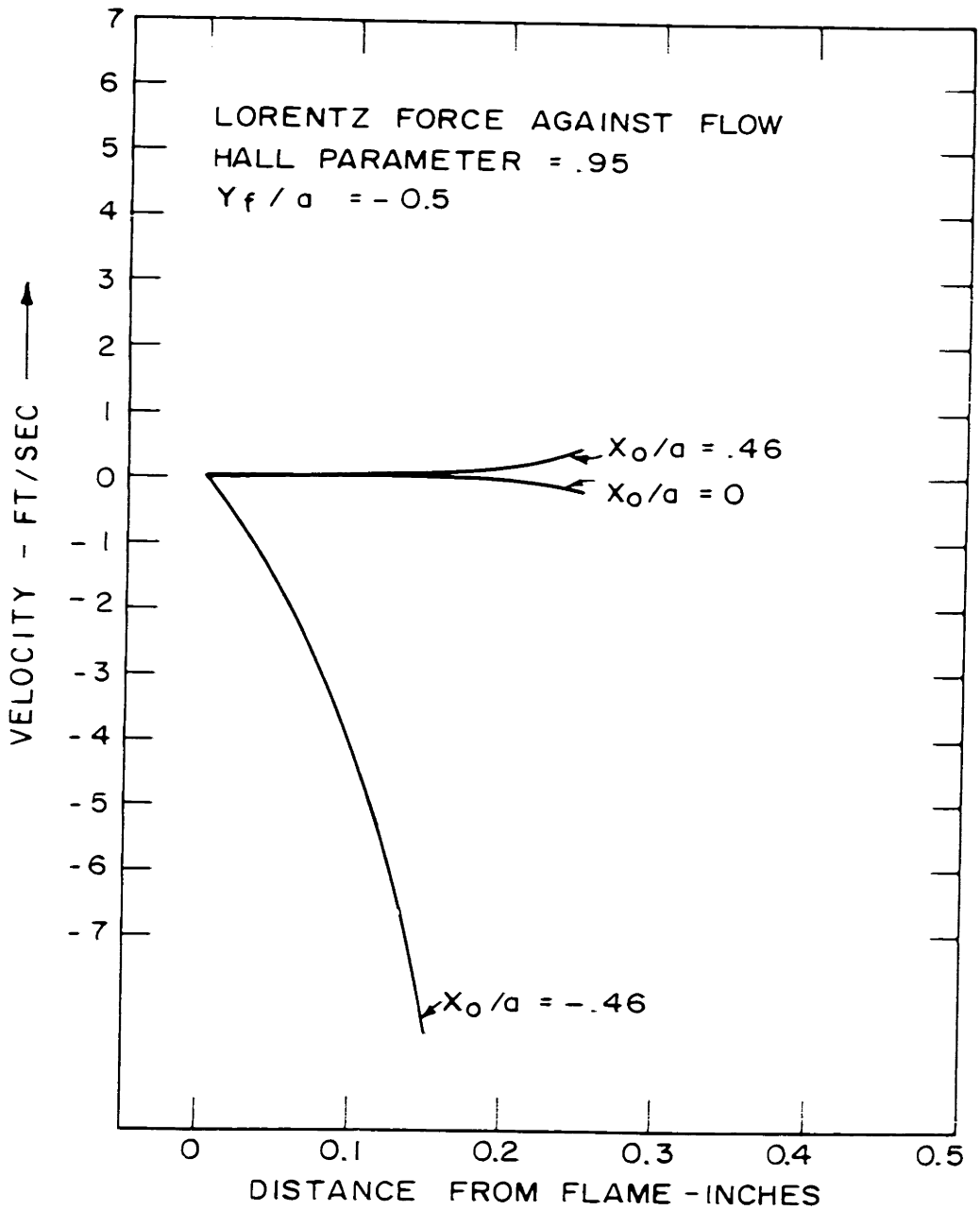

FIG. 36 PLOT OF X COMPONENT OF VELOCITY CHANGE

FIG. 37

3-VIEWS OF BURNER AND ELECTRODES MOUNTED IN LOWER HALF OF TEST SECTION (1/2 size)

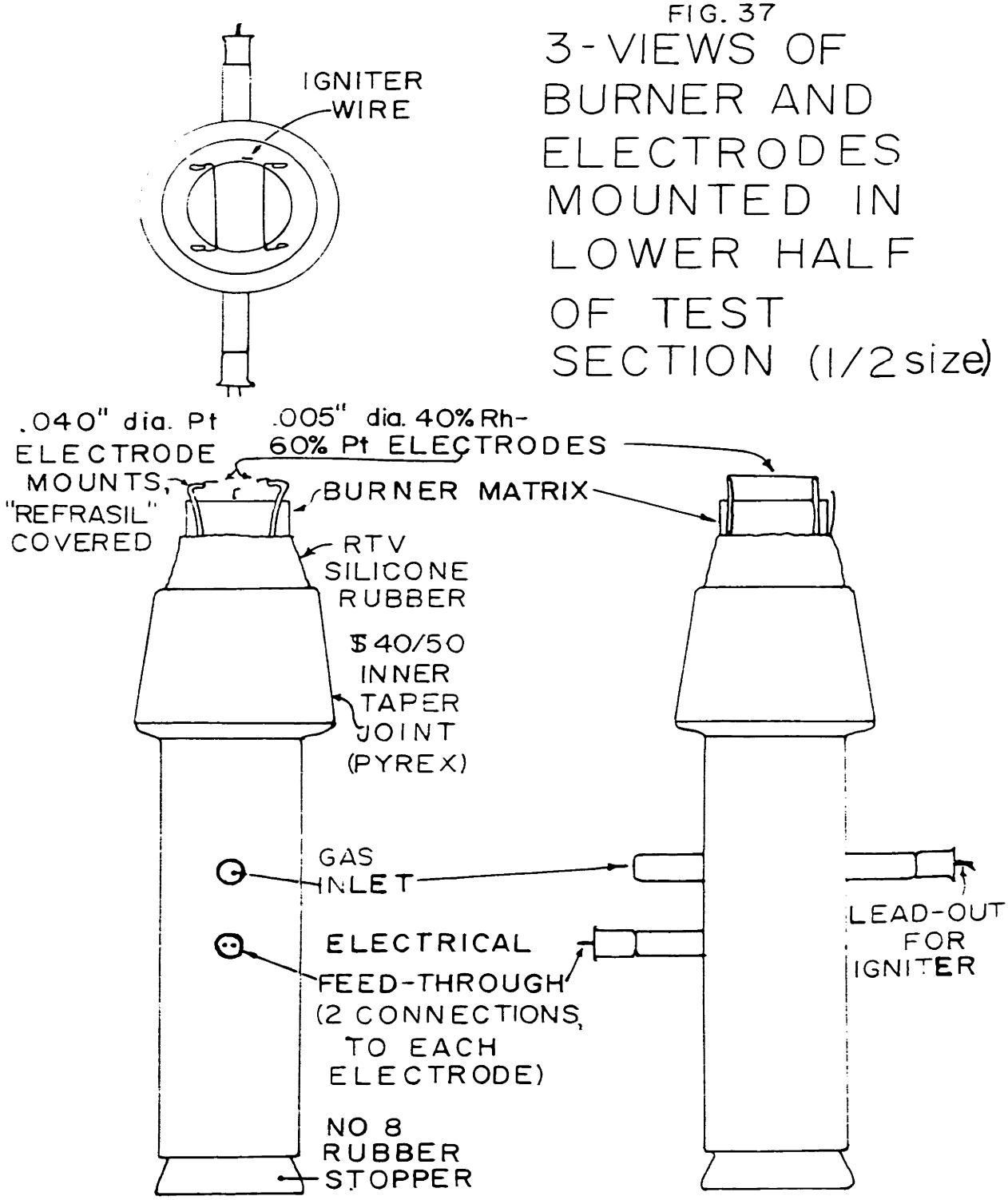

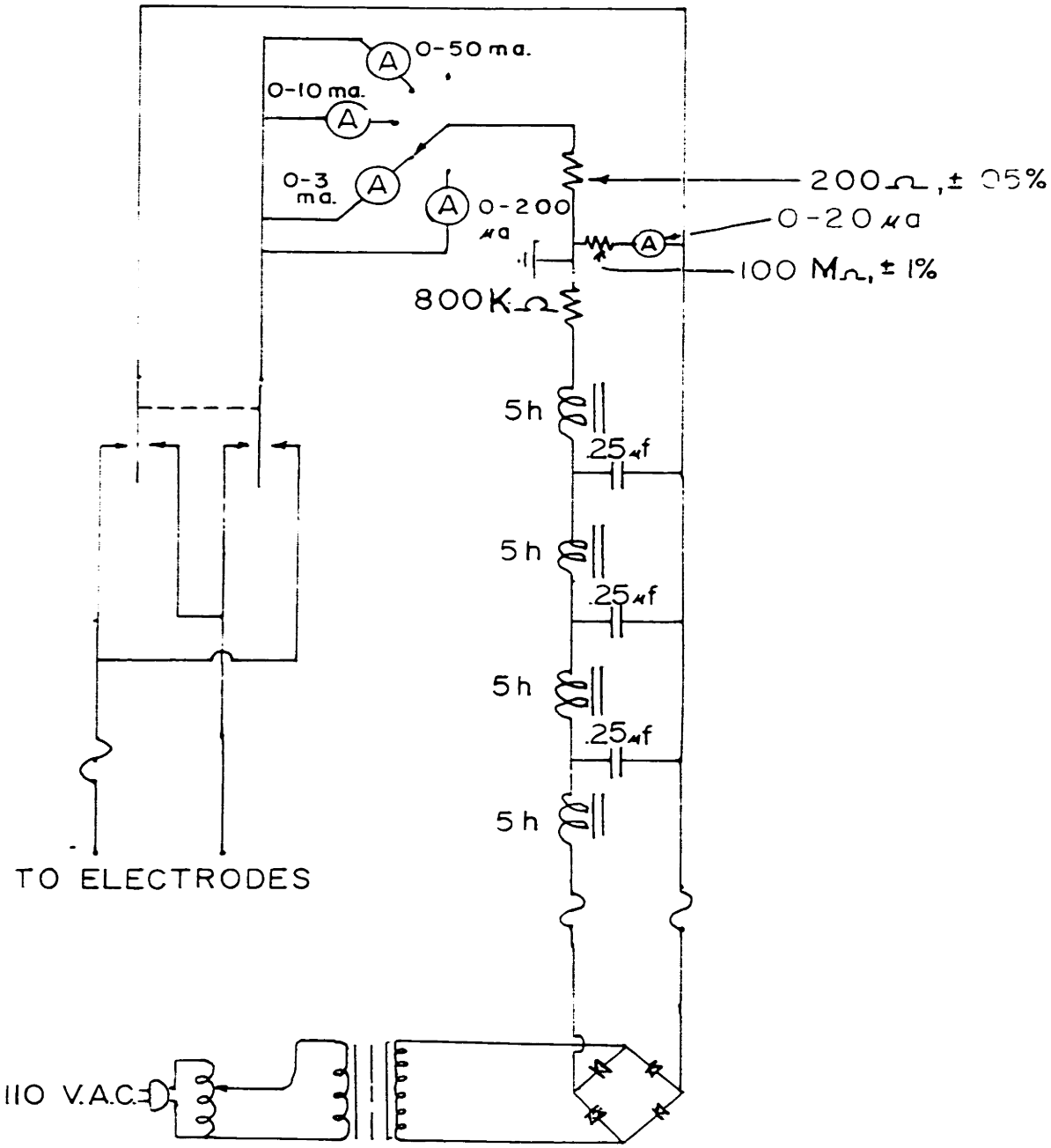

FIG. 39

ELECTRODE POWER SUPPLY

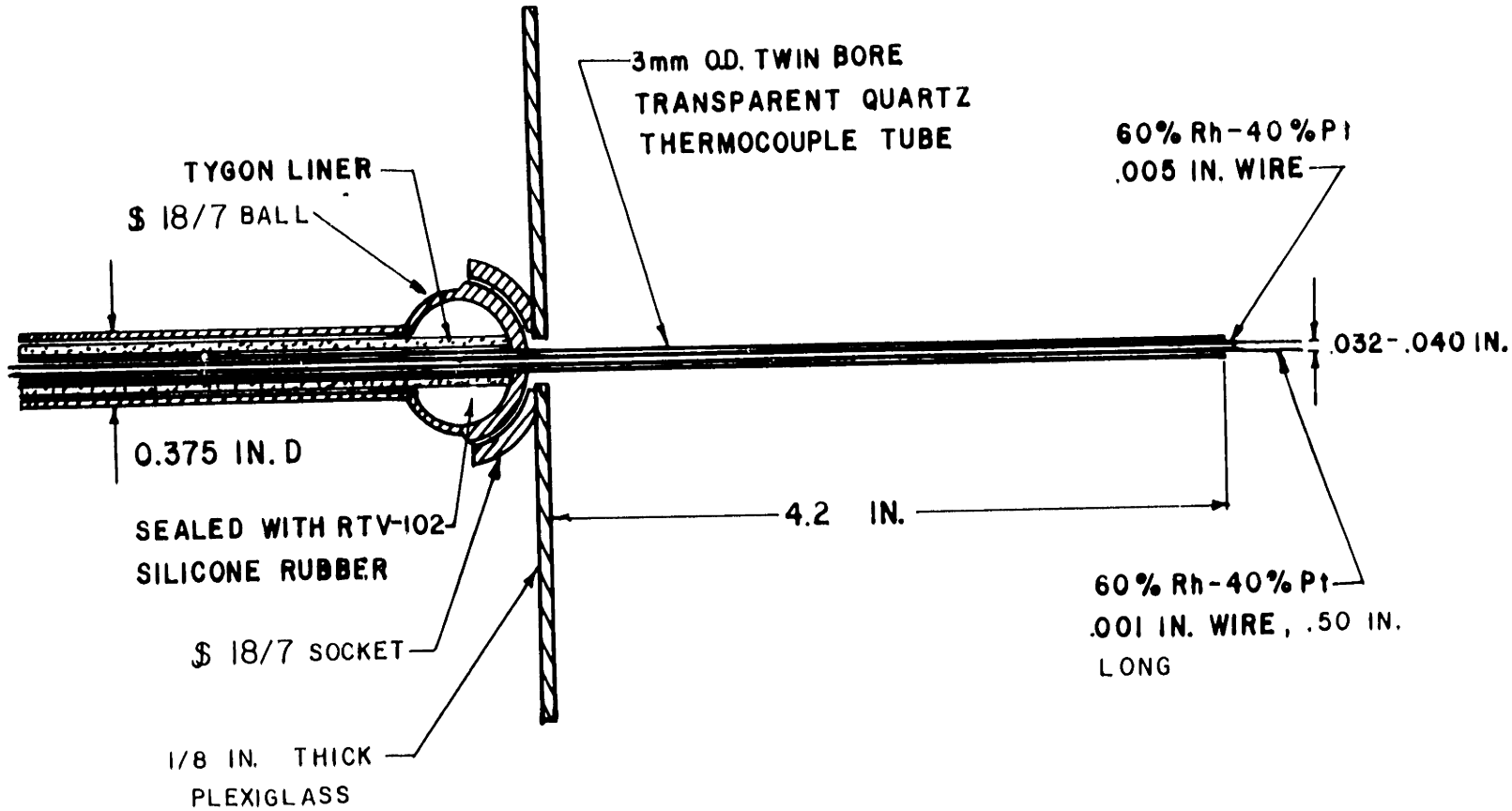

FIG. 40

E FIELD PROBE

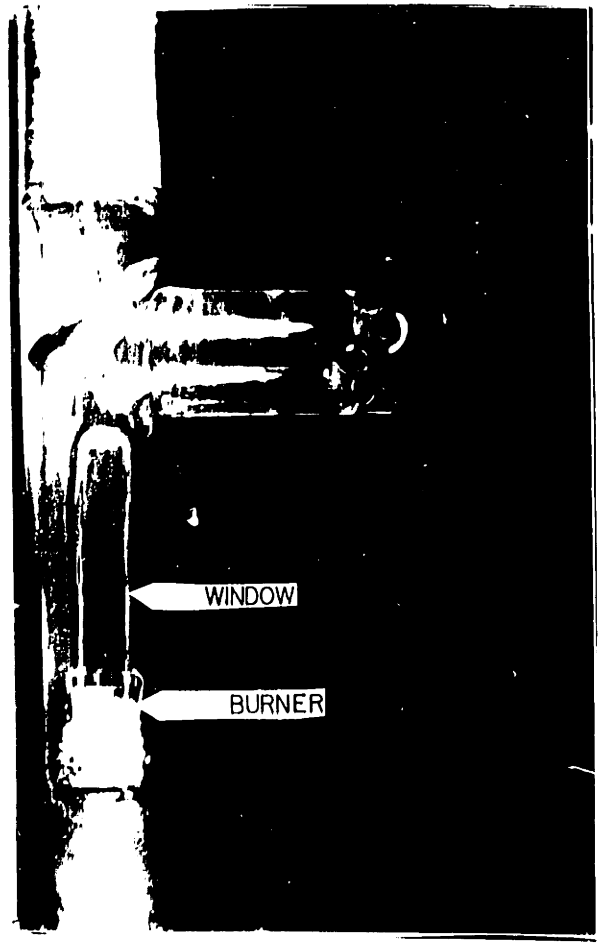

FIG 41 UPPER HALF OF TEST SECTION, WITH LOWER HALF OF TEST SECTION MOUNTED

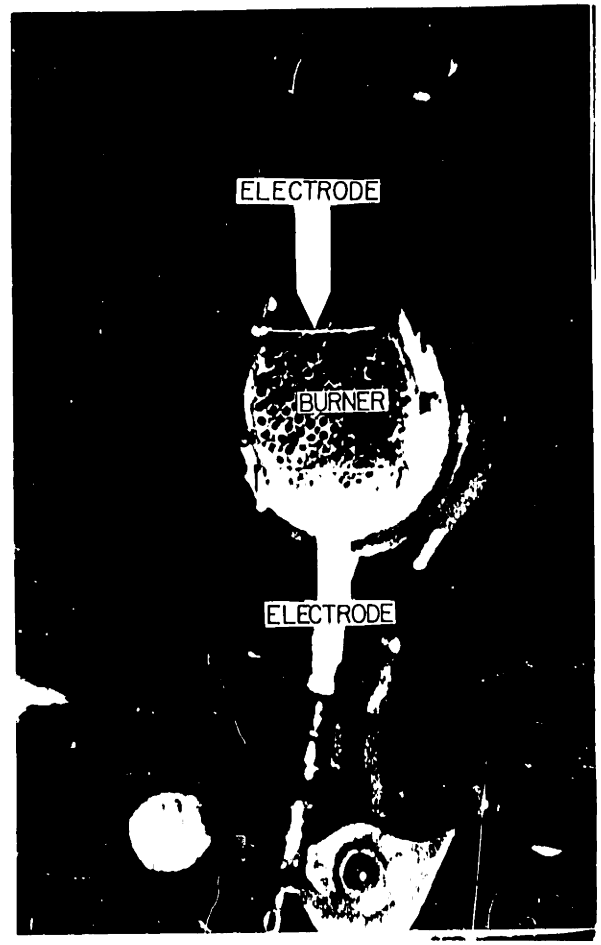

FIG 42 HEAD ON VIEW OF BURNER AND ELECTRODES

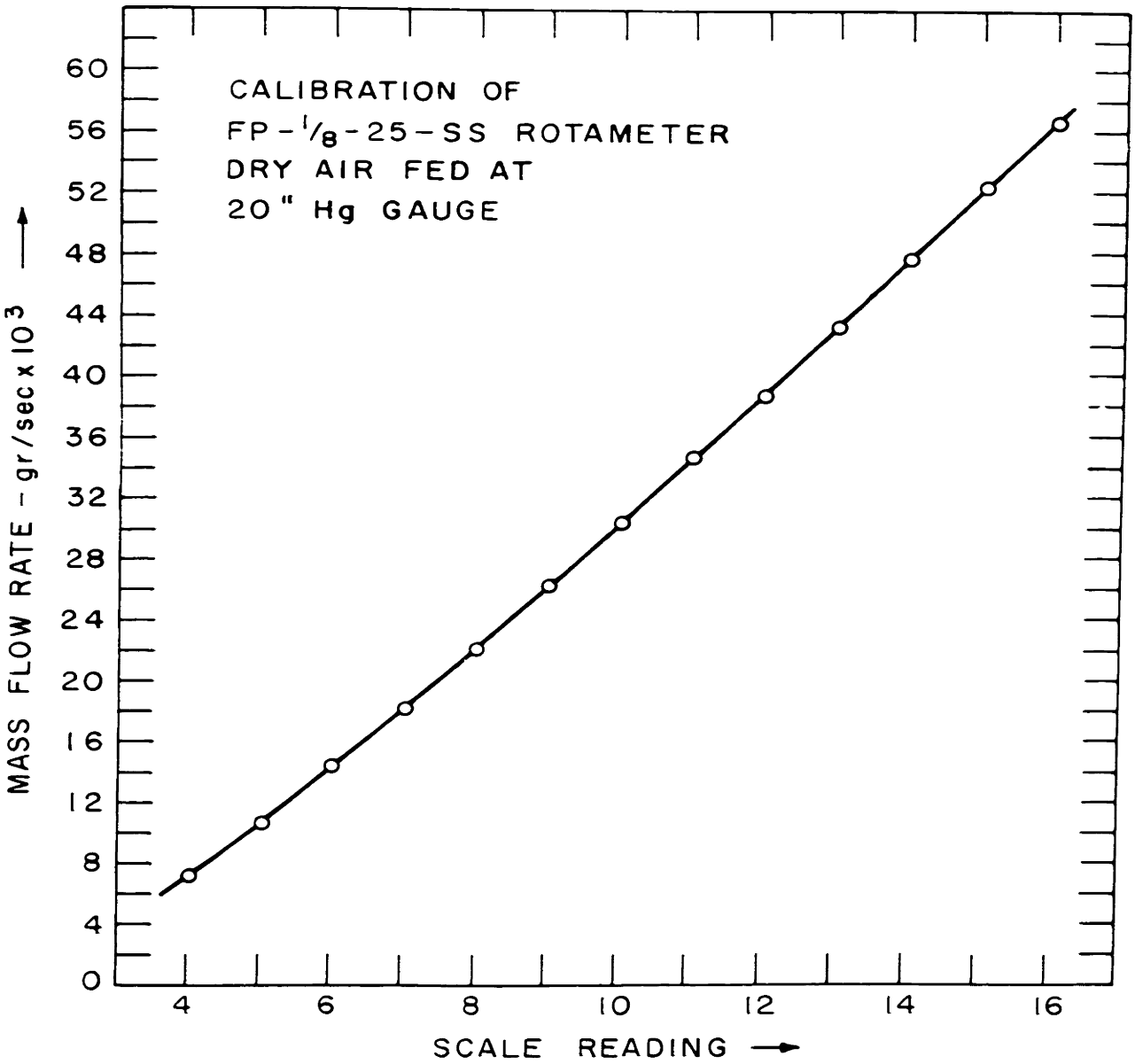
CALIBRATION OF
FP-1/8-25-SS ROTAMETER
DRY AIR FED AT
20" Hg GAUGE
MASS FLOW RATE - gr/sec x 10^3
0
4
8
12
16
20
24
28
32
36
40
44
48
52
56
60
4
6
8
10
12
14
16
SCALE READING

FIG. 43

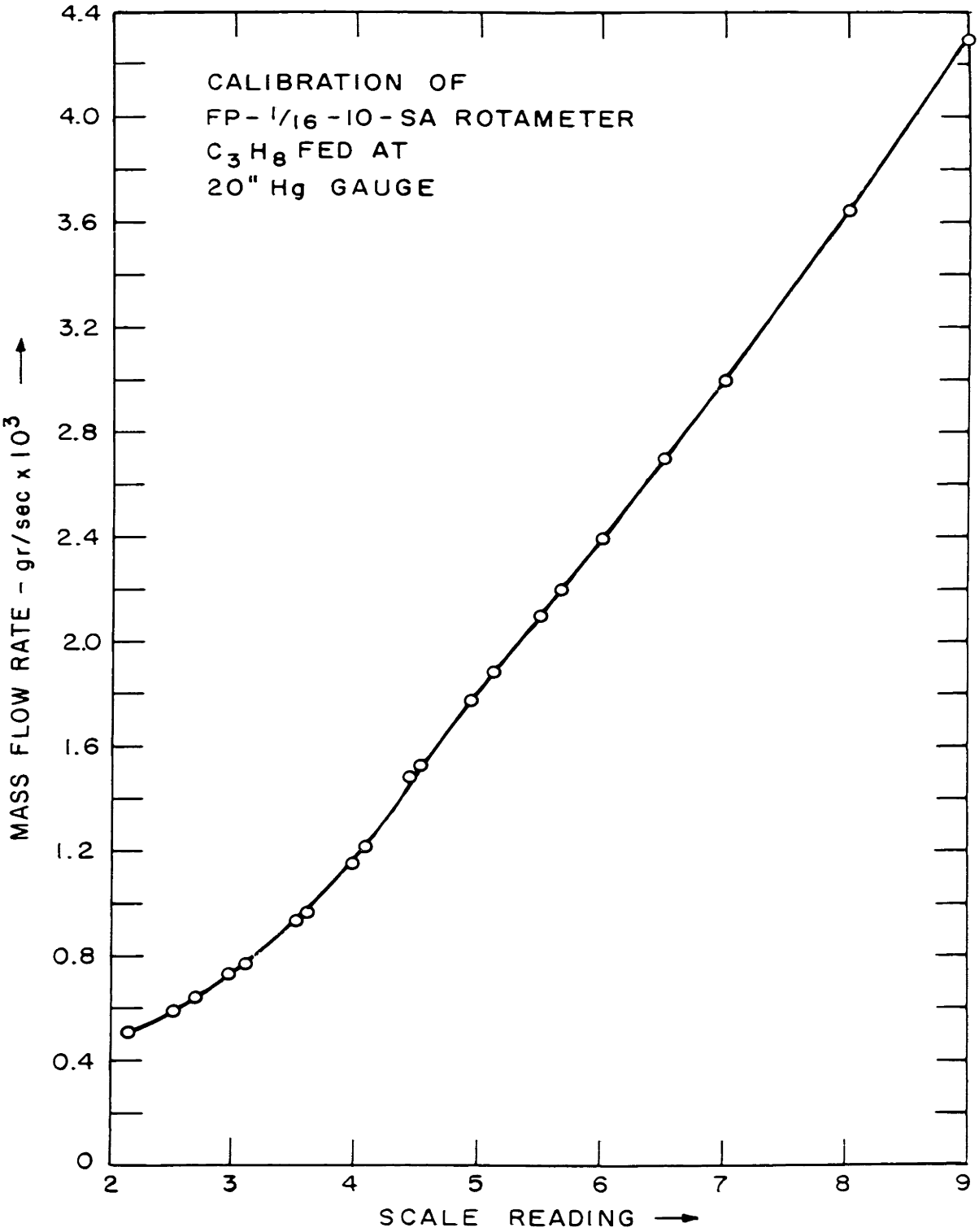
CALIBRATION OF
FP-1/16-10-SA ROTAMETER
C3H8 FED AT
20" Hg GAUGE
MASS FLOW RATE - gr/sec x 10^3
SCALE READING
4.4
4.0
3.6
3.2
2.8
2.4
2.0
1.6
1.2
0.8
0.4
0
2
3
4
5
6
7
8
9

FIG. 44

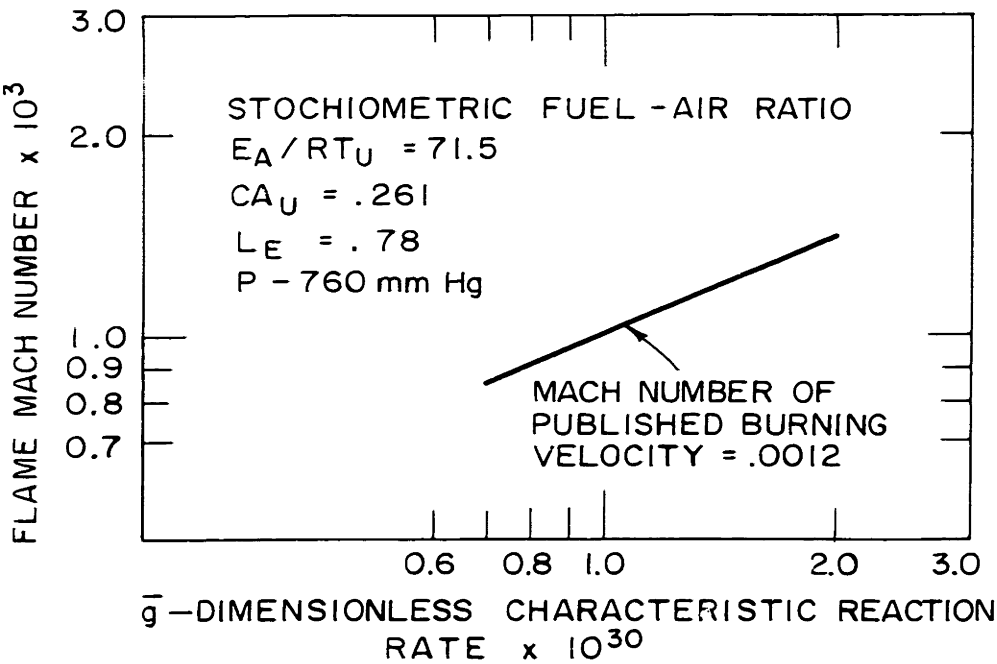

FIG. 45 DETERMINATION OF REACTION RATE CONSTANT - VARIATION OF FLAME MACH NUMBER WITH CHARACTERISTIC REACTION RATE

BIBLIOGRAPHY

N.B. The following abbreviations are used throughout this bibliography:

Third Symposium - Third Symposium on Combustion and Flame and Explosion Phenomena, Williams and Wilkins Company, Baltimore, 1949

Fourth Symposium - Fourth Symposium (International) on Combustion, Williams and Wilkins Company, Baltimore, 1953

Fifth Symposium - Fifth Symposium (International) on Combustion, Reinhold, New York, 1955

Sixth Symposium - Sixth Symposium (International) on Combustion, Reinhold, New York, 1957

Seventh Symposium - Seventh Symposium (International) on Combustion, Butterworth, London, 1959

Eighth Symposium - Eighth Symposium (International) on Combustion, Williams and Wilkins Company, Baltimore, 1962

Ninth Symposium - Ninth Symposium (International) on Combustion, Academic Press, New York, 1963

1. Ball, "A Study of a Two-Dimensional Flame", Combustion Laboratory Report, Harvard University, July, 1961
2. Barman, Soviet Mathematics and Mechanics, March, 1963
3. Beck and Toong, "Magnetogasdynamic Effects on Laminar Flame Propagation", Journal of Aero/Space Sciences,

November, 1961

4. Botha and Spalding, "The Laminar Flame Speed of Propane/Air Mixtures with Heat Extraction from the Flame", Proceedings of the Royal Society, v. 255, p. 71

5. Calcote, "Ion and Electron Profiles in Flames", Ninth Symposium

6. Cambel, "A review of Flame Stabilization by Means of Gaseous Jets", Combustion and Propulsion: Third AGARD Colloquium, eds. Thring, Fabri, Lutz, and Lefebvre; Pergamon Press, London, 1958

7. Cobine, Gaseous Conductors, Dover Publications, New York, 1958

8. Demutskii, Soviet Physics, Technical Physics, v. 7, no. 4, October, 1962

9. Demutskii and Polovin, Soviet Journal of Experimental and Theoretical Physics, v. 13, p. 1229

10. Dimmock, "The Electrical Properties of Ionized Flames", in Magnetohydrodynamics, Proceedings of the Fourth Biennial Gas Dynamics Symposium, Cambel, Anderson, and Slawsky, eds., Northwestern University Press, Evanston, 1962

11. Egerton and Thabat, Proceedings of the Royal Society, A211, p. 455, 1952

12. Fong, Bollinger, and Edse, Magnetohydrodynamic Effects on Exothermal Waves, ARL69, Office of Aerospace Research, USAF, WADC, September, 1961

13. Friedman, "Measurement of the Temperature Profile

in a Laminar Flame", Fourth Symposium

14. Fristrom, "Experimental Determinations of Local Concentrations in Flames", in Experimental Methods in Combustion Research, ed. Suruge, Pergamon Press, London, 1961

15. Fristrom, Experimental Techniques for the Study of Flame Structure, Bumblebee report no. 300, John Hopkins University, Applied Physics Laboratory, January, 1963

16. Gammon, in discussion of "A Review of Flame Stabilization by Means of Gaseous Jets", Combustion and Propulsion, Third AGARD Colloquium, eds., Thring, Fabri, Lutz, and Lefebvre; Pergamon Press, London, 1958

17. Gaydon and Wolfard, Flames, Their Structure, Radiation, and Temperature, Chapman and Hall, London, 1960

18. Gilbert, De Magnete, London, 1600

19. Gross and Esch, "Low Speed Combustion Aerodynamics", Jet Propulsion, v. 24, p.95, 1954

20. Gross, Chinitz, and Rivilin, "Magnetohydrodynamic Effects on Exothermal Waves", Journal of Aero/Space Sciences, April, 1960

21. Heinshom, "Electric and Magnetic Field Effects on Flat Flames", paper presented at the ASME Winter Annual Meeting, November, 1960

22. Helliwell, "Gas-Ionizing Shocks and Combustion Waves in Magnetohydrodynamics", Journal of Fluid Mechanics, part 3, v. 14, November, 1962

23. Helliwell, "Magneto-Gas-Dynamic Shock Waves in a Gas

with Variable Conductivity", Physics of Fluids, v.5, no. 6, June, 1962

24. Hirschfelder, "Propagation of Flames and Detonations", in Progress in Chemical Physics, v. 3, Academic Press, New York, 1962

25. Hirschfelder, Curtiss, and Bird, Molecular Theory of Gases and Liquids, Wiley, New York, 1954

26. Humphry, term paper in M.I.T. subject 2.821, Fall term, 1963-1964

27. Karlovitz, Denniston, Knapschaefer, and Wells, "Studies on Turbulent Flames", Fourth Symposium

28. Kelly, "Determination of the Velocity Field Across a Two-Dimensional Flame by a Particle Track Method", S.M. Thesis, M.I.T. Department of Mechanical Engineering, May, 1961

29. Kelly, "Electromagnetic Effects on the Propagation and Structure of Gaseous Detonations", Sc.D. Thesis, M.I.T. Department of Mechanical Engineering, July, 1965

30. Kerrebrock, J., Private Communication, June 24, 1965

31. Lewis, "Remarks on Combustion Science", Seventh Symposium

32. Lewis and Von Elbe, Combustion, Flame and Explosions in Gases, Academic Press, New York, 1961

33. Linnet, "Methods of Measuring Burning Velocities", Fourth Symposium

34. Lafitte, "Methodes du Bruler et de la Bulle de Savon", in Experimental Methods in Combustion Research, ed. Suruge, Pergamon Press, London, 1962

35. Lucheta, "An Experimental Demonstration of an Electromagnetic Effect in Flames", S.M. Thesis, M.I.T. Department of Mechanical Engineering, May, 1962

36. Maxworthy, "On the Mechanism of Bluff Body Flame Stabilization at Low Velocities", Combustion and Flame v. 6, p.233

37. McAdams, Heat Transmission, third edition, McGraw-Hill, New York, 1954

38. McVey, Term paper presented in M.I.T. subject 2.822, Spring semester, 1963

39. Minkoff and Tipper, Chemistry of Combustion Reactions, Butterworth, London, 1962

40. Mukherjee, Fueno, Eyring, and Ree, "Ions in Flames", Eighth Symposium

41. Nakamura, "Effect of the Electric Field Upon Hydrocarbon Diffusion Flames", Combustion and Flame, v.3, no.3, September, 1959

42. Pai, Fluid Dynamics of Jets, Van Nostrand, New York, 1954

43. Pai, Magnetogasdynamics and Plasma Physics, Springer-Verlag, Vienna, 1962

44. Penning, Electrical Discharges in Gases, Macmillan, New York, 1957

45. Polovin, Soviet Journal of Experimental and Theoretical Physics, v. 11, p. 1113

46. Powling, "The Flat Flame Burner", in Experimental Methods in Combustion Research, ed. Suruge, Pergamon Press, London, 1962

47. Putnam, "Comparison of Reverse Jet and Obstacle-Type Flame Holders", Jet Propulsion, v. 27, p. 177, 1957

48. Putnam and Smith, "On the Extinction Limit of Laminar Flames", Fourth Symposium

49. Robinson, "An Apparatus for the Measurement of the Dispersion of Transients in Pneumatic Transmission Lines", S.B. Thesis, M.I.T. Department of Mechanical Engineering, June, 1961

50. Shapiro, The Dynamics and Thermodynamics of Compressible Fluid Flow, Ronald Press, New York, 1954

51. Singer, "Burning Velocity Measurements on Slots: Comparison with Cylindrical Burner Determinations", Fourth Symposium

52. Spalding, Some Fundamentals of Combustion, Butterworth, London, 1955

53. Spitzer, Physics of Fully Ionized Gases, Interscience, New York, 1956

54. Stratton, Electromagnetic Theory, McGraw-Hill, New York, 1941

55. Thompson, The Electromagnet, Spon and Chamberlain, London, 1892

56. Thompson and Thompson, The Conduction of Electricity Through Gases, Third Edition, v. 2, Cambridge University Press, 1933

57. Toong, "Flame Stabilization in Boundary Layers", Combustion and Propulsion: Third AGARD Colloquium, Eds. Thring, Fabri, Lutz, and Lefebvre; Pergamon Press,

London, 1958

58. Toong, "Magnetogasdynamic Effects on Propagation of Detonation Waves", unpublished report, M.I.T., November, 1961

59. Toong and Chen, "Structure and Propagation of Laminar Flames Near a Heat Sink", Combustion and Flame, v.4, no. 4, 1960

60. Uberoi, "Flow Fields of Flame Propagating in Channels Based on the Source Sheet Approximation" Physics of Fluids, v.6, no. 8, August, 1963

61. Uberoi, "Flow Field of a Bunsen Flame by Source Sheet Approximation", American Physical Society, Fluid Dynamics Division Meeting, November 25-27, 1963

62. Von Engel, Ionized Gases, Second Edition, Oxford, 1965

63. Von Engel and Cozens, "Flame Plasmas", in Advances in Electronics and Electron Physics, v. 20, Morton and Morton, eds., Academic Press, New York, 1964

64. Weiss, Rohrer, and Longwell, "Some Effects of Fuel Reactivity and Heat Loss on Flame Stabilization", Sixth Symposium

65. Williams, Combustion Theory, Addison-Wesley, Reading, 1965

66. Wilson, The Electrical Properties of Flames and of Incandescent Solids, University of London, 1912

67. Wohl, Kapp, and Gazley, "The Stability of Open Flames", Third Symposium

68. Woodson and Melcher, Fields, Forces and Motion, notes

for M.I.T. subject 6.06, 1964

69. Wright, "Bluff Body Flame Stabilization: Blockage Effects", Combustion and Flame, v.3, no. 3, September, 1959

70. Zukoski and Marble, "Experiments Concerning the Mechanism of Flame Blowoff from Bluff Bodies", Proceedings of the Gas Dynamics Symposium on Aerothermochemistry, p. 205, Multicopy Corporation, Evanston, 1956

71. Handbook of Chemistry and Physics, 44th edition, Chemical Rubber Publishing Company, Cleveland, 1962

BIOGRAPHICAL NOTE

Roger Angelo Lucheta was born on November 26, 1940, in Louisville, Kentucky, where he attended the St. Vincent de Paul parish school and St. Xavier High School. He entered the Massachusetts Institute of Technology in 1957, where he recieved the degrees of Bachelor of Science in June, 1961, Master of Science in June, 1962, and Mechanical Engineer in February, 1964.

He has been employed by the Boeing Company and by the Aerojet-General Company, evaluating the dynamic response of a combustion chamber and turbine blade erosion in two-phase flow, respectively.